Development of novel membranes with polyketone support for removal of micropollutants and for separation of organic solvents

Liu, Cuijing

(Degree)
博士（学術）

(Date of Degree)
2020-03-25

(Date of Publication)
2022-03-25

(Resource Type)
doctoral thesis

(Report Number)
甲第7777号

(URL)
https://hdl.handle.net/20.500.14094/D1007777

Doctoral Dissertation

Development of novel membranes with polyketone support for removal of micropollutants and for separation of organic solvents

微少汚染物質の除去と有機溶媒分離を目的としたポリケトンを支持体とする新規膜の開発

January, 2020

Graduate School of Engineering

Kobe University

LIU CUIJING

Acknowledgement

It was the last summer before graduation from my master course, when I indulged in a book named "Doomsday and Cold in Wonderland" written by a Japanese writer, Murakami Haruki, one of my friend sent me the message: "Have you ever considered to study a PhD course in Japan?" To be honest, I had never thought about that. But I cannot stop thinking after receiving the message. Then, seven months later, I came here. Now, I get a PhD degree. I would like to appreciate many people for being awarded a PhD, because I would not have accomplished my PhD study if these people were not around me.

Foremost, I would like to express my greatest gratitude to my supervisor, Prof. Hideto Matsuyama, for his continuous guidance, sharing, pointed comments on my research. Also, thanks for providing me so many chances to attend conferences and symposiums, which are really helpful for me.

I would also like to thank the research staffs in our membrane center, for lending me their helping hands throughout my research. Particularly, I want to thank Dr. Daisuke Saeki, for his kind guidance at the first year of my study. I am truly grateful for Prof. Ryosuke Takagi, for his patiently and strictly revising my manuscripts, and also his plentiful, young and rich heart. I want to thank Prof. Takuji Shintani, because I have benefited a lot from his unique insights and a wealth of experience on membrane research. I truly appreciate Dr. Liang Cheng, for continuously discussing with me about membrane in interesting perspectives, and also for his humble and humorous attitude on the research. I want to thank Dr. Lifeng Fang, for always encouraging me.

I would like to express my appreciation to all my colleagues in the laboratory, for I have received a lot of help, understanding, caring from you. In addition, I learnt a lot from Japanese colleagues for their strong sense of responsibility and collective consciousness. Specially, I would like to thank all Chinese colleagues (Chuanjie Fang, Zhe Yang, Yuchen Sun, Huiyan Yang, Lei Zhang, Shengyao Wang, Wenyi Liu, Xinyu Zhang,…) for accompanying me to

grow through these three years in Japan and I will always remember the laughter we shared together. What's more, I hope I also left something meaningful for our laboratory.

Lastly, I would like to express my greatest and special appreciation to my family. Thank you for always loving me, teaching me how to keep contented and also how to walk in the storm. Particularly, I want to thank the humorous, diligence and ingenuity from my father, the rich imagination and perseverance from my mother, and the cuteness from my younger sister.

I treasure these three years, because of uncountable moments: dark and shining ones, disappointed and hopeful ones, ordinary and touched ones. Everyone one has only 24 hours a day. The task I needed to do but I did not, the responsibility I need to take but I did not, and the promises I needed to achieve but I did not. There must be someone else did all of these for me.

Thanks a lot, to all of you.

<div align="right">
Cuijing Liu

January, 2020
</div>

Contents

Chapter I General introduction

Currently, membrane separation plays more and more important roles than conventional methods in most industries due to its low energy consumption. The membranes with high selectivity, high permeability, various functions, and robust stability are highly desirable to the increasing demand. The target of this thesis is to explore the application of a newly developed material, polyketone (PK). It can be utilized in the fabrication of microfiltration membrane, forward osmosis membrane and reverse osmosis membrane. The separations via the novel membranes with PK support in aqueous and organic solvent media were studied. In detail, the removal of micropollutants from aqueous media and the separation of organic solvents were studied. In this chapter, the background of this study is presented.

I.1 Separation

Suppose that a system comprising two components exists in a vessel, as shown in Fig I.1. The second law of thermodynamics tells us that the system tends to maximize its entropy and keeps maximum disorder at its equilibrium state. A demon is able to discriminate molecules, and when he opens the hole, only one component can pass through the hole. For a while, the two molecules are separated completely and ordered situation is achieved. This process is called as separation [1]. People can get what they want from nature by separation. Therefore, separation is the key to the uses of nature.
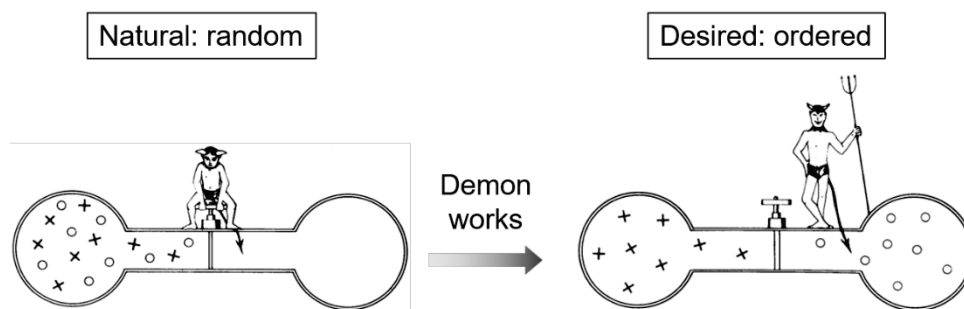
Fig. I.1 The sorting demon has transferred a random situation into an ordered one.

I.1.1 Separation system

Separation system exists everywhere, such as in our body (osmosis), in seawater treatment (distillation), in petroleum refining industry (evaporation), and so on. Generally, the media in separation systems are gas and liquid, therefore, main separations include gas phase separations and liquid phase separations. This thesis only focuses on liquid phase separations.

The targets of liquid separations are various, and here are several kinds:

- enrichment (enhancing the proportion of target component);
- dehydration (concentrating foods, biomass, organic liquid by removal of water);
- purification (removing impurities from the wanted product).

Purification is a needed process, when pure liquids (water or organic liquid) are desired from the mixtures. Two frequently encountered purifications are the purification of water from hazardous micropollutants-included aqueous media, and the purification of organic liquid from organic liquid mixtures. Because the challenges still exist in these two processes, they will be focused in this thesis.

I.1.2 Separation method

Of course, demon does not exist in nature. In order to achieve various separations, people can use energy instead of demon. The minimum amount of energy needed to achieve the separation is equal to the free enthalpy of mixing. Therefore, different systems need totally different amount of energy for separation. Generally speaking, the lower the objective molar concentration is, the higher the desired energy is. Thus, a higher price is needed for a low objective concentration, as expressed by "Sherwood-plot" in Fig. I.2 [2].

The energy of separation processes account for 10-15% of the world's energy consumption. In downstream petrochemical and manufacturing processes, around 45% of energy is associated with separations. For a given mixture, different separation approaches can be applied, which require different amount of energy. How to choose an appropriate separation approach for a given mixture? One general criterion is energy consumption.
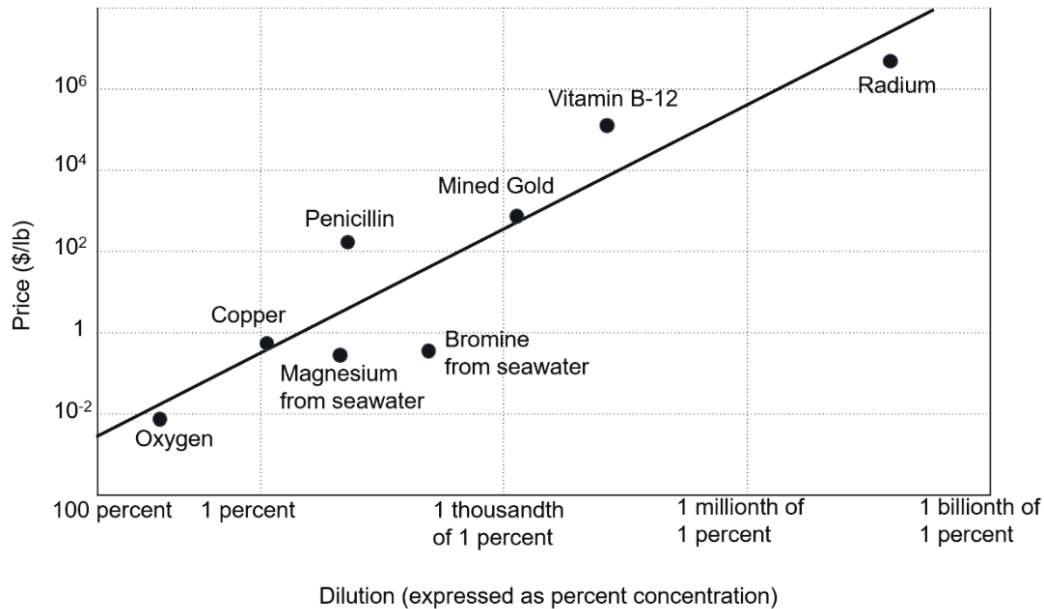
Fig. I.2 The Sherwood plot [2]. Sale price as related to the degree of the dilution of the raw material.

Generic separation approaches include:

- thermal based methods including distillation and evaporation: heat is supplied for one liquid component gasification
- other conventional methods: centrifugation, crystallization, adsorption, extraction
- membrane separation

Thermal driven processes are dominating now, in which distillation accounts for 80% of energy consumption [3]. Membrane-based separation would use 90% less energy than distillation [4], if appropriate membrane and process are designed. Taking the seawater desalination as an example, the ideal energy cost of producing pure water from typical seawater via an ideal separation process is only around 1 kWh m^{-3}, calculated from the thermodynamics. Considering the applied pressures to provide fluxes and the stir energy to minimize concentration polarization, the real energy cost in membrane process is roughly 4.5 kWh m^{-3}. On the other hand, the heat of vaporize the same amount of pure water is approximately 640 kWh m^{-3}. Even though this cost can be cut to 50 kWh m^{-3} by optimizing

multistage flash processes, it is clear that more than one order higher energy is needed in in thermal-based processes than that in membrane process [5].

The successful energy reduction in water purification by membrane technology leads us to consider the similar huge potentials for separations in organic liquids as well. Even the great success of membrane separation in aqueous media has been achieved, its separation in organic liquids is still in development. Considering that most of industries involve the separations in organic liquids, such as the recovery of catalysts [6], dyes [7] and antibiotics [8] from the organic solvents during production, and the separation of one kind of organic liquid from organic liquid mixtures, the application of membrane process for organic liquids separation is highly desired.

In summary, faced with the facts of the huge demand of various separations and current dominating energy-intensive separation technologies, membrane technology is expected to be an energy-efficient alternative.

I.2 Membrane process

Membrane process is a rapidly emerging technology. The benefits of membrane process include lower energy consumption explained in the section I.1, and as well as other aspects listed as follows:

- variable membrane properties
- easy combination with other processes (hybrid processing)
- mild operation conditions (easy operation)
- easy scale-up
- small footprint

The membrane is the heart of membrane process, and generally, it is defined as *a selective barrier between two phases and the term "selective" being inherent to a membrane or a membrane process* [1]. A schematic representation of membrane separation is shown in Fig. I.3. The driven forces in membrane separation can be gradients in pressure, concentration, electrical potential or temperature. An overview of various membrane processes is listed in Table I.1.
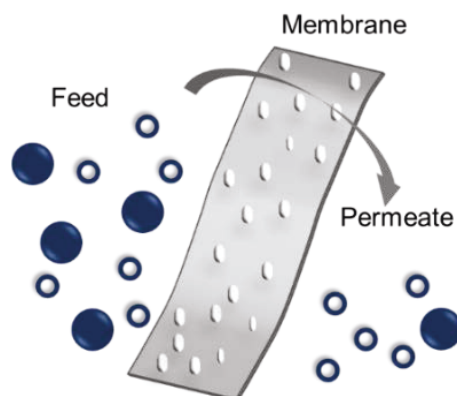
Fig. I.3 A scheme of two-phase system separated by a membrane.

Table I.1 Some membrane processes, and the corresponding driving forces and mechanisms

Membrane process	Driving force	Separation mechanism
Microfiltration (MF)	ΔP	Sieving
Ultrafiltration (UF)	ΔP	Sieving
Nanofiltration (NF)	ΔP	Sieving/Donnan exclusion
Reverse osmosis (RO)	ΔP	Solution-diffusion
Gas separation (GS)	ΔP	Solution-diffusion/Kundsen flow
Forward osmosis (FO)	ΔC	Solution-diffusion
Dialysis (D)	ΔC	Sieving
Electrodialysis (ED)	ΔE	Donnan exclusion
Membrane distillation (MD)	$\Delta T/\Delta P$	Vapor-liquid equilibrium
Pervaporation (PV)	$\Delta T/\Delta P$	Solution-diffusion

ΔP: pressure difference, ΔC: concentration difference, ΔE: electric potential difference, ΔT: temperature difference.

I.2.1 Pressure driven membrane process

Pressure driven membrane separation is the most widely used membrane process. According to the size of target molecules, it can be classified into microfiltration (MF), ultrafiltration (UF), nanofiltration (NF), reverse osmosis (RO). Figure I.4 shows the commonly operative range of these membrane processes in aqueous media and as well as in organic media. Operation pressure depends on the size of the retained solutes.

MF and UF are filtration processes which remove relatively large contaminants (such as bacterial, virus, and proteins) from a feed with a porous membrane. These processes are applied primarily in aqueous media. Because MF/UF processes can only remove relatively large molecules, they cannot guarantee high water quality. In order to produce a water of higher quality economically using the low pressure driven process, MF/UF is commonly combined with other processes (e.g. adsorption and catalytic process). For example, positive charged polymers coating to endow membranes with adsorption ability towards negative charged dyes [9], enzyme immobilization to endow membranes with catalytic ability, and so on. In which, enzyme immobilized MF membranes play important roles in the micropollutant degradation in the aqueous media. In this thesis, a removal of micropollutants from aqueous media is investigated using enzyme immobilized MF membranes, because micropollutants widely exist and have become a big environmental concern nowadays.

NF is mainly used with low TDS (total dissolved solids) water resources, for example, surface water and ground water. The purpose of NF filtration is a softening (polyvalent cation removal) and a removal of precursors that may produce by-products in disinfection such as natural or synthetic organic matters. Besides the applications in aqueous media, recently, NF separation of organic media has also attracted much attention as an organic solvent nanofiltration (OSN). OSN plays important roles in separation of solutes with molecular weight (M_w) larger than 200 Da, which can be antibodies, catalysts, dyes, and so on, as shown in Fig. I.4. This separation is of importance for most industries, such as pharmaceutical industry and chemical industry.

RO is a separation process which is the reverse of the normal osmosis process. In RO process, a solvent is permeated through a membrane from one side with high solute

concentration to another side with low solute concentration by applying a pressure higher than an osmotic pressure. RO membrane is considered to be semipermeable, allowing the passage of only solvent but not solute. This process requires a high applied pressure, due to the high resistance from the dense membrane. In organic media, organic solvent reverse osmosis (OSRO) membranes are expected to show high selectivity towards the solutes with M_w below 100 Da, which will be very useful for the separation of organic liquid mixtures, such as the separation of alcohol and hydrocarbon mixture. As it stands now, the development of OSRO membranes is in very infancy stage. In this thesis, the OSRO separation of organic liquid mixtures is further investigated.
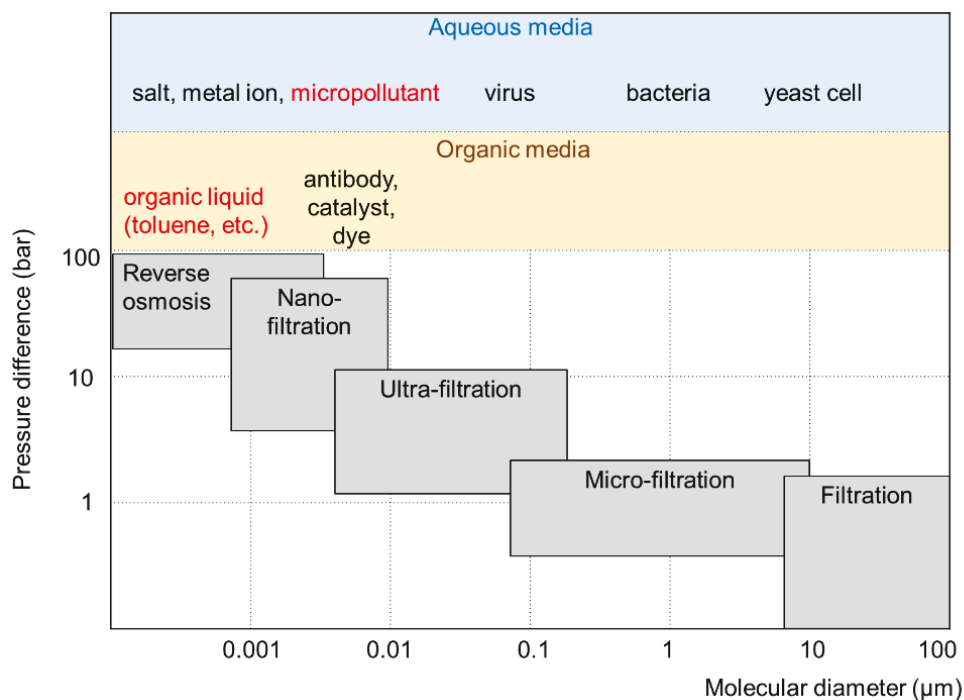
Fig. I.4 The filtration spectrum of commonly used pressure driven membrane processes in aqueous and organic media.

I.2.2 Forward osmosis membrane process

Forward osmosis (FO) is a membrane separation process driven by osmotic pressure created by the different concentrations between draw solution and feed solution, as shown in

Fig. I.5 [10]. FO process reduces the costs associated with a pumping, and a system construction with high pressure system, since an externally applied hydraulic pressure is not required. It is reported that the energy consumption in FO seawater desalination was 0.84 kWh/m^3, while 2 – 6 kWh/m^3 is needed when RO process is applied [11]. Therefore, FO process has drawn much attention over the past decades, mainly due to its less energy consumption while maintaining similar separation ability with RO process.

Because of osmotic pressure-driven, the fouling in FO is less compacted and more reversible than that in RO process, which allows the membrane cleaning easier. Thus, FO process is very suitable as an efficient pretreatment process before RO process, particularly for the feed solutions with high fouling property. In most applications, FO separation is coupled with other processes to form a hybrid system, and these systems are expected to surpass the single process [12]. The commonly used FO hybrid systems are listed in Table I.2. These systems have wide usage in desalination, wastewater treatment, fertigation, and so on [13-15]. Especially, it has been proved that FO is promising to remove micropollutants from water [16-18].

Considering the above advantages (low energy and low fouling) of FO process, in this thesis, hybrid FO process is used in the micropollutant removal from the aqueous media.
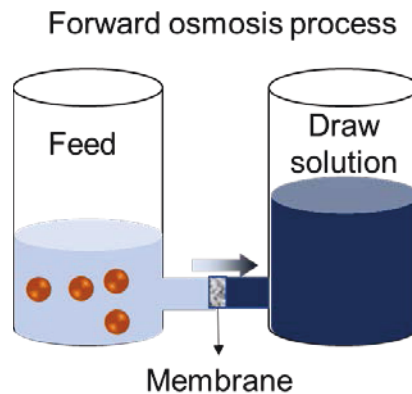
Fig. I.5 Schematic illustration of typical FO process composed of FO membrane, feed and draw solution. Pure water was moved from feed solution to draw solution by an osmotic pressure.

Table I.2 Some hybrid FO processes and the main applications

Hybrid process	Examples	The functions of FO part
FO + Membrane	FO-RO	Advanced pretreatment process in desalination
	RO-FO	Concentrate RO brine in desalination
	FO/MD[1]	Advanced pretreatment for MD operation
FO + Catalysis	FO-MBR[2]	Improve retention for higher MBR efficiency
	FO-ECO[3]	Improve retention for higher ECO efficiency

[1]   MD: membrane distillation

[2]   MBR: membrane bioreactor

[3]   ECO: Electrochemical oxidation

I.3 Membrane structure

Commonly used membranes are categorized into two types based on structure, symmetric and asymmetric as shown in Fig. I.6. The symmetric membranes have a symmetric cross section, while the asymmetric membranes consist of a skin layer and a support. For the asymmetric membranes, the skin layer assumes a practical filtration. If the materials of skin layer and supporting layer are the same, it is called as an integrally skinned asymmetric (ISA) membrane; while, when the materials are different, it is called as a thin film composite (TFC) membrane.

MF and UF membranes are usually symmetric or ISA membranes. Most NF, RO and FO membranes are TFC membranes, composing a porous support (usually MF or UF membranes) and a dense selective layer (usually polyamide made from interfacial polymerization).
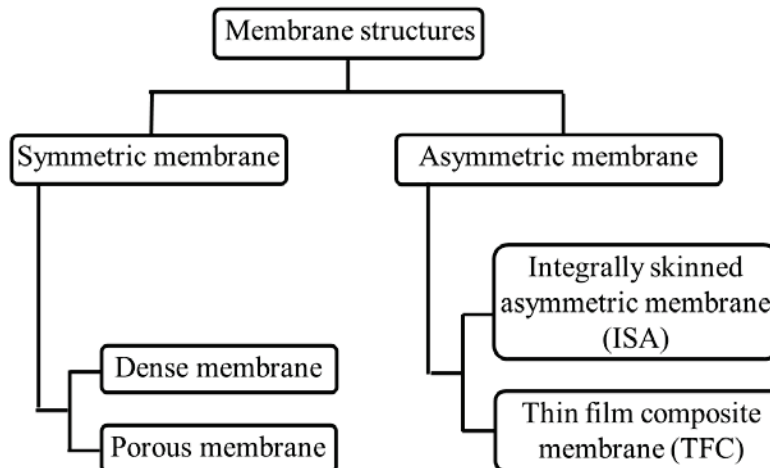
Fig. I.6 The types of commonly used membrane structures.

I.4 Membrane material

Membrane material is the key to the application of membranes in various separations. The mechanical properties and ease of processing are vital considerations for membrane materials. In addition, for water purification, antifouling must be considered, and for separations in organic media, solvent resistance is the most important consideration. Currently, many kinds of membrane materials have been developed, which can be divided into polymeric and inorganic materials. Common inorganic materials are confronted with high cost, few variety and difficult processing. Therefore, the most commonly used membrane materials are polymeric. This thesis focuses on polymeric materials.

I.4.1 Hydrophobic membrane materials

Figure I.7 lists some frequently used hydrophobic polymers. In Fig. I.7(A), polyvinylidene fluoride (PVDF) is soluble in many solvents such as dimethylformamide (DMF), dimethylacetamide (DMAc), glyceryl triacetate (GTA), N-methyl pyrrolidone (NMP), and polycarbonate (PC). Thus, PVDF is easy to form membrane via phase inversion methods, including nonsolvent induced phase separation (NIPS) and thermally induced phase separation (TIPS). PVDF is often used in the fabrication of MF membranes. Polysulfone (PSf) and polyethersulfone (PES) are the most important synthetic polymer materials now. They

can be fabricated as MF and UF membranes, and also are frequently employed as the porous supports of TFC membranes including NF, RO and FO membranes.

Considering the good chemical resistance of polymers shown in Fig. I.7(B), they can be used not only in aqueous but also in organic solvents. For example, polyacrylonitrile (PAN) and polyimide (PI) are largely explored for the supports for OSN membranes, but a pre-crosslinking step is necessary to provide high organic solvent resistance [19].

Despite the excellent chemical and thermal stability of the hydrophobic materials, there are some concerns. Firstly, many pollutants in water resources are hydrophobic, such as proteins and bacterial, which are easy to adsorb onto these hydrophobic membranes. The adsorption results in membrane fouling, and thus decreases the operation flux and/or increases the energy consumption. Secondly, faced with the various separation targets, modification of membranes is necessary, such as the hydrophilic modification for antifouling, the adsorption groups introduction for adsorptive membrane, the reactive groups grafting for catalysis, and so on. Nevertheless, most hydrophobic materials only contain inert groups possessing low reactivity, making them difficult to be functionalized.
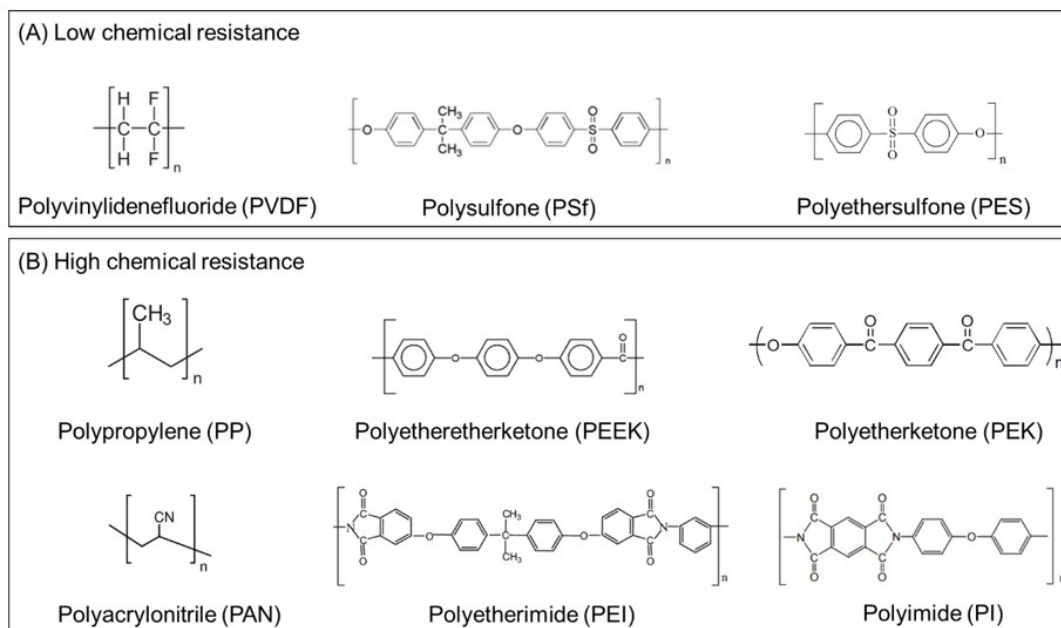
Fig. I.7 Some hydrophobic polymer materials frequently used as membrane materials.

I.4.2 Hydrophilic membrane materials

As hydrophobic polymers have some problems explained in part I.4.1, hydrophilic polymers are more attractive as membrane materials due to their low adsorption tendencies and the existence of functional groups [20, 21]. Mainly, two classes of hydrophilic membrane materials have been successfully developed. The best-known class is cellulose and its derivatives, including regenerated cellulose, cellulose acetate, cellulose triacetate, and so on [22]. As shown in Fig. I.8, the regenerated cellulose belongs to polysaccharide, and the molecular weight is around 500,000 to 1,500,000 Da. Benefited from its regular liner chain and intermolecular hydrogen bonding between hydroxyl groups, it is quite crystalline [23]. However, there are some problems to use cellulose as a membrane material. Firstly, it is difficult to be processed because of its high molecular weight and thus insoluble in common solvents [22]. Secondly, cellulose is very sensitive to biological degradation, which limits its application.

Another class of hydrophilic materials is polyamides [24]. Aliphatic polyamides, such as nylon-6 and nylon 6-6, are of greater interest as MF membranes. Aromatic polyamides, such as poly(m-phenylene isophtalamide), are also preferred due to their excellent mechanical, chemical, and thermal stability. In addition, polyamides usually are used as the selective layer materials for TFC NF and TFC RO membranes. The polyamides can be formed via interfacial polymerization using amine monomers and chloride monomers. The most commonly used monomers are m-phenylenediamine (MPD) and trimesoyl chloride (TMC) [25].

The above hydrophilic membranes are solvent resistant due to the strong interactions between main chains [26], which makes them potential to be employed in organic media. But they are confronted with difficult processing problem. Novel membrane materials with high hydrophilicity, robust solvent resistance, easy-processable and easy-functionable are highly desired. Such membranes are expected to show low fouling property in aqueous media and stable separation ability in organic media.

Cellulose   Nylon-6   Poly(m-phenylene isophtalamide)
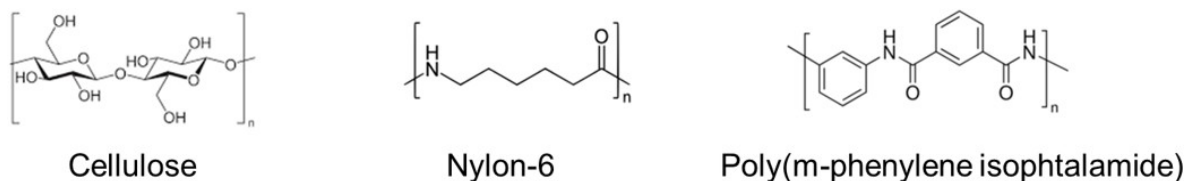
Fig. I.8 The chemical structure of cellulose, polyamides (nylon-6 and poly(m-phenylene isophtalamide)).

I.4.3 Polyketone (PK)

Aliphatic polyketone (PK) is a class of hydrophilic polymers of great current interest. PK polymers are prepared by the polymerization of α-olefins and carbon monoxide in a perfectly 1:1 alternating sequence using palladium catalysts. This synthesis was first reported in 1941 and the production of PK subsequently became appealing in academic and industrial areas. Initially, The US and Japan companies challenged to commercialize PK polymer. In 2013, Hyosung Corporation in Korea became the first company in the world to succeed in making this polymer using an economically efficient way, and the product was named as POLYKETONE. The simplest aliphatic PK is the polymer of ethylene and carbon monoxide, which can be regarded as a homopolymer of the repeat unit CH_2-CH_2-C=O [27] and the structure is shown in Fig. I.9. Now, Asahi Kasei Corporation in Japan can synthesize and provide this kind of PK.

PK has a crystalline melting point typical between 255 and 260 °C and it has higher chemical resistance than many other plastic materials. According to the report from Hyosung Corporation, POKETONE has a chemical resistance and impact resistance superior to nylon by more than 30% and 230% compared to Nylon, respectively. In addition, POKETONE has 14 times better abrasion resistance than polyoxymethylene (POM), and has the advantage of reducing friction noise.

Two main reasons why PK is promising as a membrane material are its functional properties, which can be modulated by changing the carbonyls into a wide variety of other groups [28] and meanwhile, outstanding solvent resistance [29]. These two characteristics endow PK membrane easy to be functioned to be applied in aqueous media and the potential

usage in organic media. Despite these advantages, PK membranes have been rarely reported, particularly for the applications in organic solvents. The wider usage of PK polymer in membrane technology is deserved to be explored. Thus, PK was used as the main membrane materials in this thesis.

The PK membranes can be fabricated by electrospinning [30], melt spinning and drawing [31], and NIPS [32, 33] methods. NIPS is preferred due to its superior adjustability of fabrication parameters.
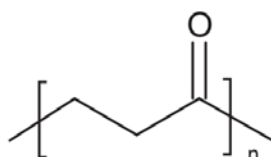
Fig. I.9 Chemical structure of polyketone material made from ethylene and carbon monoxide by Asahi Kasei Corporation.

I.5 Membrane process for micropollutant treatment in aqueous media

I.5.1 Micropollutant

The world is experiencing serious water shortages. By 2025, an estimated 1.8 billion people will be faced with water scarcity, and two-thirds of the population may be living in communities with lack of clean water supply [34]. Only 2.5 wt% of water on Earth is fresh water. Considering the fact that the increasing worldwide contamination of freshwater resources, the clean water must be produced from various water resources to satisfy the huge demands of drinking water [35].

There are many pollutants existing in water resources, such as proteins, oils, micropollutants, and so on. Among these pollutants, micropollutants have become an issue of increasing environmental concern. Micropollutants consist of a vast array of substances, including endocrine-disrupting compounds (EDCs), steroid hormones, pesticides, pharmaceuticals (PhACs), personal care products (PPCPs), industrial chemicals, and so on. Although most of these compounds are existed at low concentrations in water (up to several µg/L), many of them raise considerable concerns. The possible adverse effects of

micropollutant on the environment and human beings have been addressed, including short-term and long-term toxicity, endocrine disrupting effects and antibiotic resistance of microorganisms.

I.5.2 Sole membrane process

The large diversity of micropollutants create challenges for water treatment processes [36]. It has been reported that conventional municipal wastewater (WW) treatment processes are unlikely to remove micropollutants [37]. Micropollutants that could not be fully removed will eventually enter the environment and are transferred along the food chains. Thus, it is highly demanded to remove micropollutant more efficiently from water with powerful strategies.

Membrane processes are promising to be used to remove micropollutants [38-40]. However, sole membrane process can physically concentrate, but not eliminate micropollutants. If the degradation process can be combined with the membrane process, the harmful micropollutants will be removed and degraded simultaneously. Here, we consider the combination of degradation process with membrane process. Compared to various degradation approaches, including UV/O_3 oxidation, electrochemical degradation, and microorganism degradation, enzyme degradation is a mild, facile, and green approach.

I.5.3 Enzyme membrane bioreactors (EMBRs)

I.5.3.1 Enzyme and enzyme catalysis

Enzyme is one kind of important biocatalysts, and most enzymes are protein. Different enzymes have different catalytic functions. According to the definition of International Union of Pure and Applied Chemistry (IUPAC), enzymes are divided into six kinds based on the reaction type and mechanism: oxidoreductases, hydrolases, transferase, lyase, isomerase, and synthetase. Compared with the chemical catalysts, enzyme catalysis has the advantages such as high catalytic rate, high specificity, no pollution. Therefore, enzyme is used in wide applications. Table I.3 lists some commercially available enzymes and the corresponding applications.

Specifically, laccase belongs to oxidase enzyme, and can decompose many kinds of micropollutants. Thus, laccase is very promising to be used for micropollutant treatment [41]. The degradation mechanism of laccase is shown in Fig. I.10. Laccases couple the oxidation of the substrates to the reduction of O_2 to H_2O via Cu atoms in laccase. The Cu atoms are divided into Type1 (T1), Type2 (T2), and binuclear Type3 (T3) Cu sites due to the different spectroscopic characteristics. An electron is firstly donated to the substrate by the T1 and the following reactions occur subsequently, such as polymerization and/or dimerization. At the meantime, an internal electron transfers from the reduced T1 to the T2/T3 cluster, and oxygen is reduced to water.

Table I.3 Some common enzymes and the corresponding applications.

Enzyme	Field	Application
Protease	Detergent	Removal of organic coloring
Glucanase	Sugar manufacturing	Saccharification
Lipase	Fine chemical industry	Hydrolysis or esterification of grease
Laccase	Micropollutant removal	Environmental protection
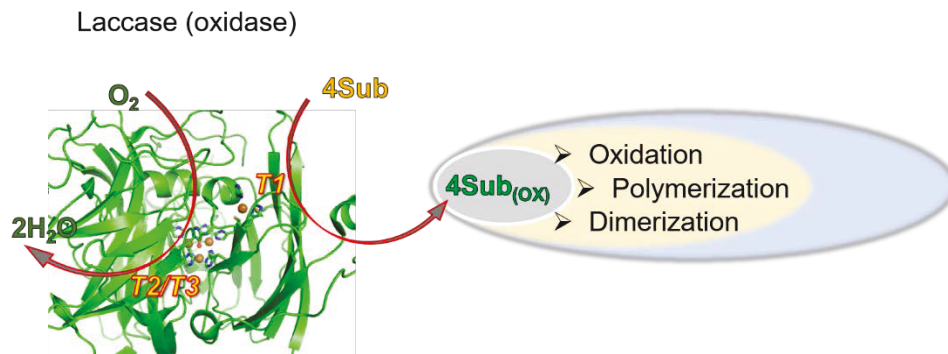
Fig. I.10 The catalytic mechanism of laccase toward substrates.

I.5.3.2 The kinds of EMBRs

Combining enzyme catalysis with membrane process becomes attractive over the past years, because this is an integration of low energy-cost and green-degradation process. The combination system is called as EMBRs. Generally speaking, these are two forms of EMBRs as shown in Fig. I.11. In type 1, enzyme exists in the free forms, and can be retained in the feed via membrane retention, electrostatic repulsion, and so on. Membrane only acts as a selective barrier. The small sized products can pass through the membrane. In this type of combination, the reaction rate is high, because of the sufficient contact of enzyme and substrates. And also, the operation is very facile, by simply adding free enzyme into the substrate solution. However, it is worth noting that enzymes are proteins, which trend to foul the membrane in this type of EMBRs. As introduced before, FO membrane has a high antifouling property, and also the dense separation layer can fully retain the enzymes in the feed solution side. Thus, the coupling of enzyme catalysis with FO process is intriguing, due to the wide use of both processes in practice. Considering there are no related reports combining these two processes, it was investigated in this thesis and the results were reported in Chapter II.

Even the process of type1 EMBRs is mild and green, enzyme is difficult to be recycled from the operation system after usage. Besides, enzyme stability in the operation needs to be concerned. For example, the existence of organic solvent in aqueous media may sharply lower the activity of free enzyme. These drawbacks can be eased by enzyme immobilizing, as type 2 shown in Fig. I.11. Here, membranes act as the supports for the immobilization of enzymes. Expect for keeping the catalytic activity, enzyme has other advantages after immobilization: (1) immobilized enzyme is easier for usage and reuse; (2) immobilized enzyme makes the reaction more controllable; (3) the product is easy to be separated; (4) in most cases, the stability of enzyme would be improved after immobilization; (5) MF and UF membranes are also can be coupled with enzyme catalysis, because there is no need to use dense membranes to retain enzymes in feed solution, like FO or RO or NF membranes.

In type 2, the immobilization methods must be carefully considered. A desired method provides high activity retention and high stability after immobilization. Adsorption, entrapment, and covalent bonding are commonly used for immobilization. Especially, the

covalent attachment can efficiently prevent enzyme migration and also can ensure high enzyme mobility. In addition, organic solvent may weaken the physical interaction between enzyme and membrane matrix. Thus, covalent bonding is preferred when organic solvent exists in the catalytic system. A novel and simple covalent method was explored in this thesis in Chapter III. The catalytic activity and stability of immobilized enzyme in organic solvent-included aqueous media was discussed in Chapter IV.
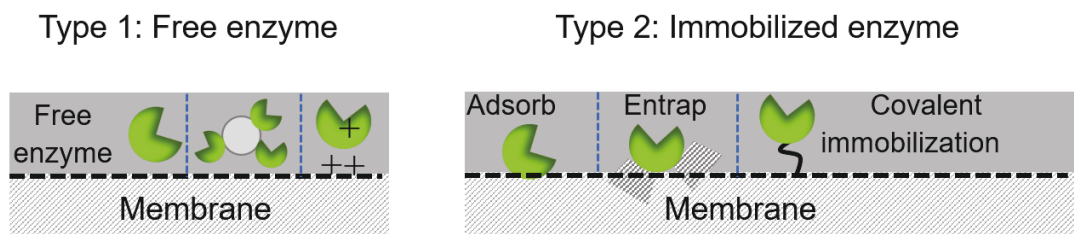
Fig. I.11 The two types to combine enzymes and membranes.

I.6 Membrane process for separations in organic media

Benefiting from low energy consumption, small footprint, operation simplicity and green process, membrane processes have been extensively used in water treatment as presented in the above parts. However, in practice, the separations in organic media are also frequently encountered in many industries such as pharmacy and chemical industries. Currently, the energy intensive distillation process dominates the separations in organic liquids. The membrane separation in organic media is highly desired to provide an alternative solution with low energy consumption.

The main membrane separation systems for organic liquids include the concentration of macromolecules in organic solvents and the separation of mixed organic liquids [42]. The corresponding processes, known as organic solvent nanofiltration (OSN) and organic solvent reverse osmosis (OSRO), respectively, have emerged over 50 years ago [3, 43].

Many of reported OSN and OSRO membranes are TFC composite membranes, comprising of a thin polyamide skin layer formed via interfacial polymerization and a porous substrate made from different materials. The polyamide layers are highly crosslinked, and can tolerate

harsh organic liquids. However, the typical supporting materials for TFC membranes (PSf, PES) will swell or be dissolved in organic media. The membrane separation in organic media is still challenging. One main difficulty is the exploration of high solvent resistant supports which are favorable for interfacial polymerization.

I.6.1 Organic solvent nanofiltration (OSN)

OSN is a separation process targeting the retention of organic solutes with molecular weights ranging from 200 to 1000 g/mol from an organic liquid. The first OSN pilot was launched in the 1990s, targeting a lube oil dewaxing application, which reduced energy use by 20% and capital costs by 60% compared with the conventional thermal distillation [44]. Recently, OSN membranes have been widely explored, which cover wide applications such as production purification, solvent recovery, catalyst recycling in pharmacy, and petroleum and chemistry industries [7, 25, 45-47]. For the supports of OSN membranes, many of these studies have focused on crosslinking common conventional polymer membrane substrates, such as polyimide (PI) and poly(ether imide) (PEI) and poly(ether ether ketone) (PEEK) [48-51].

However, OSN membranes can only efficiently reject the solutes larger than 200 Da. For the solute smaller than 200 Da, OSRO membranes are needed. The most common application occasion is the separation of organic liquid mixtures, such as alcohol and hydrocarbon mixtures [52-54].

I.6.2 Organic solvent reverse osmosis (OSRO)

In 1970, Sourirajan investigated the separation of alcohols and hydrocarbons using integrally cellulose acetate membranes. But unfortunately, hydrocarbons tended to collapse the membrane structures [52]. In the following 20 years after this study, organic solvent-resistant membranes made from polyacrylonitrile, cellulose acetate butyrate, and aromatic polyamide were also developed. However, the separation factors for organic substances were unsatisfactory and lower than 3.0 [53, 55, 56]. Even OSRO is promising for the separation

of molecules with Mw below 100 Da, it is very infancy and only a few studies have been reported [57]. Compared with OSN, OSRO separation is more difficult to be achieved.

On the one hand, higher solvents tolerance of supports is needed to obtain high separation performance. Most of the reported supports for TFC membranes need crosslinking, and the swelling still occurs during separation, which decreases the separation ability. As introduced in part I.4.3, PK is a promising candidate. Therefore, the PK was used as the support for interfacial polymerization, and the obtained TFC membrane was used to test the OSRO separation of organic liquid mixtures in this thesis. The results were shown in Chapter V.

On the other hand, higher crosslinking degree of polyamide layers are expected to provide higher separation ability. Thus, the fabrication parameters of interfacial polymerization were optimized in order to improve the separation factor. The results were shown in Chapter VI.

I.7 Purpose of this study

During last decades, membranes play more and more important roles in the wastewater treatment and as well as the separations in the organic solvents. Novel membrane materials are still needed for the diversification of membrane applications. As reported in our pervious study, PK polymer is easy to fabricate MF membrane via NIPS method, which achieves efficient oil/water separation [58]. Furthermore, interfacial polymerization can be performed onto this MF membrane to form a defect-free selective layer. Benefited from the porous structure of MF support membrane, this thin film composite membrane can be performed as a FO membrane endowed with high flux [33]. Considering various advantages of PK polymer, further development of PK based membranes and membrane processes is worthwhile. In this study, PK based membranes are fabricated, and their applications for micropollutant treatment from aqueous media and for organic liquid mixtures separations are focused.

For micropollutant treatment in aqueous media, two kinds of EMBR are designed. One is the combination of free enzyme and PK based FO membrane process, and the other one is the immobilizing enzyme onto PK based MF membrane. The enzyme immobilization method was also explored.

For organic liquid mixtures separations, PK based OSRO membrane was fabricated and the separation performance of a series of organic liquid mixtures was investigated. Furthermore, the fabrication condition of OSRO membrane was optimized to obtain better separation performance.

I.8 Scope of this study

This thesis was divided into 7 parts. The chapters expect for background and conclusion are shown in Fig. I.12. Each part is described as follows:

In **Chapter I**, the background as well as the purpose of this study is introduced. The scope of this thesis is also presented.

In **Chapter II**, PK based FO membrane was fabricated. Then enzyme catalysis was coupled with the FO process. The result hybrid system was used in micropollutant removal from aqueous media. To be specific, laccase enzyme was used as the model enzyme. TCP was used as the model micropollutant. The laccase enzyme was added into the feed solution at the beginning of FO filtration. The performance of hybrid system, sole FO process, sole enzyme catalysis process was compared and discussed. It was found that the degradation efficiency of hybrid system was higher than that of sole enzyme catalysis due to the concentration of enzyme during the FO process. Also, the fouling property of this enzyme-coupled membrane process was discussed.

In **Chapter III,** considering the limitations of free enzyme, such as the difficulty in recycling and instability, an efficient enzyme immobilization method was explored. Trypsin and lipase enzyme were used as model enzymes, due to their wide usage. Regenerate cellulose MF membrane is chosen as a model membrane due to the easy functionability resulted from the hydroxyl groups and also commercial availability. The enzyme immobilization density, activity and activity retention were evaluated. The results showed both trypsin and lipase could be efficiently immobilized and also exhibited good activity retentions. Therefore, the explored immobilization method was expected to be used to immobilize most enzymes onto membranes with hydroxyl functional groups.

In **Chapter IV**, laccase enzyme was immobilized onto PK based MF membranes using the developed method in Chapter III. In practical application, it is very common that enzyme catalysis needs to be conducted in the organic solvent-included aqueous media. Therefore, the main target of this chapter is to improve the catalytic ability of enzyme towards micropollutants in organic solvent-included aqueous media, via enzyme immobilization. Polyketone membrane was used as a support because it had functional groups (ketone groups), which were easy to be transferred to hydroxyl groups. Another important consideration was the excellent stability of PK membrane in many kinds of organic solvents. Regenerate cellulose (RC) membranes were used as a comparison. It was found that PK based membrane could immobilize higher enzyme amount and obtained higher activity retention than RC membrane. The mechanism of the above results was put forward and verified. The micropollutants decomposition of immobilized laccase was more efficient than that of free laccase when organic solvents existed in the aqueous media.

In **Chapter V**, due to the robust solvent resistance of PK based membrane, it is interesting to explore its separation ability in pure organic solvents. In this chapter, the interfacial polymerization was conducted on PK microporous membranes to form a dense separation layer, and this TFC membrane was explored as organic solvent reverse osmosis (OSRO) membrane. The separation of organic liquid mixtures was performed using this OSRO membrane. It was found that big nonpolar liquids could be efficiently separated from the small polar liquids by this membrane.

In **Chapter VI**, the separation ability of the OSRO membrane developed in Chapter V was further improved through an appropriate heat treatment. The effect of heat treatment procedures on the separation factor was investigated.

In **Chapter VII**, the summary and conclusions of this dissertation were given.
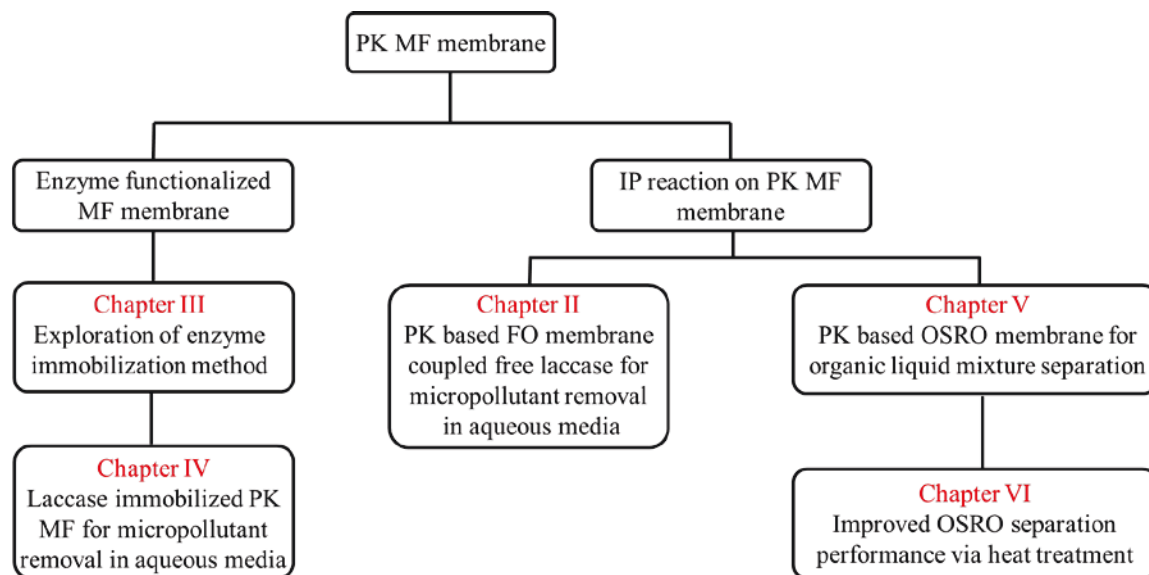
Fig. I.12 The experimental design of this thesis.

Reference

[1] M. Mulder, Basic principles of membrane techology, Springer Netherlands, Dordrecht, 1996.

[2] M. Ranjan, H.J. Herzog, Feasibility of air capture, Enrgy Proced, 4 (2011) 2869-2876.

[3] R.P. Lively, D.S. Sholl, From water to organics in membrane separations, Nat Mater, 16 (2017) 276-279.

[4] D.S. Sholl, R.P. Lively, Seven chemical separations to change the world, Nature, 533 (2016) 316-316.

[5] W.J. Koros, R.P. Lively, Water and beyond: Expanding the spectrum of large-scale energy efficient separation processes, AIChE J, 58 (2012) 2624-2633.

[6] L. Huang, J. Chen, T.T. Gao, M. Zhang, Y.R. Li, L.M. Dai, L.T. Qu, G.Q. Shi, Reduced Graphene Oxide Membranes for Ultrafast Organic Solvent Nanofiltration, Adv Mater, 28 (2016) 8669-8674.

[7] B. Liang, H. Wang, X.H. Shi, B.Y. Shen, X. He, Z.A. Ghazi, N.A. Khan, H. Sin, A.M. Khattak, L.S. Li, Z.Y. Tang, Microporous membranes comprising conjugated polymers with rigid backbones enable ultrafast organic-solvent nanofiltration, Nat Chem, 10 (2018) 961-967.

[8] D.Q. Shi, Y. Kong, J.X. Yu, Y.F. Wang, J.R. Yang, Separation performance of polyimide nanofiltration membranes for concentrating spiramycin extract, Desalination, 191 (2006) 309-317.

[9] C.J. Liu, L.A. Cheng, Y.F. Zhao, L.P. Zhu, Interfacially crosslinked composite porous membranes for ultrafast removal of anionic dyes from water through permeating adsorption, Journal of Hazardous Materials, 337 (2017) 217-225.

[10] B.D. Coday, P. Xu, E.G. Beaudry, J. Herron, K. Lampi, N.T. Hancock, T.Y. Cath, The sweet spot of forward osmosis: Treatment of produced water, drilling wastewater, and other complex and difficult liquid streams, Desalination, 333 (2014) 23-35.

[11] S. Phuntsho, H.K. Shon, S. Hong, S. Lee, S. Vigneswaran, J. Kandasamy, Fertiliser drawn forward osmosis desalination: the concept, performance and limitations for fertigation, Rev Environ Sci Bio, 11 (2012) 147-168.

[12] L. Chekli, S. Phuntsho, J.E. Kim, J. Kim, J.Y. Choi, J.S. Choi, S. Kim, J.H. Kim, S. Hong, J. Sohn, H.K. Shon, A comprehensive review of hybrid forward osmosis systems: Performance, applications and future prospects, J Membr Sci, 497 (2016) 430-449.

[13] S.F. Zhao, L.D. Zou, D. Mulcahy, Brackish water desalination by a hybrid forward osmosis-nanofiltration system using divalent draw solute, Desalination, 284 (2012) 175-181.

[14] Q.C. Ge, P. Wang, C.F. Wan, T.S. Chung, Polyelectrolyte-Promoted Forward Osmosis-Membrane Distillation (FO-MD) Hybrid Process for Dye Wastewater Treatment, Environ Sci Technol, 46 (2012) 6236-6243.

[15] K.Y. Wang, M.M. Teoh, A. Nugroho, T.S. Chung, Integrated forward osmosis-membrane distillation (FO-MD) hybrid system for the concentration of protein solutions, Chem Eng Sci, 66 (2011) 2421-2430.

[16] X. Jin, J.H. Shan, C. Wang, J. Wei, C.Y.Y. Tang, Rejection of pharmaceuticals by forward osmosis membranes, J Hazard Mate, 227 (2012) 55-61.

[17] B.D. Coday, B.G.M. Yaffe, P. Xu, T.Y. Cath, Rejection of Trace Organic Compounds by Forward Osmosis Membranes: A Literature Review, Environ Sci Technol, 48 (2014) 3612-3624.

[18] R.V. Linares, V. Yangali-Quintanilla, Z.Y. Li, G. Amy, Rejection of micropollutants by clean and fouled forward osmosis membrane, Water Res, 45 (2011) 6737-6744.

[19] B. Liang, X. He, J. Hou, L. Li, Z. Tang, Membrane Separation in Organic Liquid: Technologies, Achievements, and Opportunities, Adv Mater, (2018) 1806090.

[20] B. Jung, Preparation of hydrophilic polyacrylonitrile blend membranes for ultrafiltration, J Membr Sci, 229 (2004) 129-136.

[21] J.F. Blanco, Q.T. Nguyen, P. Schaetzel, Novel hydrophilic membrane materials: sulfonated polyethersulfone Cardo, J Membr Sci, 186 (2001) 267-279.

[22] Z.W. Ma, M. Kotaki, S. Ramakrishna, Electrospun cellulose nanofiber as affinity membrane, J Membr Sci, 265 (2005) 115-123.

[23] J. Kim, S. Yun, Z. Ounaies, Discovery of cellulose as a smart material (vol 39, pg 4202, 2006), Macromolecules, 39 (2006) 5583-5583.

[24] Z.B. Zhang, X.L. Zhu, F.J. Xu, K.G. Neoh, E.T. Kang, Temperature- and pH-sensitive nylon membranes prepared via consecutive surface-initiated atom transfer radical graft polymerizations, J Membr Sci, 342 (2009) 300-306.

[25] S. Karan, Z.W. Jiang, A.G. Livingston, Sub-10 nm polyamide nanofilms with ultrafast solvent transport for molecular separation, Science, 348 (2015) 1347-1351.

[26] S.L. Liu, J.A. Zeng, D.D. Tao, L.N. Zhang, Microfiltration performance of regenerated cellulose membrane prepared at low temperature for wastewater treatment, Cellulose, 17 (2010) 1159-1169.

[27] J.M. Lagaron, A.K. Powell, N.S. Davidson, Characterization of the structure and crystalline polymorphism present in aliphatic polyketones by Raman spectroscopy, Macromolecules, 33 (2000) 1030-1035.

[28] Y.S. Jung, A. Canlier, T.S. Hwang, An efficient and facile method of grafting Allyl groups to chemically resistant polyketone membranes, Polymer, 141 (2018) 102-108.

[29] N. Ataollahi, K. Vezzu, G. Nawn, G. Pace, G. Cavinato, F. Girardi, P. Scardi, V. Di Noto, R. Di Maggio, A Polyketone-based Anion Exchange Membrane for Electrochemical Applications: Synthesis and Characterization, Electrochim Acta, 226 (2017) 148-157.

[30] O. Ohsawa, K.H. Lee, B.S. Kim, S. Lee, I.S. Kim, Preparation and characterization of polyketone (PK) fibrous membrane via electrospinning, Polymer, 51 (2010) 2007-2012.

[31] P. Gupta, J.T. Schulte, J.E. Flood, J.E. Spruiell, Development of high-strength fibers from aliphatic polyketones by melt spinning and drawing, J Appl Polym Sci, 82 (2001) 1794-1815.

[32] C.J. Liu, D. Saeki, L. Cheng, J.Q. Luo, H. Matsuyama, Polyketone-based membrane support improves the organic solvent resistance of laccase catalysis, J Colloid Interf Sci, 544 (2019) 230-240.

[33] M. Yasukawa, S. Mishima, M. Shibuya, D. Saeki, T. Takahashi, T. Miyoshi, H. Matsuyama, Preparation of a forward osmosis membrane using a highly porous polyketone microfiltration membrane as a novel support, J Membr Sci, 487 (2015) 51-59.

[34] J. Eliasson, The rising pressure of global water shortages, Nature, 517 (2015) 6-6.

[35] D.J. Miller, D.R. Dreyer, C.W. Bielawski, D.R. Paul, B.D. Freeman, Surface Modification of Water Purification Membranes, Angew Chem Int Edit, 56 (2017) 4662-4711.

[36] Y.L. Luo, W.S. Guo, H.H. Ngo, L.D. Nghiem, F.I. Hai, J. Zhang, S. Liang, X.C.C. Wang, A review on the occurrence of micropollutants in the aquatic environment and their fate and removal during wastewater treatment, Sci Total Environ, 473 (2014) 619-641.

[37] S. Kim, K.H. Chu, Y.A.J. Al-Hamadani, C.M. Park, M. Jang, D.H. Kim, M. Yu, J. Heo, Y. Yoon, Removal of contaminants of emerging concern by membranes in water and wastewater: A review, Chem Eng J, 335 (2018) 896-914.

[38] L.D. Nghiem, A.I. Schafer, M. Elimelech, Pharmaceutical retention mechanisms by nanofiltration membranes, Environ Sci Technol, 39 (2005) 7698-7705.

[39] M. Lopez-Munoz, A. Sotto, J.M. Arsuaga, B. Van der Bruggen, Influence of membrane, solute and solution properties on the retention of phenolic compounds in aqueous solution by nanofiltration membranes, Sep Purif Technol, 66 (2009) 194-201.

[40] Y. Yoon, P. Westerhoff, S.A. Snyder, E.C. Wert, J. Yoon, Removal of endocrine disrupting compounds and pharmaceuticals by nanofiltration and ultrafiltration membranes, Desalination, 202 (2007) 16-23.

[41] N. Mita, S. Tawaki, H. Uyama, S. Kobayashi, Laccase-catalyzed oxidative polymerization of phenols, Macromol Biosci, 3 (2003) 253-257.

[42] T. Tsuru, M. Miyawaki, T. Yoshioka, M. Asaeda, Reverse osmosis of nonaqueous solutions through porous silica-zirconia membranes, AIChE J, 52 (2006) 522-531.

[43] L.L. Xia, J. Ren, M. Weyd, J.R. McCutcheon, Ceramic-supported thin film composite membrane for organic solvent nanofiltration, J Membr Sci, 563 (2018) 857-863.

[44] R.M. Gould, L.S. White, C.R. Wildemuth, Membrane separation in solvent lube dewaxing, Environ Prog, 20 (2001) 12-16.

[45] I.B. Valtcheva, P. Marchetti, A.G. Livingston, Cross linked polybenzimidazole membranes for organic solvent nanofiltration (OSN): Analysis of crosslinking reaction mechanism and effects of reaction parameters, J Membr Sci, 493 (2015) 568-579.

[46] L. Perez-Manriquez, P. Neelakanda, K.V. Peinemann, Tannin-based thin-film composite membranes for solvent nanofiltration, J Membr Sci, 541 (2017) 137-142.

[47] C. Li, S.X. Li, L. Lv, B.W. Su, M.Z. Hu, High solvent-resistant and integrally crosslinked polyimide-based composite membranes for organic solvent nanofiltration, J Membr Sci, 564 (2018) 10-21.

[48] Y.Y. Hai, J.L. Zhang, C. Shi, A.Y. Zhou, C.Y. Bian, W. Li, Thin film composite nanofiltration membrane prepared by the interfacial polymerization of 1,2,4,5-benzene tetracarbonyl chloride on the mixed amines cross-linked poly(ether imide) support, J Membr Sci, 520 (2016) 19-28.

[49] X.Y. Guo, D.H. Liu, T.T. Han, H.L. Huang, Q.Y. Yang, C.L. Zhong, Preparation of Thin Film Nanocomposite Membranes with Surface Modified MOF for High Flux Organic Solvent Nanofiltration, AIChE J, 63 (2017) 1303-1312.

[50] M.F.J. Solomon, Y. Bhole, A.G. Livingston, High flux membranes for organic solvent nanofiltration (OSN)-Interfacial polymerization with solvent activation, J Membr Sci, 423 (2012) 371-382.

[51] M.F. Jimenez-Solomon, P. Gorgojo, M. Munoz-Ibanez, A.G. Livingston, Beneath the surface: Influence of supports on thin film composite membranes by interfacial polymerization for organic solvent nanofiltration, J Membr Sci, 448 (2013) 102-113.

[52] W.J. Adam, B. Luke, P. Meares, The Separation of Mixtures of Organic Liquids by Hyperfiltration, J Membr Sci, 13 (1983) 127-149.

[53] Y. Fang, S. Sourirajan, T. Matsuura, Reverse osmosis separation of binary organic mixtures using cellulose acetate butyrate and aromatic polyamide membraes, J Appl Polym Sci, 44, (1992) 1959-1969.

[54] S. Sourirajan, Separation of Hydrocarbon Liquids by Flow under Pressure through Porous Membranes, Nature, 203 (1964) 1348.

[55] H. Nomura, S. Yoshida, M. Seno, H. Takahashi, T. Yamabe, Permselectivities of Some Aromatic-Compounds in Organic Medium through Cellulose-Acetate Membranes by Reverse-Osmosis, J Appl Polym Sci, 22 (1978) 2609-2620.

[56] W.J. Adam, B. Luke, P. Meares, The Separation of Mixtures of Organic Liquids by Hyperfiltration, J Membr Sci, 13 (1983) 127-149.

[57] M.L. Jue, D.Y. Koh, B.A. McCool, R.P. Lively, Enabling Widespread Use of Microporous Materials for Challenging Organic Solvent Separations, Chemistry of Materials, 29 (2017) 9863-9876.

[58] L. Cheng, D.M. Wang, A.R. Shaikh, L.F. Fang, S. Jeon, D. Saeki, L. Zhang, C.J. Liu, H. Matsuyama, Dual Superlyophobic Aliphatic Polyketone Membranes for Highly Efficient Emulsified Oil-Water Separation: Performance and Mechanism, Acs Appl Mater Inter, 10 (2018) 30860-30870.

Chapter II Enzyme-aided forward osmosis (E-FO) process to enhance removal of micropollutants from water resources

II.1 Introduction

The shortage of water has plagued many communities: more than 1.2 billion people in the world lack access to safe drinking water [1, 2]. The increasing pollution of water resources by human activities further aggravates the water crisis. As mentioned in **Chapter I**, part I.5, there is a vast and expanding array of micropollutants resulting from the use of pesticides, personal care products, plasticizers, endocrine disruptor chemicals (EDCs), pharmaceuticals, steroid hormones, and other products [2], causing deleterious effects on aquatic ecosystems and human health even at trace concentration levels due to inherent bioaccumulation and considerable carcinogenic properties [3, 4]. Micropollutants in relatively high concentrations (μg/L) have been found in wastewater effluents owing to incomplete removal by conventional treatment processes [2]. For example, traditional activated carbon adsorption and coagulation are less effective owing to the low concentration of micropollutants and competitive adsorption by natural organic matter [5]. The development of low energy technologies with a high micropollutants removal efficiency is crucial for affordable portable water production.

Forward osmosis (FO) has emerged as a promising membrane technology for potable water production, because of the high rejection by the membranes, similar to that of reverse osmosis (RO), and low energy consumption by using the natural osmotic process to draw water molecules from a feed solution (FS) to a draw solution (DS) via a semipermeable membrane [6, 7], as well as a low membrane fouling potential with easy flux recovery. Osmotic pressure leads to a loose and low-density accumulation layer of foulants on the FO membranes, which can easily be cleaned. In contrast, a conventional RO process driven by

high hydraulic pressure remains an energy-intensive operation, and a compact and dense fouling layer (e.g. scaling, organic fouling, and biofouling) is usually formed on the RO membranes. Thus, FO is considered to be promising in treating water with high salinity and intensive fouling, while lowering total energy consumption by using hybrid processes with RO, membrane distillation (MD) and other techniques [8].

As regards to removal of micropollutants, previous studies have confirmed the good performance of the FO process. Single FO processes can achieve higher rejection of those trace contaminants than RO processes mainly due to the reverse salt flux that helps reduce target solute flux in the FO process [9]. The hybrid FO-RO system even shows significantly high rejection (> 99%) of micropollutants provided by the dual barrier of FO and RO membranes. However, these target contaminants are merely physically concentrated in the feed water, and not eliminated, and they will ultimately be accumulated in a closed-loop system. A relatively high level of contaminants remaining in the feed requires additional detoxification treatments before safe disposal [10]. On the contrary, the accumulated contaminants will likely pass through the membrane by adsorption and diffusion in long-term operations, resulting in contamination of the product water [2, 6, 11-14], and severe membrane fouling.

Integrating micropollutant detoxification processes with the FO process is believed to be a promising energy- and cost-effective solution for simultaneous clean water production and FO concentrate treatment [15]. Available advanced oxidation strategies, such as electrochemical oxidation and chemical oxidation using hydrogen peroxide, ozone, or UV radiation are possible approaches. Liu et al. have proposed an electrochemical oxidation-FO hybrid process that can reject pharmaceuticals in the feed water by 98% and remove the pharmaceuticals in feed by 99% [15]. However, drawbacks of these methods are high energy consumption, the need for complex devices and unknown byproducts with equal or greater toxicity than the parent chemical [16-18]. Alternatively, biological protocols are potentially a green and low-cost approach owing to their high selectivity, environment friendliness, and technical feasibility [19]. Integrating microbial transformation with FO process, called osmosis membrane bioreactor (OMBR), was firstly proposed in 2008 and have captured

tremendous attention [20-22], however, the membranes suffered from problematic fouling and biodegradation via the biomass in the activated sludge [23, 24]. Compared with microorganism-based catalysis, enzymatic catalysis is expected to cause less membrane deterioration, along with a higher catalytic efficiency and a lower fouling potential. The use of isolated enzymes targeting specific chemicals holds promise as a more systematic and controllable biological treatment [19]. Many micropollutants can be oxidized by a variety of enzymes such as peroxidase, tyrosinase, and laccase [25, 26]. Taking laccase as an example, the catalytic mechanism and typical reactions were shown in Fig. II.1 [27]. Therefore, in this study, we report the first example of coupling enzyme catalysis with FO process, hereafter assigned as E-FO, for sustainable clean water production with highly efficient micropollutant degradation, as shown in Fig. II.2. Due to the continuous recovery of water from feed solution during filtration, the enzyme is concentrated, and thus E-FO is expected to exhibit higher degradation efficiency than single enzyme catalysis in bioreactor (BR). Meanwhile, owing to the degradation of micropollutants by enzyme in E-FO, less micropollutants adsorption and leakage through membrane are anticipated than in the single FO process. The main aim of this work is to verify the above concept.

2, 4, 6-trichlorophenol (TCP) and bisphenol A (BPA) were used as the model micropollutants. TCP, a carcinogen with high toxicity, is formed by emissions of fossil fuel combustion, municipal waste incineration, and chlorination of water containing phenol [28]. BPA is well-known as an endocrine disruptor and one of the highest productions and consumption volume chemicals in the world [29]. Laccase was used as a model enzyme because of its catalytic ability towards a variety of aromatic compounds, particularly phenolics including TCP and BPA [30]. The possible products of the TCP and BPA were also shown in the Fig. II.1. Generally speaking, the products are less harmful than the micropollutants. Due to their wide substrate specificity, many phenolic micropollutants, pesticide, personal care products, dye molecules from wastewater effluents can be degraded [19]. A lab-made polyamide thin film composite (TFC) membrane prepared by interfacing polymerization (IP) on a polyketone (PK) substrate, referred to as PK-IP, was employed as the FO membrane. The micropollutant removal performance of E-FO was then evaluated. To

be specific, the TCP degradation efficiencies in the feed solution of E-FO and in BR were measured. The leaked TCP in a permeate and adsorption amount on the membrane in E-FO and in FO processes were also measured and then compared. At last, the fouling tendency of E-FO process was investigated for possible long-term operation and compared with that of enzyme-aided reverse osmosis (E-RO).
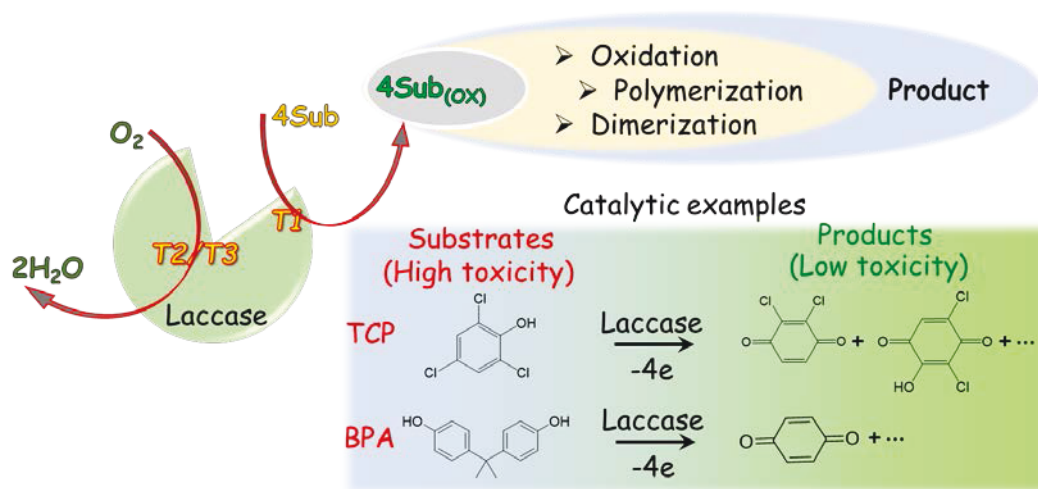
Fig. II.1 The mechanism and examples of laccase catalysis toward 2, 4, 6-trichlorophenol (TCP) and bisphenol A (BPA).
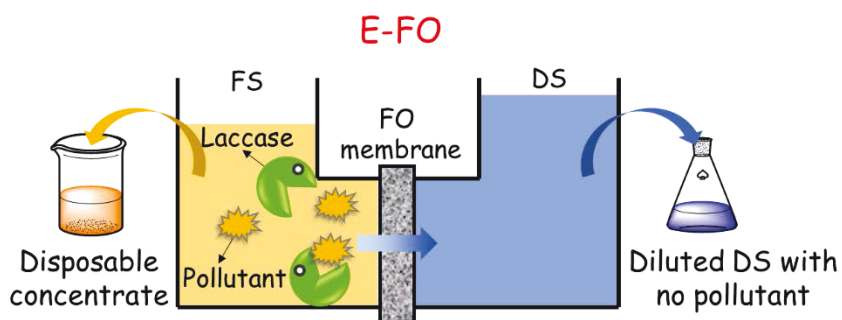
Fig. II.2 Schematic diagram of enzyme-aided FO (E-FO) process for the removal of micropollutants from water. FS and DS indicate the feed solution and the draw solution, respectively.

II.2 Experimental

II.2.1 Materials
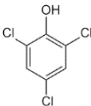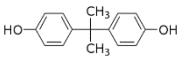
Polyketone (PK) polymer (molecular weight: 200,000 g mol^{-1}, Asahi Kasei Co., Tokyo, Japan) was used to fabricate a porous PK supporting layer for synthesis of thin film composite (TFC) FO membrane. Resorcinol, methanol, acetone, and hexane (Wako Pure Chemical Co., Osaka, Japan), were used in the PK support layer fabrication. 1,3,5-benzenetricarbonyl trichloride (TMC), 10-camphorsulfonic acid (CSA), hexamethylphosphoric triamide (HMPA) (Tokyo Kasei Co., Tokyo, Japan), 1,3-phenylene diamine (MPD), sodium dodecyl sulfate (SDS), and triethyl amine (TEA) (Wako Pure Chemical Co., Japan) were used to fabricate the polyamide layer of lab-made TFC membranes via interfacial polymerization (IP). A commercial polysulfone (PSf) substrate (CF30K, Nitto, Osaka, Japan) was obtained for fabrication of a control polyamide TFC membrane. In addition, a commercial FO membrane made of cellulose triacetate (CTA) material with embedded polyester screen support (CTA-ES, Fisher, USA), and a commercial TFC RO membrane (ES20, Nitto, Osaka, Japan) were also obtained for membrane filtration tests.

TCP and BPA (Sigma-Aldrich Co. LLC, USA) were used as the model micropollutants, and their properties were listed in Table II.1. The stock solutions of TCP and BPA were prepared by dissolving them in methanol with a concentration of 10.2 mM (2000 ppm) and 8.7 mM (2000 ppm), respectively, and stored at -20°C for future use. Laccase from *Trametes versicolor* (powder, light brown, ≥ 0.5 U mg^{-1}, molecular weight: 63 KDa, Sigma-Aldrich Co. LLC, USA) was used as a model enzyme. 2, 2'-azino-bis (3-ethylbenzothiazoline-6-sulfonic acid) (ABTS) (Sigma-Aldrich Co. LLC) was used as a model substrate to evaluate the activity of laccase.

HCl solution (0.1 M) and H$_2$SO$_4$ solution (1 M) (Sigma-Aldrich Co. LLC, USA) were used for adjusting the pH of the feed solution and the draw solution samples in the solid phase extraction process (explained in Section II.2.5.1), respectively. Sodium chloride (NaCl) (Wako Pure Chemical Co., Japan) was used in draw solution preparation. Acetonitrile (Wako Pure Chemical Co., Japan) was used as the mobile phase in high performance liquid chromatography (HPLC) analysis and also as enzyme inactivation agent. Oasis HLB

cartridges (6 mL/200 mg, Waters, Milford, MA, USA) were used in the solid phase extraction process. Nylon syringe filters (0.22 μm, Membrane Solution, Kent, WA, USA) were used for purifying the sample for HPLC analysis. Milli-Q water (Millipore, Billerica, MA, USA) was used in all cases.

Table II.1 Physicochemical properties of selected micropollutants

	Structure	Molecular weight (g/mol)	Log D[1]	PKa[2]
TCP		197	3.69	6.23
BPA		228	3.32	9.6

[1] Distribution coefficient

[2] Acid dissociation constant

II.2.2 Membrane fabrication

The porous PK substrate was prepared via the typical non-solvent induced phase separation process (NIPS) [31-33]. PK powder was firstly dissolved in a resorcinol/water solution (65/35 wt. %) to form a 10 wt. % PK solution. The degassed homogeneous polymer solution was cast on a clean glass plate at a thickness of 400 μm and subsequently, the plate was immersed in a coagulation bath containing methanol/water (35/65 wt. %) for 20 min. Finally, the formed PK membranes were washed in acetone, and then hexane for 20 min each, and dried in air for future use. The IP process was then performed on the PK substrates for the synthesis of PK-based TFC FO membrane [31], referred to as PK-IP. The aqueous phase contained 2 wt. % MPD, 1.1 wt. % TEA, 3 wt. % HMPA, 2.3 wt. % CSA, and 0.15 wt. % SDS. The oil phase contained 0.15 wt. % TMC in hexane. Briefly, the aqueous solution was first poured onto the top surface of PK substrate and removed after 5 min. Then, the hexane solution was covered on the top surface to allow IP reaction for 2 min. After draining the

excess hexane solution, the formed membrane was heated at 90 °C for 10 min and then gently washed by Milli-Q water and stored in Milli-Q water for further use.

Similarly, the IP process was performed on the commercial PSf substrate to obtain a control TFC membrane named as PSf-IP. According to another report [34], an aqueous solution with optimized constitution was used, including 2 wt. % MPD, 2 wt. % TEA, 4 wt. % CSA, and 0.25 wt. % SDS, whereas the oil phase was kept the same as PK-IP fabrication. The retention time for aqueous and oil phases was 1 min and 30 s, respectively. The following heat treatment was conducted at 100 °C for 5 min. At the same time, for better comparison, the same IP processes and post-treatment conditions of PK-IP were conducted on PSf membrane and the resulted membrane was named as PSf-IP-contrast.

II.2.3 Evaluation of laccase activity

The laccase activity in the sample solutions was evaluated by the monitoring the oxidation rate of a model substrate, ABTS, to ABTS$^+$, in order to test its activity stability. A 150 µL of sample was taken from the feed solution in E-FO and in BR systems at fixed time intervals. Then, each sample was added into 3 mL ABTS aqueous solution (0.5 mM, pH 5.5). The increase in absorbance at 420 nm (ΔAbs_{420nm}; extinction coefficient $\varepsilon_{420} = 36.0$ mM^{-1} cm^{-1}) was recorded using a UV-Vis spectrometer (V-630, Jasco, Tokyo, Japan) for 2 min at 25 °C. The normalized laccase activity was obtained according to Eq. (II.1):

$$\text{Normalized laccase activity} = \frac{\text{Sample } (\Delta Abs_{420nm})}{\text{Initial } (\Delta Abs_{420nm})} \tag{II.1}$$

where Sample (ΔAbs_{420nm}) and Initial (ΔAbs_{420nm}) were the values of ΔAbs_{420nm} for the sample after a certain of reaction time and the sample taken at reaction time zero, respectively.

The effect of NaCl concentrations varying from 0 to 170 mM on the laccase activity was also investigated. After adding the designated amount of NaCl to the laccase solution (0.8 µM, 0.5 L), the normalized laccase activity relative to the activity without NaCl addition was evaluated.

II.2.4 Enzyme reaction between TCP and laccase

To choose suitable reaction conditions for the following E-FO process study, the enzyme reaction between laccase and TCP model micropollutant was analyzed with Michaelis–Menten equation. The enzyme reaction is given by

$$E + S \underset{k_{-1}}{\overset{k_1}{\rightleftharpoons}} ES \overset{k_{cat}}{\rightarrow} E + P$$
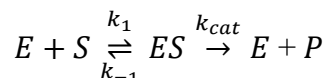
where E, S, ES, and P indicate enzyme, substrate, complex and product, respectively. k_1, k_{-1}, and k_{cat} are the reaction rate constants in the reaction. According to this mechanism, the reaction rate, v, is given by the Michaelis–Menten equation, Eq. (II.2).

$$v = \frac{k_{cat}[E]\,[S]}{K_m + [S]} = \frac{V_{max}\,[S]}{K_m + [S]} \tag{II.2}$$

Here, K_m is the Michaelis–Menten constant. $[E]$ and $[S]$ indicate the molar concentration of enzyme and substrate, respectively.

K_m and k_{cat} were determined by plotting the reaction rate as a function of TCP concentration while keeping the enzyme concentration at 0.8 µM. At first, a designated amount of laccase was added into a 0.5 L feed solution (pH 5.5) containing 0.005-1.015 mM TCP in a conical flask, to initiate the reaction process. After certain reaction time, 0.5 mL sample was taken from the conical flask, and mixed with 0.5 mL of acetonitrile for laccase inactivation. Then, the mixture was filtrated by a nylon membrane with 0.22 µm pore size to remove impurities for HPLC analysis. Thirty microlites of filtered mixture was injected into a Shim-pack GIST C18 column (4×250 mm). The isocratic elution was performed by pumping the mixture of acetonitrile and water (50/50 v/v) at a flow rate of 0.6 mL min^{-1} at 40 °C. A UV detector (SPD-20A) was used to measure TCP concentration at 295 nm. The initial degradation rate was obtained from the gradient of smoothed time course curve of TCP at time zero. Subsequently, the effect of enzyme concentrations on the reaction rate was experimentally evaluated under a fixed TCP concentration of 0.051 mM and different laccase concentrations from 0.4 to 1.6 µM.

II.2.5 Membrane filtration
II.2.5.1 Membrane filtration without enzyme catalysis

Membrane filtrations in the FO and RO modes without enzyme addition were conducted to evaluate the intrinsic separation performances of the commercial and the lab-made dense membranes in terms of pure water flux, rejection of NaCl (only for the RO mode), and rejection of the micropollutants (TCP and BPA). In addition, the reverse NaCl flux was measured for the FO mode, and 0.6 M NaCl was employed as DS. The experimental set-ups were schematically shown in Fig. II.3. For all filtration tests, the system was firstly equilibrated by pure water filtration for 2 h. Then, FS contained 0.051 mM TCP, 0.044 mM BPA, or 34.2 mM NaCl, were charged to the test system according to the targets.
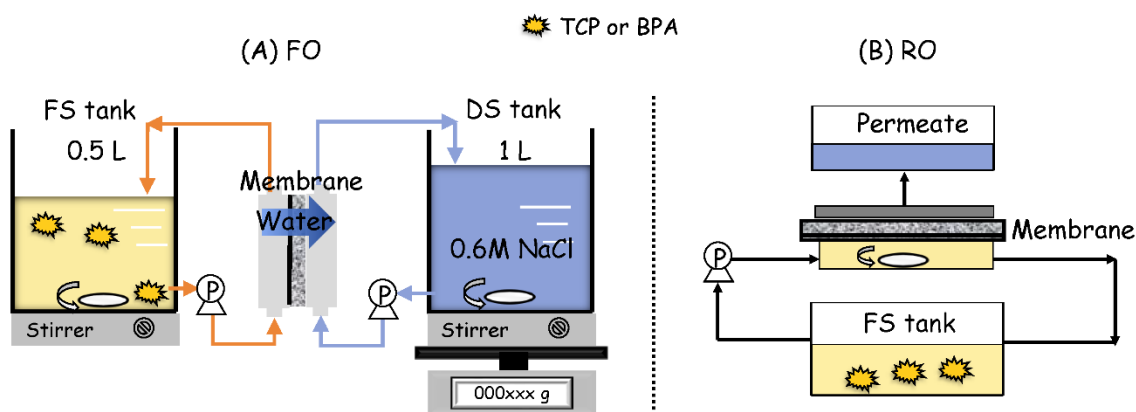
Fig. II.3 Schematic diagrams of the forward osmosis (FO) and reverse osmosis (RO) testing systems. In FO process, water flux and reverse salt flux was measured using water as FS. 0.051 mM (10 ppm) TCP, 0.044 mM (10 ppm) BPA, or 34.2 mM (2000 ppm) NaCl was used as FS for the rejection determination of the corresponding components, respectively.

Specifically, for the FO mode, a laboratory scale FO device consisted of a 0.5 L FS tank, an acrylic glass membrane cell with an effective membrane area of 17.7 cm^2, and a 1 L DS tank placed onto an electronic balance. The flow rate for both FS and DS was controlled at 0.3 L min^{-1} by two circulation pumps, and the temperature was kept at $20 \pm 2°C$ by a cooling system. Active layer faced feed solution (AL-FS) mode was used in this study owing to its low fouling propensity [35].

For the RO mode, a cross-flow filtration unit with an effective membrane area of 8.04 cm^2 was operated under an applied pressure of 10 bar as described in our previous study [36]. The FS was introduced to the cell at 9.9 mL min^{-1} by a plunger pump (NPL-120, Nihon Seimitsu Kagaku, Tokyo, Japan). The FS within the cell was magnetically stirred at 500 rpm to reduce concentration polarization on the membrane surface.

Water fluxes (Lm^{-2}h^{-1}, LMH) in RO and FO modes were obtained by Eq. (II.3),

$$\text{Water flux} = \frac{M}{a \times t} \text{ (LMH)} \tag{II.3}$$

where M (L) is the volume of accumulated permeate, a (m^2) the membrane area, t (h) the filtration time. M was estimated from the weight of accumulated permeate (in permeate side for RO and DS side for FO) by assuming that the density of permeate was unity.

Solute rejections in the RO mode were obtained by comparing the solute concentrations of feed and permeate in steady state after 12 h of filtration. For the FO mode, the solute concentrations of FS and DS were compared at a water recovery of 50%. Solute rejection (R) was calculated by Eq. (II.4),

$$R = \left(1 - \frac{C_{p-a-b}}{C_{f-a-b}}\right) \times 100 \text{ (\%)} \tag{II.4}$$

where C_{p-a-b} and C_{f-a-b} is the solute concentrations in permeate and in feed, respectively. The symbol *p* denotes the permeate, *f* the feed, *a* the filtration mode (RO or FO), and *b* the test solute (NaCl, TCP or BPA). For example, $C_{p-RO-NaCl}$ indicates the NaCl concentration of permeate in the RO mode. The concentration of NaCl was measured by a conductivity meter (B-771, Horiba, Kyoto, Japan). The concentration of TCP and BPA was measured by HPLC analysis with no acetonitrile addition at a UV wavelength of 295 and 280 nm, respectively.

For the FO mode, the solute concentrations in permeate, C_{p-FO-b}, was obtained with Eq. (II.5),

$$C_{p-FO-b} = \left(\frac{C_{d-FO-b}V_d}{V_p}\right) \tag{II.5}$$

where $C_{d\text{-}FO\text{-}b}$ and V_d are the solute concentrations (mol L^{-1}) in DS and the volume (L) of DS at the end of filtration, respectively. V_p is the reduced volume (L) of FS by permeation into DS. For example, at 50% water recovery, the value of V_p was 0.25 L.

Since the diluted permeate in FO process may lead to a concentration below the detection limit, and the high NaCl concentration in sample can cause damage to HPLC column, solid phase extraction was used for extract micropollutants leaching into DS for following HPLC analysis to determine the corresponding $C_{d\text{-}FO\text{-}b}$. The procedures of the solid phase extraction process were described as follows. Firstly, 5 mL of MeOH and 5 mL of Milli-Q water were added in sequence to the HLB cartridge for pre-conditioning. Secondly, 250 mL of H$_2$SO$_4$ acidified solution sample of DS (pH 1.5-2) was loaded onto the cartridge at a flow rate of 5-10 mL min^{-1} with the aid of a vacuum pump. Thirdly, nitrogen gas was purged to dry the cartridge for 60 min. Finally, 5 mL of MeOH was used for micropollutant elution.

$C_{f\text{-}FO\text{-}b}$ is the averaged concentration of test solute b in feed to offset the concentration effect of FS and was defined by Eq. (II.6).

$$C_{f-FO-b} = \frac{C_{0b}+C_{1b}}{2} \text{ (mol L}^{-1}) \tag{II.6}$$

where C_{0b} and C_{1b} are the concentrations at the beginning and the end of FO experiments, respectively. The reverse NaCl flux (mM m^{-2}h^{-1}) in the FO mode was obtained by recording the volume reduction and salt concentration of FS.

II.2.5.2 Enzyme aided membrane filtration (E-FO)

The membrane showing superior FO performances was further characterized in E-FO filtrations. The experimental setup of E-FO was the same as used in the FO process, illustrated in Section II.2.5.1. In E-FO, the model enzyme, laccase, was added to the FS. The initial composition of the FS was denoted as xTyE, where x and y indicate the TCP and enzyme concentrations (ppm), respectively. For example, 10T50E represents 10 ppm TCP and 50 ppm enzyme in the FS. For the FO mode without enzyme addition, the FS composition was denoted as xT.

The TCP degradation efficiencies in E-FO, FO, and BR modes were compared. To exclude the effect of TCP adsorption within the operation system, in this section, BR was

also operated in the same FO setup but with a water-impermeable polypropylene film mounted inside the membrane cell instead of a permeable FO membrane. Then, the water filtration did not take place and all feed solution remained in the feed tank.

The amounts of the micropollutant in the feed and permeate as well as that adsorbed on the membranes in E-FO and in FO filtrations were compared. The micropollutant adsorption amounts on the membranes after filtrations were experimentally determined using the following extraction procedure. First, the membrane removed from the test cell was gently washed with Milli-Q water several times. The excess water on the membrane surface was allowed to drain off. Two small pieces of membrane disks with 20 mm and 25 mm in diameters, giving a total membrane area of 8.04 cm^2 were cut and then submerged in 2 mL methanol in a sealed flask. Then the flask was placed on a shaker at a speed of 120 rpm at 20°C for 12 h. 1 mL of solution sample was taken out and was subjected to HPLC analysis after the extraction process. To ensure data reproducibility, three tests were carried out for each operation condition by using a new membrane sample each time.

II.2.6 Evaluation of antifouling properties

The water flux variations during E-FO filtrations were monitored at three different FS compositions, namely, 10T50E, 10T100E, 20T50E. To reflect the effect of DS dilution on water flux, a base line was obtained by using Milli-Q as FS. After that, the feed solution containing micropollutant and enzyme was operated, and the water flux variation was recorded. The difference between this water flux variation and the baseline was the decreased water flux attributed to fouling. The initial water flux subtracted this water flux difference to get the corrected water flux only attributed to fouling. In the meantime, E-RO filtrations were also conducted using the same FS of E-FO at an applied pressure of 10 bar, the water flux variations were recorded and compared with that of E-FO.

II.3 Results and discussion

II.3.1 Selection of a suitable FO membrane

A desired FO membrane should possess a porous and hydrophilic substrate layer with low mass transfer resistance, which is usually characterized by a low structural parameter (S-value) [31], as well as a dense skin layer possessing high rejections of both draw solutes (e.g. NaCl) and micropollutants. Previous studies have reported that TFC membranes produced by IP usually exhibit higher rejection of micropollutants than cellulose acetate based membranes [37, 38] due to its dense skin layer. However, conventional TFC membranes based on hydrophobic supports (e.g. PSf) characterizing high S-values usually display low FO fluxes [34]. To date, development of an ideal support for FO membranes fabrication is still in the early stages [39]. Our previous study has verified that a hydrophilic and highly porous PK membrane can be used to obtain low S-value TFC FO membranes [31]. Therefore, in this study, a PK-IP polyamide TFC membrane was fabricated and compared with a lab-made PSf-IP membrane and commercial CTA-ES (Fisher) and ES20 (Nitto) membranes in water permeability and micropollutant rejection. Fig. II.4 shows a typical FO filtration test in AL-FO mode using 0.051 mM (10 ppm) TCP as FS, and 0.6 M NaCl as DS. The similar TCP rejections obtained by ES20, PSf-IP, PSf-IP-contrast and PK-IP membranes were attributed to their similar polyamide skin layers. In contrast, CTA-ES membrane rejected TCP by only 16 %, possibly due to its large pore size and high affinity to non-polar micropollutants, such as TCP [40]. In addition, the TCP rejections were compared under similar fluxes (6 ~ 8 LMH) for all the membranes and the result was shown in Fig. II.5. The same membrane tended to provide a little bit higher rejection at a higher flux and vice versa. Still, all the TFC membranes exhibited similar rejections. On the other hand, PSf-IP showed higher flux than that of PSf-IP-contrast indicating the optimized fabrication condition of PSf-IP. Even similar TCP rejection was obtained using the commercial TFC membrane (ES20), the water flux was extremely lower than PK-IP. High water flux is also a very important point in FO process. So, it is not recommended to use commercial TFC membranes in FO and E-FO processes even if it is convenient. Therefore, the superior PK-IP membrane was selected as the desirable FO membrane in this work.

Table II.2 further compares the performances of PK-IP in the RO and FO filtrations. Higher rejections of both TCP and BPA were achieved in the FO mode. This benefit is

attributed to the reverse NaCl flux (80.0 ± 10.0 mM m^{-2}h^{-1}) from DS to FS, which hindered the permeation of micropollutants from FS to DS through adsorption and pore diffusion. Similar results were reported in the previous study [9]. The relatively lower rejection of TCP than that of BPA can be explained by the smaller molecular weight of TCP (see Table II.1), according to the dominant size exclusion-based separation mechanism for neutral solutes [41]. Since the removal of TCP is more challenging, the following work focused on TCP removal.
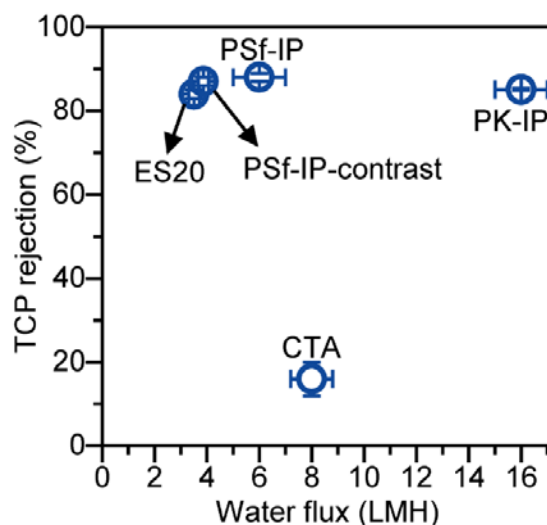
Fig. II.4 Water flux and TCP rejection (10 ppm) of PK-IP and other membranes in the FO mode (AL-FS). 0.051 mM (10 ppm) TCP was used as FS and 0.6 M NaCl was employed as DS. Water flux was the initial water flux, and the TCP rejection was measured at 50% water recovery.
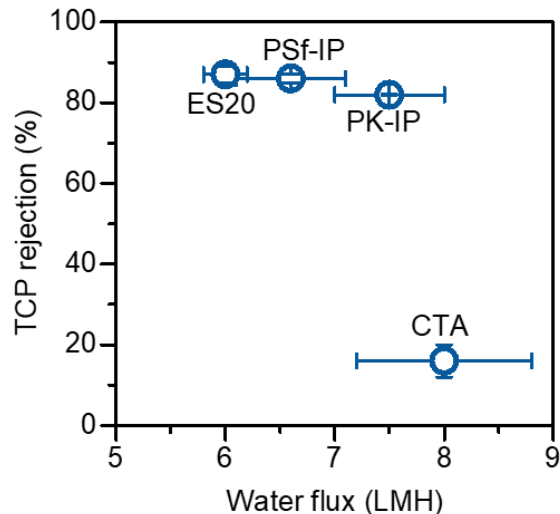
Fig. II.5 The TCP rejections of membranes under similar water flux. 2.4 M NaCl was used as the draw solution for ES20 and PSf-IP. 0.3 M NaCl was used for PK-IP membrane. 0.6 M NaCl was used as the draw solution for CTA membrane.

Table II.2 Comparison of PK-IP membrane performances in RO and FO modes

	RO mode	FO mode[1]
Water permeability	2.40 ± 0.20 LMH bar^{-1}	16.0 ± 1.0 LMH
NaCl rejection[2]	$94.1 \pm 2.6\%$	——
NaCl reverse flux	——	80.0 ± 10.0 mM m^{-2}h^{-1}
TCP rejection[3]	$77.8 \pm 3.9\%$	$85.1 \pm 0.2\%$
BPA rejection[4]	$97.3 \pm 1.6\%$	$99.5 \pm 0.1\%$

[1] Determined in AL-FS mode. Using 0.6 M NaCl as a draw solution. Measured at the beginning of the filtration.

[2] Measured in the RO mode with 34.2 mM (2000 ppm) NaCl at 20°C and 10 bar.

[3] Measured with 0.051 mM (10 ppm) TCP at 20°C at 50% water recovery.

[4] Measured with 0.044 mM (10 ppm) BPA at 20°C at 50% water recovery.

II.3.2 Stability and viability of enzyme in membrane filtration

Enzymatic degradation of micropollutants usually takes several hours [42], and its reaction efficiency is essentially influenced by the chosen experimental conditions. To assure a high efficiency of E-FO system, a suitable water flux should match the enzyme degradation rate. If water flux through the membrane is too high, the time for enzyme catalysis may be too short and a certain amount of micropollutants may pass through a membrane before they are degraded by enzymes. On the contrary, if water flux is too low or negligible, the operation regime is roughly equivalent to BR without water outflow, and extra time and energy are needed to recover clean water from the BR treated effluent. In addition, a qualified E-FO process is expected to concentrate enzymes in FS with increasing water recovery. Since enzyme catalytic rate usually increases with substrate and enzyme concentrations to a certain extent, the enzyme catalytic reaction is expected to be accelerated by this concentration effect as compared to the conventional BR process. To test the viability and advantages of E-FO process, comparative studies were conducted to obtain the preliminary information including FO operation time, enzyme stability, and enzyme condensation in the E-FO process, using laccase as the model enzyme, and ABTS as the model substrate.

Fig. II.6(A) shows that water recovery in the E-FO process increased linearly with process time. After around 10 h, E-FO recovered 50% water from FS. This water recovery rate is acceptable for practical FO operation. Meanwhile, increasing laccase activity in E-FO was confirmed from Fig. II.6(B), indicating that laccase in FS was successfully retained and concentrated by the dense skin layer of PK-IP membrane. In contrast, during the 10 h BR test without solution volume change, laccase activity barely changed.

Another issue of concerned is the inevitable reverse passage of draw solutes (NaCl in this study) from DS to FS. Salt may inhibit microbial or enzyme catalysis and therefore, influence the sustainability of the E-FO process [43]. Laccase activity at different NaCl concentrations was measured in batches as illustrated in Fig. II.6(C). There was no salt inhibition effect observed for the NaCl concentrations below 35 mM. For the PK-IP based FO process with 0.6 M NaCl as DS, the NaCl concentrations in FS were 2.8 mM and 17 mM at 50% and 90%

water recovery, respectively. It can be concluded that the NaCl reverse salt flux has no detrimental effect on the enzyme catalytic reaction incorporated in the E-FO process.
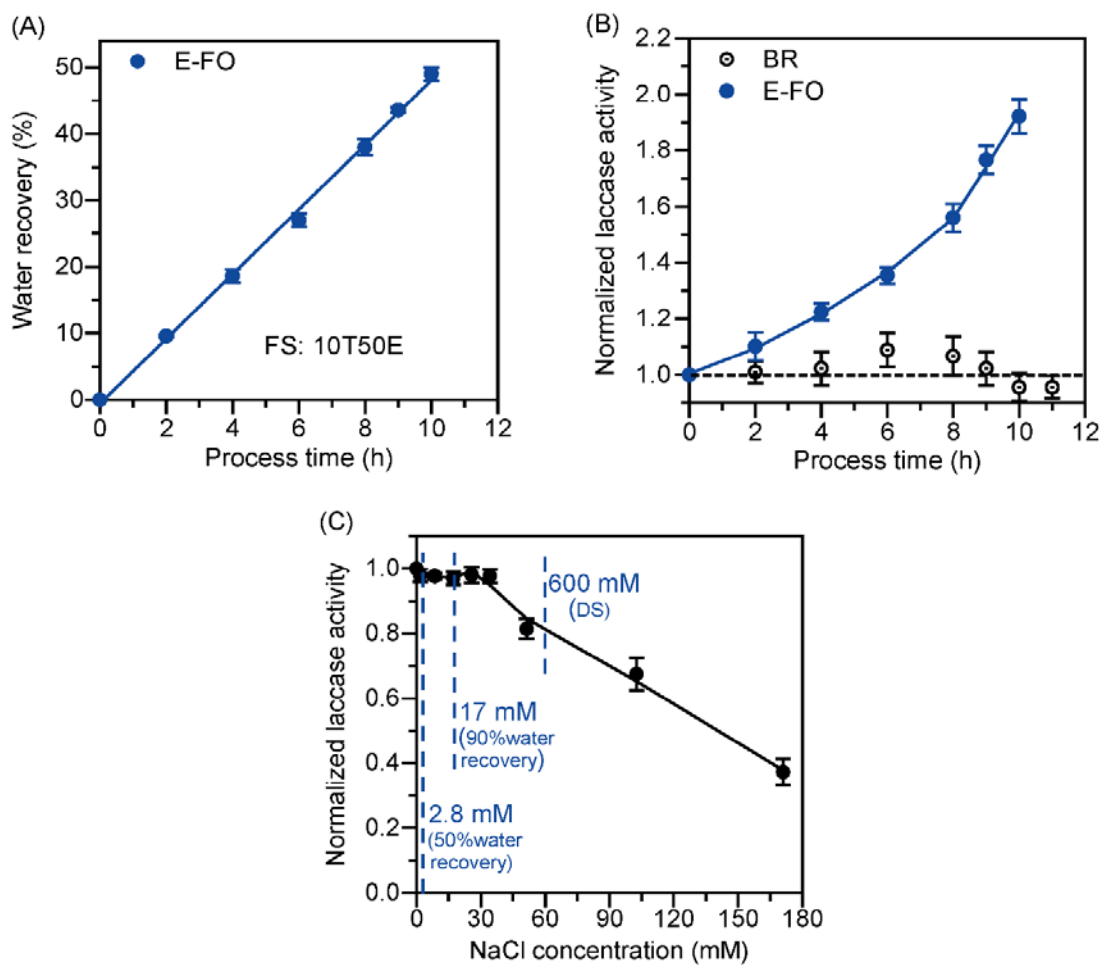
Fig. II.6 (A) Relationship between water recovery and process time for FS containing 0.051 mM (10 ppm) TCP and 0.8 µM (50 ppm) laccase (10T50E), and 0.6 M NaCl as DS for E-FO modes. (B) Normalized laccase activity towards ABTS during 10T50E treatment in single enzyme catalysis in bioreactor (BR) and E-FO processes. (C) Normalized laccase activity of laccase solution (0.8 µM) with different NaCl concentration towards ABTS.

II.3.3 Enzyme (laccase) reaction with TCP

II.3.3.1 Degradation of micropollutants in BR

The BR process using laccase to degrade TCP was studied to understand the catalytic characteristics, using a model solution containing 0.051 mM (10 ppm) TCP and 0.8 µM (50 ppm) enzyme, i.e. 10T50E. In HPLC spectra shown in Fig. II.7(A), the peak at a retention time of 9 min decreased continuously with the reaction, while the peak at 3 min sharply increased, indicating the metabolism of TCP. The peaks at around 9 min and 3 min are attributed to TCP and oxidation products, respectively [44]. The main oxidation product of TCP by laccase catalysis is dichloro-1,4-benzoquinone, and another possible product is 2,6-dichloro-3-hydroxy-1,4-benzoquinone [44-46]. Both products are considered to be less harmful than original TCP. Fig. II.8(A) shows the time course of TCP degradation in BR process. The fitted curve is quite smooth, indicating the continuous degradation of TCP with increasing reaction time. The initial degradation rate can be reflected by the slope of the fitted curve at time zero. Then, the effect of initial substrate (TCP) concentration in solution on initial TCP degradation rate was evaluated at 0.8 µM laccase, as shown in Fig. II.8(B). This result was analyzed with the Michaelis-Menten equation, Eq. (II.2). K_m and V_{max} were determined to be 0.82 mM and 0.155 mM h^{-1}, respectively, and then k_{cat} was determined as 194 h^{-1}, given $V_{max} = k_{cat} [E]$ and $[E] = 0.8$ µM in Fig. II.8(B). The theoretical curve (shown as solid line) calculated with Eq. (II.2) implies that the enzyme reaction can be explained well by the Michaelis-Menten kinetics. Fig. II.8(C) shows the degradation rate as a function of enzyme concentration. Similarly, the enzyme reaction can be described well by the theoretical curve generated by applying Eq. (II.2) with $k_{cat} = 194$ h^{-1} and $K_m = 0.82$ mM (listed in Table II.3).
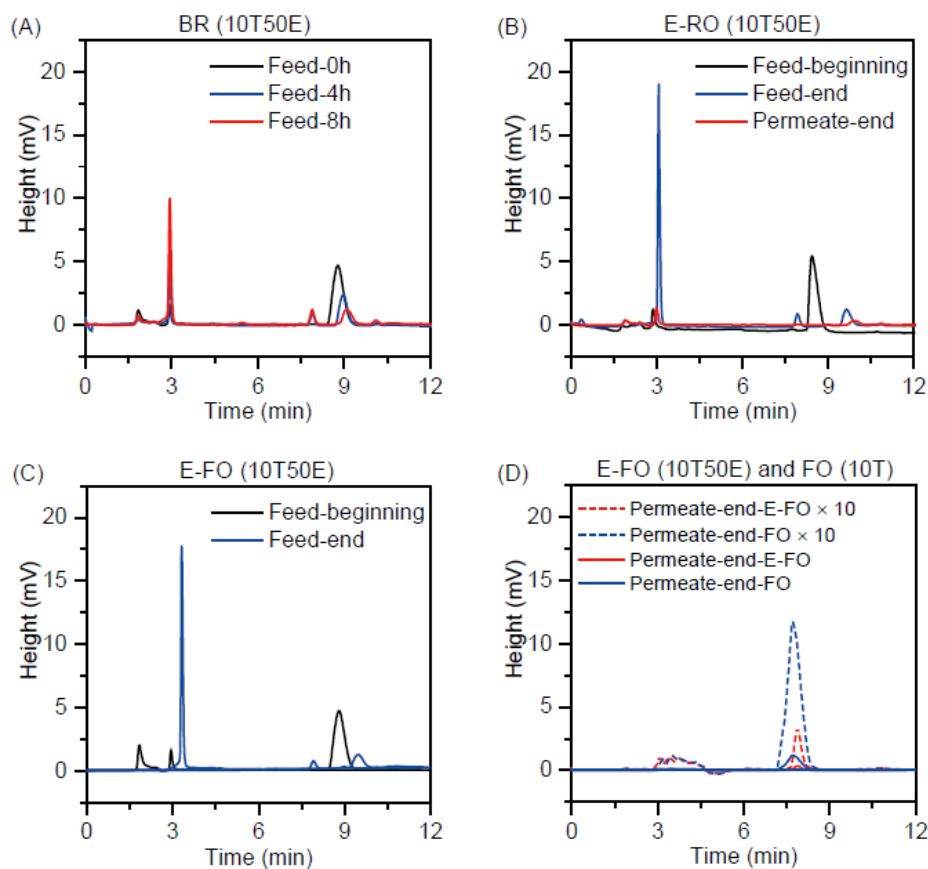
Fig. II.7 (A) The HPLC spectra of feed solutions during different catalytic time using 10 ppm TCP and 50 ppm laccase (10T50E) as a model in bioreactor (BR) mode. (B) The HPLC spectra of feed solutions of E-RO at the beginning (Feed-beginning) and at the end of the filtration (Feed-end), as well as the permeate at the end of the filtration (Permeate-end) at 50% water recovery. (C) The HPLC spectra of feed solutions of E-FO at the beginning (Feed-beginning) and at the end of the filtration (Feed-end) at 50% water recovery. (D) The measured HPLC spectra of permeate solutions of E-FO (permeate-end-E-FO × 10) and FO (permeate-end-FO × 10) at the 50% water recovery. The procedure for sample treatment was as follows. 250 mL solution was taken out from the draw solution (total volume: 1250 mL) at the end of the filtration, and was concentrated via solid phase extraction (SPE) process. 5 mL methanol was used to wash out the micropollutant, and used as the sample of the above spectra. Therefore, the obtained spectra were 10 times concentrated ones. The measured spectra were divided by 10 and showed as the solid lines.
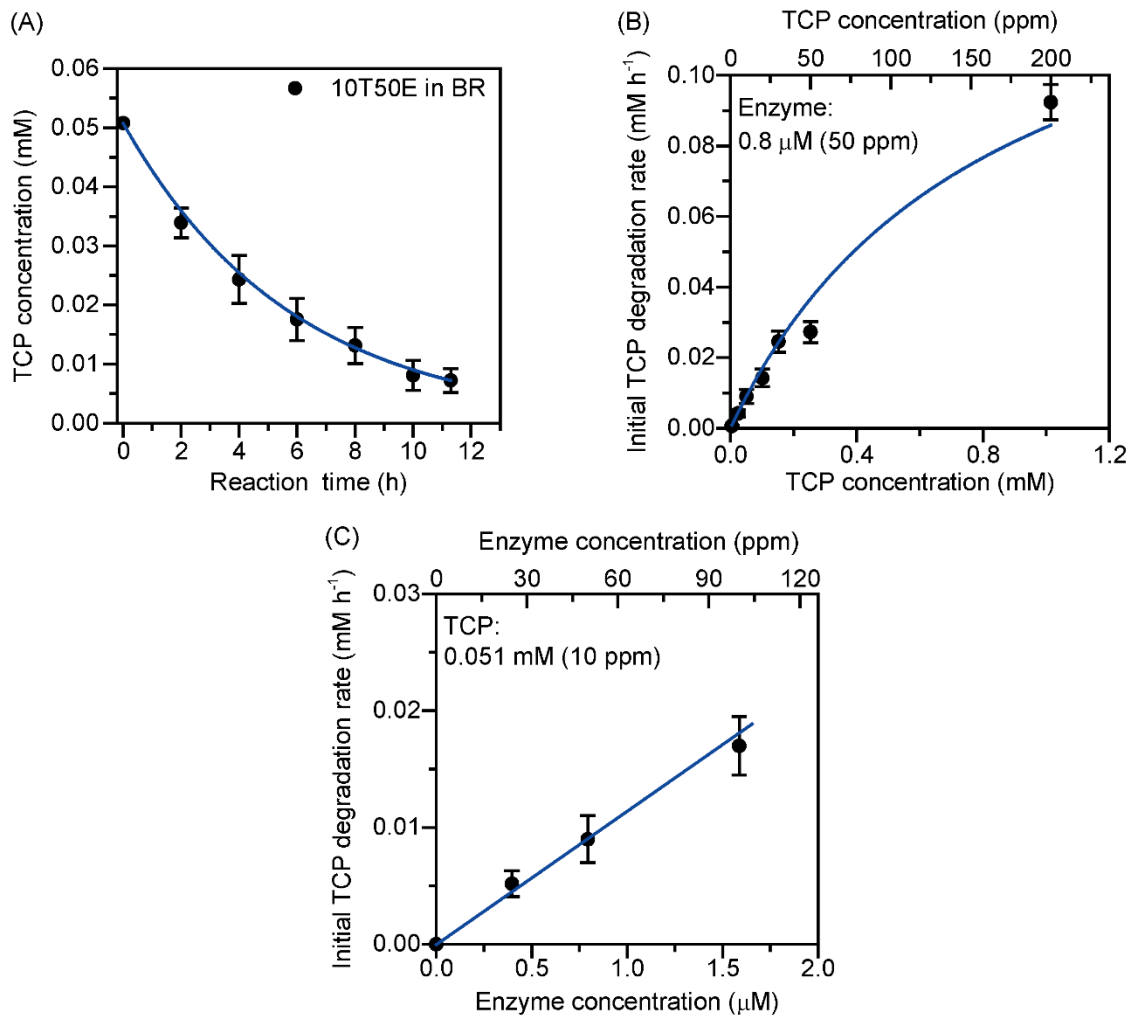
Fig. II.8. (A) Degradation course of 0.051 mM (10 ppm) TCP via and 0.8 µM (50 ppm) laccase. The symbols are the measured data, and the solid line is the smoothed curve. (B) Effect of TCP concentration on the initial degradation rate of TCP. The laccase concentration was fixed at 0.8 µM. (C) Effect of laccase concentration on the initial degradation rate of TCP. The TCP concentration was fixed at 0.051 mM. Both the solid lines in (B) and (C) show the theoretical line calculated with the Michaelis-Menten equation putting k_{cat} and K_m as 194 h^{-1} and 0.82 mM, respectively.

Table II.3 Parameters for laccase reaction with TCP

K_m (mM)	k_{cat} (h^{-1})
0.82	194

II.3.3.2 Micropollutants degradation in E-FO

The 10T50E solution and 0.6 M NaCl were used as FS and DS of the E-FO process, respectively, where an initial FO flux of 16 LMH was observed. Fig. II.9 summarizes the time course of normalized TCP amounts present in FS of E-FO, BR, and FO (with TCP but no enzyme addition). A baseline accounting for the TCP adsorption within the FS side of the FO device was obtained by circulating the FS containing only TCP through the pump, tubing, and half membrane cell equipped with a dense polypropylene film. The amount of TCP in the baseline run only slightly deceased as a function of operation time, and only 0.4 mg was adsorbed around 10 h process time. In the case of a typical FO test, the decrease of TCP amount in FS was slightly larger than the baseline run, which can be attributed to the incomplete TCP rejection by the PK-IP membrane and/or the TCP adsorption onto the membrane. FO line (red line) shows 80% TCP was retained in FS side at 10 h process time. Considering the adsorption amount on the device (0.4 mg), the TCP rejection was around 85%, which was consistent with the value in Table II.2. As for the BR process with enzyme involvement, the TCP amount declined as expected by enzymatic degradation. Furthermore, a faster degradation rate was obtained in E-FO than in BR due to the enhanced enzyme activity by membrane concentration as discussed above. After about 10 h of E-FO filtration, 50% water recovery was reached, and 95% of feed TCP in FS was degraded.

The effects of initial laccase and TCP concentrations, as well as operation fluxes on TCP removal efficiency were further evaluated, as shown in Fig. II.10. Under all investigated conditions, faster TCP degradation rates were observed in E-FO than in BR. At a higher E-FO flux of 23 LMH, 50% water recovery was achieved after 7 h operation, however, only 80% of TCP was degraded, indicating the inadequate time for enzyme catalysis. This

emphasizes that the designed water flux should match with the catalysis rate in order to achieve high clearance of micropollutants in one-step E-FO process.
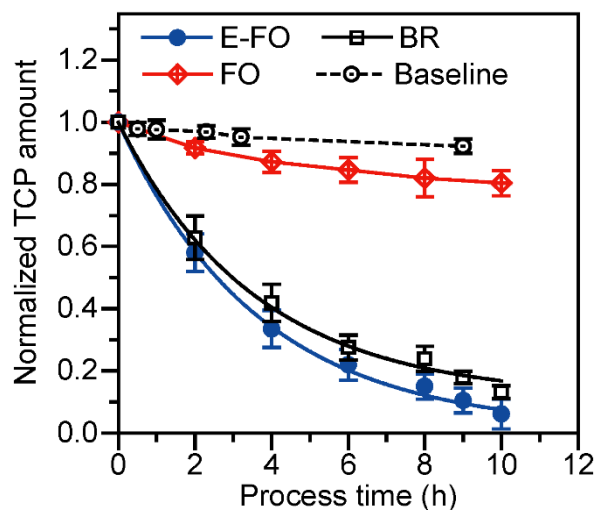
Fig. II.9 Course of normalized TCP amounts in FS of E-FO, BR, and FO process. The FS of E-FO and BR was the mixture of 0.051 mM (10 ppm) TCP and 0.8 µM (50 ppm) enzyme (10T50E), while for FO, the FS was 0.051 mM (10 ppm) TCP (10T). Blue filled circles, black open squares, red crossing diamonds, and black open circles with center dots represent E-FO, BR, FO, and baseline, respectively.
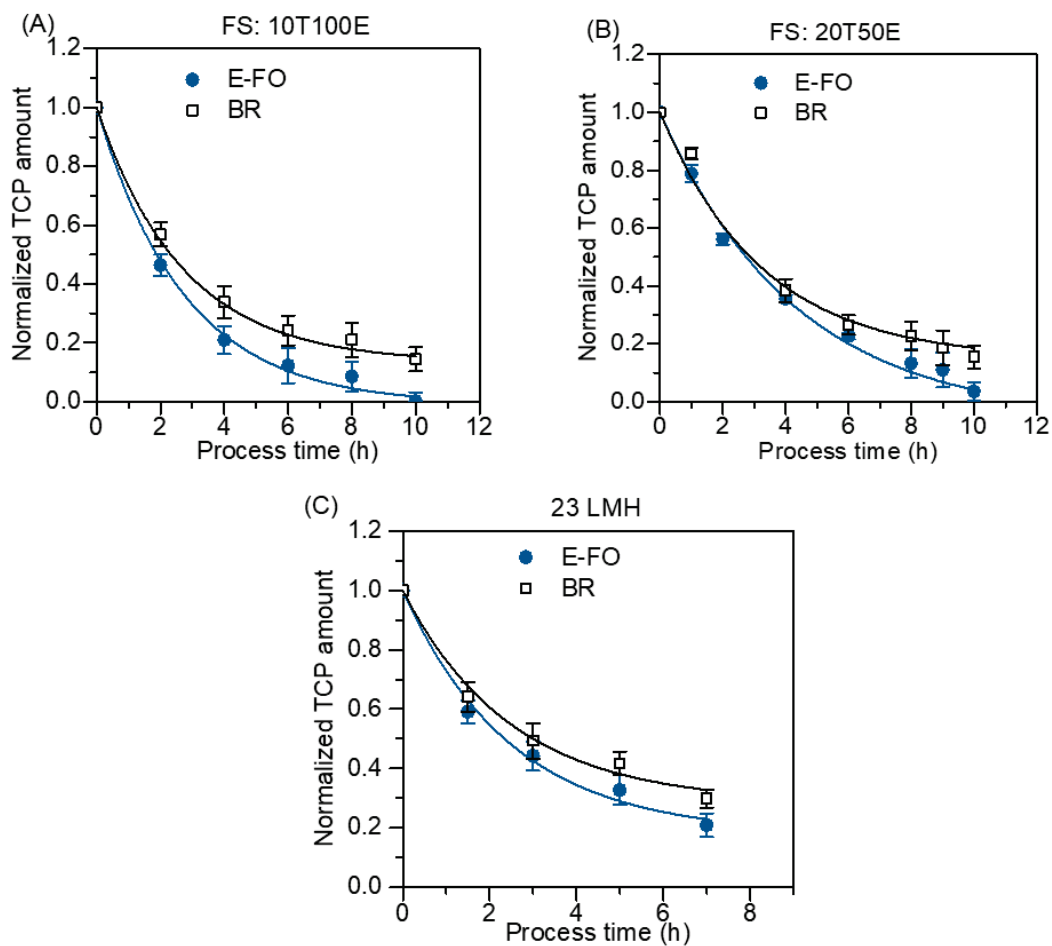
Fig. II.10 The time course of TCP amount in FS of E-FO and BR process in different FS conditions: (A) 10T100E, (B) 20T50E, (C) 10T50E at a FO flux of 23 LMH.

II.3.3.3 Micropollutants in permeate and on membrane

The coupling of enzymatic catalysis and FO separation enables the efficient elimination of micropollutants in FS, which will directly affect the concentration of micropollutants in the permeate and also their adsorption on membrane. Systematic investigations on this issue were carried out under different operation conditions. Fig. II.11(A) shows the TCP amount detected in the permeate and adsorbed on the membrane after the FO and E-FO filtrations with certain time. The TCP amount in the permeate was obtained with Eq. (II.5). In the FO

test, the TCP permeation gradually increased from 5.48 to 10.0 µM with increasing process time from 4.3 to 10 and 16.7 h (corresponding to increasing water recovery from 20 to 50 and 90%). This is because the concentrated TCP molecules in FS would lead to higher adsorption and partition in membrane pores and thus higher permeation through membrane. The membrane adsorption amount increased from 0.015 to 0.02 µmol cm^{-2} with increasing process time from 4.3 to 10 h, and then kept at around 0.021 µmol cm^{-2} at 16.7 h. Thanks to the efficient enzyme catalyzed TCP elimination, the TCP permeation in E-FO process decreased from 2.35 to 1.05 and 0.9 µM, while the amount of membrane adsorbed TCP reduced from 0.0045 to 0.0019 and 0.0013 µmol cm^{-2} at the end of filtration (90% water recovery). Compared to the FO test, the E-FO test shows 11.0 times lower TCP permeation and 16.6 times lower adsorption after 16.7 h operation. Fig. II.11(B) shows the effect of varying initial TCP concentrations in FS from 5.08 to 102 µM on the TCP permeation and membrane adsorption. In FO, the absolute TCP amount in permeate increased as expected, although the calculated membrane rejection increased from 84.9 to 92.2%, similar to the previous report [47]. The membrane adsorption also sharply increased to 0.02 µmol cm^{-2} at 50.7 µM TCP. By contrast, the E-FO tests with 5.08 and 102 µM TCP showed 2.6 and 6.9 times lower TCP permeation, along with 5.3 and 18.3 times lower TCP adsorption on membrane, respectively.

Fig. II.11(C) shows that on increasing laccase concentration in FS from 0 to 0.8 µM, the TCP permeation and membrane adsorption sharply reduced as expected, due to higher degradation rate (see Fig. II.8(C)). Further increasing laccase concentration to 1.59 µM only slightly improved the TCP elimination because that the relative scarcity of substrate (TCP) would limit the enzymatic reaction in this case. Too high enzyme addition is not cost-effective and brings undesired high fouling potential to membranes. On the other hand, to further confirm the measured amounts, the mass balance of TCP in feed, on the membrane and in the permeate was examined, using 10T as a feed solution, and the results shown in Table II.4 verified the reliability of the data.

Besides, considering the potential secondary pollution by the products, the permeate of E-RO and E-FO were analyzed using 10T50E as a model system. E-RO exhibited very low

product peak in permeate (Fig. II.7(B)), while E-FO showed undetectable product peak in permeate (Fig. II.7(D)), even though large amount of products existed in the feed solution (Fig. II.7(C)). This indicates that most oxidation products were rejected by the PK-IP membrane, especially in E-FO mode, avoiding the secondary pollution. The detailed analysis of HPLC spectra were displayed in the supporting information. The above results indicate that the proposed E-FO process is very efficient in retaining and eliminating micropollutants, which can effectively suppress contamination of product water and membrane fouling.
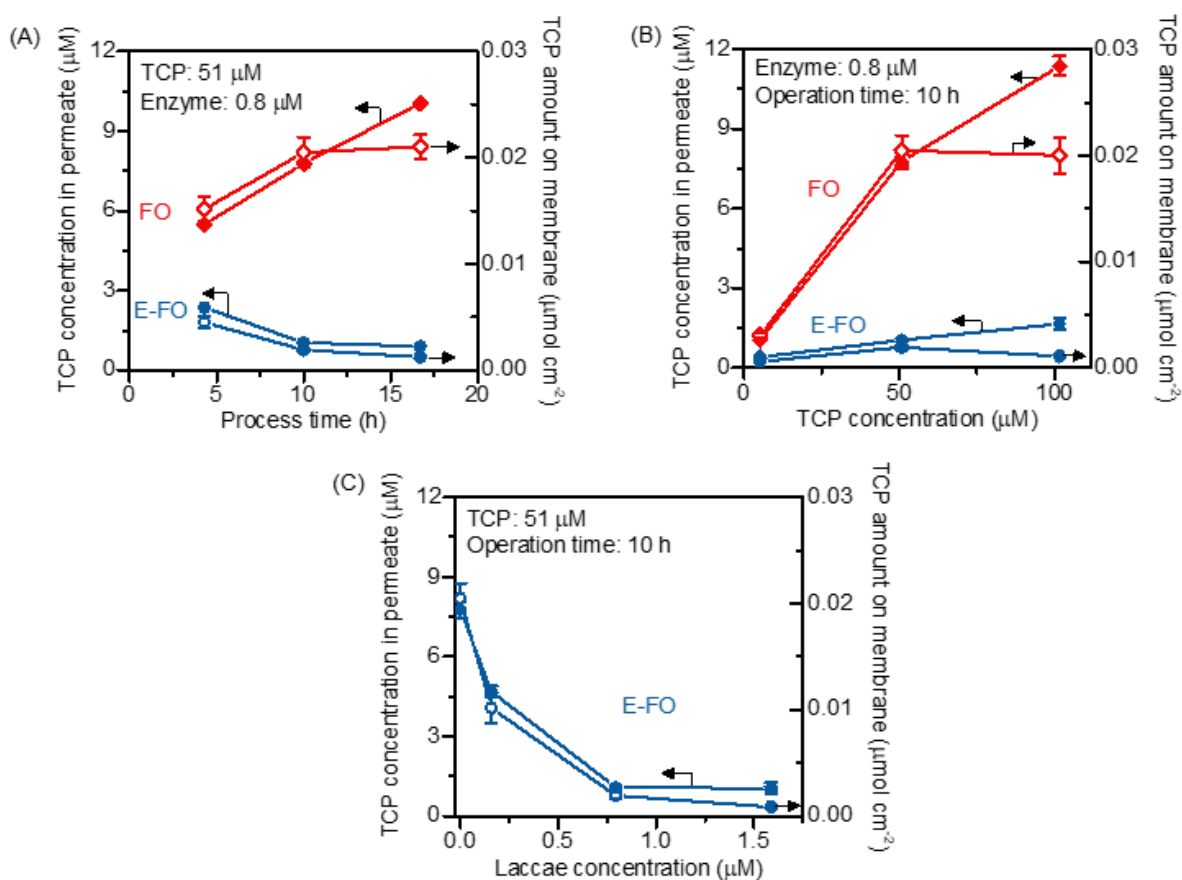
Fig. II.11 TCP concentration in permeate (µM) and TCP amount on membranes (µmol cm^{-2}) in FO and E-FO processes. (A) Effect of process time for 10T50E. (B) Effect of TCP concentration under 0.8 µM (50 ppm) laccase at 10 h process time. (C) Effect of laccase concentration under 51 µM (10 ppm) TCP at 10 h process time.

Table II.4 The mass balance of TCP amounts during FO process [1]

Mass distribution (mg)	FO[2]
Input TCP amount	**5**
Adsorption on tubes of FS side	0.4
FS	4.02
Membrane	0.072
DS	0.385
Catalysis by laccase	0
Sum of the above amounts **(Calculated total amount)**	**4.9**

[1] Only the average values are listed in the table.

[2] 10 ppm TCP was used as the feed solution and the system was operated for 10 h, achieving 50% water recovery.

II.3.4 Fouling trend

Membrane fouling caused by various pollutants present in real water is one of the major challenges in membrane technology, leading to increasing operation cost and reduction in membrane productivity and lifespan [48]. Therefore, it is essential to evaluate the antifouling characteristic of the proposed E-FO process with PK-IP membrane. Fig. II.12 shows the water flux variations as a function of operation time during filtrations of three different solutions. The decrease of water flux due to the dilution of DS was corrected. Almost no flux decrease occurred in the E-FO filtrations for all three cases. However, when the same feed solutions were subjected to the E-RO filtrations, the flux decline became apparent, particularly at higher TCP and laccase concentration, indicting the typical fouling phenomenon [49]. The flux declined by 45% at the worst case (10T100E) for E-RO, while

E-FO showed no decline. This result was consistent with another study in which the water permeability reduced by at least 30% in a similar E-RO process for 20 ppm BPA and 75 ppm enzyme [41]. High hydraulic pressure applied in E-RO would promote the adsorption and accumulation of laccase, micropollutants, or other oxidation products on the membrane, giving rise to severer membrane fouling. For example, at 10 ppm TCP concentration, the 10T100E feed solution (100 ppm enzyme) showed faster flux decline than that of 10T50E (50 ppm enzyme). This result indicates higher enzyme concentration leads to the high fouling tendency. In addition to fouling resistance, the different aspects of E-FO, FO, BR, and E-RO were also compared, as summarized in Table II.5. In our opinion, the E-FO exhibits the best comprehensive performance and is more resilient and sustainable for the long-term operation.
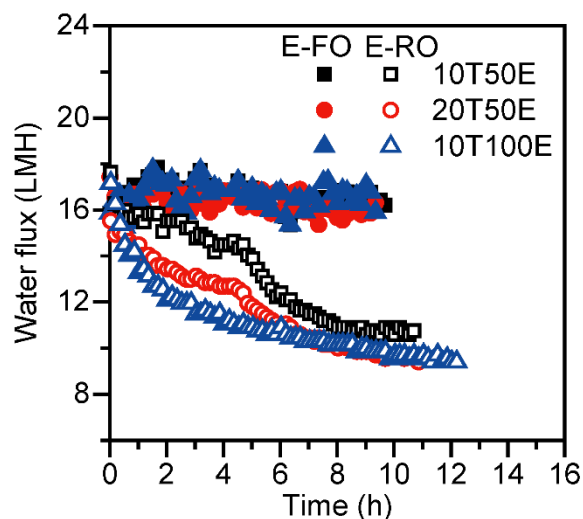
Fig. II.12 Time course of water flux in E-FO (closed symbols) and E-RO (open symbols). The concentrations of TCP and enzyme in FS were recorded in the figure.

Table II.5 Comparison of E-FO, FO, BR, and E-RO

	E-FO	FO	BR	E-RO
Quality of product water	high	low	——	high
TCP accumulation in FS and on membrane	low	high	low	low
Operation pressure	low	low	——	high
Membrane fouling tendency	low	low	——	high

II.4 Conclusions

The study has proved the applicability of the hybrid enzyme-aided FO (E-FO) process for enhanced micropollutants removal. PK-IP TFC membrane was firstly explored as the optimal FO membrane possessing high flux and high micropollutants rejection (taking TCP and BPA as examples). In the E-FO process, the enzyme in FS was concentrated with increasing operation time, leading to higher catalytic degradation ability than that of a single bioreactor (BR) operation. Owing to the enzymatic degradation in E-FO, the permeation of micropollutants and the membrane adsorption apparently reduced as compared to a typical FO process, leading to low risk of product water contamination and also low membrane fouling tendency. The E-FO process sustained nearly constant operation fluxes, whereas the control E-RO process showed obvious flux decline because of membrane fouling. This study shows that the proposed simple E-FO process can potentially be a powerful and sustainable platform for simultaneous rejection and elimination of micropollutants to produce high quality potable water.

Reference

[1] M.A. Montgomery, M. Elimelech, Water and sanitation in developing countries: Including health in the equation, Environ Sci Technol, 41 (2007) 17-24.

[2] A.I. Schafer, I. Akanyeti, A.J.C. Semiao, Micropollutant sorption to membrane polymers: A review of mechanisms for estrogens, Adv Colloid Interface Sci, 164 (2011) 100-117.

[3] U.I. Gaya, A.H. Abdullah, M.Z. Hussein, Z. Zainal, Photocatalytic removal of 2,4,6-trichlorophenol from water exploiting commercial ZnO powder, Desalination, 263 (2010) 176-182.

[4] T.A. Ternes, M. Meisenheimer, D. McDowell, F. Sacher, H.J. Brauch, B.H. Gulde, G. Preuss, U. Wilme, N.Z. Seibert, Removal of pharmaceuticals during drinking water treatment, Environ Sci Technol, 36 (2002) 3855-3863.

[5] P.A. Quinlivan, L. Li, D.R.U. Knappe, Effects of activated carbon characteristics on the simultaneous adsorption of aqueous organic micropollutants and natural organic matter, Water Res, 39 (2005) 1663-1673.

[6] J.L. Cartinella, T.Y. Cath, M.T. Flynn, G.C. Miller, K.W. Hunter, A.E. Childress, Removal of natural steroid hormones from wastewater using membrane contactor processes, Environ Sci Technol, 40 (2006) 7381-7386.

[7] S.F. Zhao, L. Zou, C.Y.Y. Tang, D. Mulcahy, Recent developments in forward osmosis: Opportunities and challenges, J Membr Sci, 396 (2012) 1-21.

[8] S. Lee, C. Boo, M. Elimelech, S. Hong, Comparison of fouling behavior in forward osmosis (FO) and reverse osmosis (RO), J Membr Sci, 365 (2010) 34-39.

[9] M. Xie, L.D. Nghiem, W.E. Price, M. Elimelech, Comparison of the removal of hydrophobic trace organic contaminants by forward osmosis and reverse osmosis, Water Res, 46 (2012) 2683-2692.

[10] L. Chekli, S. Phuntsho, J.E. Kim, J. Kim, J.Y. Choi, J.S. Choi, S. Kim, J.H. Kim, S. Hong, J. Sohn, H.K. Shon, A comprehensive review of hybrid forward osmosis systems: Performance, applications and future prospects, J Membr Sci, 497 (2016) 430-449.

[11] A.J.C. Semiao, M. Foucher, A. Schafer, Removal of adsorbing estrogenic micropollutants by nanofiltration membranes: Part B-Model development, J Membr Sci, 431 (2013) 257-266.

[12] A.J.C. Semiao, A.I. Schafer, Estrogenic micropollutant adsorption dynamics onto nanofiltration membranes, J Membr Sci, 381 (2011) 132-141.

[13] A.J.C. Semiao, A. Schafer, Removal of adsorbing estrogenic micropollutants by nanofiltration membranes. Part A-Experimental evidence, J Membr Sci, 431 (2013) 244-256.

[14] L.D. Nghiem, A.I. Schafer, Adsorption and transport of trace contaminant estrone in NF/RO membranes, Environ Eng Sci, 19 (2002) 441-451.

[15] P.X. Liu, H.M. Zhang, Y.J. Feng, C. Shen, F.L. Yang, Integrating electrochemical oxidation into forward osmosis process for removal of trace antibiotics in wastewater, J Hazard Mater, 296 (2015) 248-255.

[16] K.V. Plakas, V.C. Sarasidis, S.I. Patsios, D.A. Lambropoulou, A.J. Karabelas, Novel pilot scale continuous photocatalytic membrane reactor for removal of organic micropollutants from water, Chem Eng J, 304 (2016) 335-343.

[17] J. Benner, T.A. Ternes, Ozonation of Metoprolol: Elucidation of Oxidation Pathways and Major Oxidation Products, Environ Sci Technol, 43 (2009) 5472-5480.

[18] E.M. Fiss, K.L. Rule, P.J. Vikesland, Formation of chloroform and other chlorinated byproducts by chlorination of triclosan-containing antibacterial products, Environ Sci Technol, 41 (2007) 2387-2394.

[19] L.F. Stadlmair, T. Letzel, J.E. Drewes, J. Grassmann, Enzymes in removal of pharmaceuticals from wastewater: A critical review of challenges, applications and screening methods for their selection, Chemosphere, 205 (2018) 649-661.

[20] W.H. Luo, M. Xie, X.Y. Song, W.S. Guo, H.H. Ngo, J.L. Zhou, L.D. Nghiem, Biomimetic aquaporin membranes for osmotic membrane bioreactors: Membrane performance and contaminant removal, Bioresour Technol, 249 (2018) 62-68.

[21] X.H. Wang, J.F. Zhang, V.W.C. Chang, Q.H. She, C.Y.Y. Tang, Removal of cytostatic drugs from wastewater by an anaerobic osmotic membrane bioreactor, Chem Eng J, 339 (2018) 153-161.

[22] E.R. Cornelissen, D. Harmsen, K.F. de Korte, C.J. Ruiken, J.J. Qin, H. Oo, L.P. Wessels, Membrane fouling and process performance of forward osmosis membranes on activated sludge, J Membr Sci, 319 (2008) 158-168.

[23] A. Drews, Membrane fouling in membrane bioreactors-Characterisation, contradictions, cause and cures, J Membr Sci, 363 (2010) 1-28.

[24] L. Chen, Y.S. Gu, C.Q. Cao, J. Zhang, J.W. Ng, C.Y. Tang, Performance of a submerged anaerobic membrane bioreactor with forward osmosis membrane for low-strength wastewater treatment, Water Res, 50 (2014) 114-123.

[25] Q.G. Huang, W.J. Weber, Transformation and removal of bisphenol A from aqueous phase via peroxidase-mediated oxidative coupling reactions: Efficacy, products, and pathways, Environ Sci Technol, 39 (2005) 6029-6036.

[26] M. Yoshida, H. Ono, Y. Mori, Y. Chuda, K. Onishi, Oxidation of bisphenol A and related compounds, Biosci Biotech Bioch, 65 (2001) 1444-1446.

[27] S.M. Jones, E.I. Solomon, Electron transfer and reaction mechanism of laccases, Cell Mol Life Sci, 72 (2015) 869-883.

[28] B.H. Hameed, I.A.W. Tan, A.L. Ahmad, Adsorption isotherm, kinetic modeling and mechanism of 2,4,6-trichlorophenol on coconut husk-based activated carbon, Chem Eng J, 144 (2008) 235-244.

[29] B.S. Rubin, Bisphenol A: An endocrine disruptor with widespread exposure and multiple effects, J Steroid Biochem, 127 (2011) 27-34.

[30] M. Fernandez-Fernandez, M.A. Sanroman, D. Moldes, Recent developments and applications of immobilized laccase, Biotechnol Adv, 31 (2013) 1808-1825.

[31] M. Yasukawa, S. Mishima, M. Shibuya, D. Saeki, T. Takahashi, T. Miyoshi, H. Matsuyama, Preparation of a forward osmosis membrane using a highly porous polyketone microfiltration membrane as a novel support, J Membr Sci, 487 (2015) 51-59.

[32] L. Cheng, D.M. Wang, A.R. Shaikh, L.F. Fang, S. Jeon, D. Saeki, L. Zhang, C.J. Liu, H. Matsuyama, Dual Superlyophobic Aliphatic Polyketone Membranes for Highly Efficient Emulsified Oil-Water Separation: Performance and Mechanism, Acs Appl Mater Inter, 10 (2018) 30860-30870.

[33] L.F. Fang, L. Cheng, S. Jeon, S.Y. Wang, T. Takahashi, H. Matsuyama, Effect of the supporting layer structures on antifouling properties of forward osmosis membranes in AL-DS mode, J Membr Sci, 552 (2018) 265-273.

[34] Y. Zhang, K. Nakagawa, M. Shibuya, K. Sasaki, T. Takahashi, T. Shintani, T. Yoshioka, E. Kamio, A. Kondo, H. Matsuyama, Improved permselectivity of forward osmosis membranes for efficient concentration of pretreated rice straw and bioethanol production, J Membr Sci, 566 (2018) 15-24.

[35] W.C.L. Lay, Q.Y. Zhang, J.S. Zhang, D. McDougald, C.Y. Tang, R. Wang, Y. Liu, A.G. Fane, Study of integration of forward osmosis and biological process: Membrane performance under elevated salt environment, Desalination, 283 (2011) 123-130.

[36] D. Saeki, S. Nagao, I. Sawada, Y. Ohmukai, T. Maruyama, H. Matsuyama, Development of antibacterial polyamide reverse osmosis membrane modified with a covalently immobilized enzyme, J Membr Sci, 428 (2013) 403-409.

[37] S. Yuksel, N. Kabay, M. Yuksel, Removal of bisphenol A (BPA) from water by various nanofiltration (NF) and reverse osmosis (RO) membranes, J Hazard Mater, 263 (2013) 307-310.

[38] K. Kimura, S. Toshima, G. Amy, Y. Watanabe, Rejection of neutral endocrine disrupting compounds (EDCs) and pharmaceutical active compounds (PhACs) by RO membranes, J Membr Sci, 245 (2004) 71-78.

[39] Q. Saren, C.Q. Qiu, C.Y.Y. Tang, Synthesis and Characterization of Novel Forward Osmosis Membranes based on Layer-by-Layer Assembly, Environ Sci Technol, 45 (2011) 5201-5208.

[40] D. Bhanushali, S. Kloos, D. Bhattacharyya, Solute transport in solvent-resistant nanofiltration membranes for non-aqueous systems: experimental results and the role of solute-solvent coupling, J Membr Sci, 208 (2002) 343-359.

[41] I. Escalona, J. Grooth, J. Font, K. Nijmeijer, Removal of BPA by enzyme polymerization using NF membranes, J Membr Sci, 468 (2014) 192-201.

[42] J. Lin, Y.J. Liu, S. Chen, X.Y. Le, X.H. Zhou, Z.Y. Zhao, Y.Y. Ou, J.H. Yang, Reversible immobilization of laccase onto metal-ion-chelated magnetic microspheres for bisphenol A removal, Int J Biol Macromol, 84 (2016) 189-199.

[43] X.H. Wang, B. Yuan, Y. Chen, X.F. Li, Y.P. Ren, Integration of micro-filtration into osmotic membrane bioreactors to prevent salinity build-up, Bioresour Technol, 167 (2014) 116-123.

[44] R. Sarma, M.S. Islam, A.F. Miller, D. Bhattacharyya, Layer-by-Layer-Assembled Laccase Enzyme on Stimuli -Responsive Membranes for Chloro-Organics Degradation, Acs Appl Mater Inter, 9 (2017) 14858-14867.

[45] X.F. Hu, H.H. Ji, L. Wu, Singlet oxygen photogeneration and 2,4,6-TCP photodegradation at Pt/TiO_2 under visible light illumination, Rsc Adv, 2 (2012) 12378-12383.

[46] C.J. Liu, D. Saeki, L. Cheng, J.Q. Luo, H. Matsuyama, Polyketone-based membrane support improves the organic solvent resistance of laccase catalysis, J Colloid Interf Sci, 544 (2019) 230-240.

[47] K. Kimura, G. Amy, J.E. Drewes, T. Heberer, T.U. Kim, Y. Watanabe, Rejection of organic micropollutants (disinfection by-products, endocrine disrupting compounds, and pharmaceutically active compounds) by NF/RO membranes, J Membr Sci, 227 (2003) 113-121.

[48] G. Han, C.Z. Liang, T.S. Chung, M. Weber, C. Staudt, C. Maletzko, Combination of forward osmosis (FO) process with coagulation/flocculation (CF) for potential treatment of textile wastewater, Water Res, 91 (2016) 361-370.

[49] D.J. Miller, D.R. Dreyer, C.W. Bielawski, D.R. Paul, B.D. Freeman, Surface Modification of Water Purification Membranes, Angew Chem Int Edit, 56 (2017) 4662-4711.

Chapter III A novel strategy to immobilize enzymes on microporous membranes via dicarboxylic acid halides

III.1 Introduction

Enzymes are types of proteins that act as biological catalysts by recognizing target substrates. There are various different types of enzymes such as proteases, amylases, cellulases, and lipases that facilitate the decomposition or synthesis of organic matter in living organisms [1]. Compared to ordinary catalysts, the reaction rates and selectivity of enzymes with respect to their substrates are exceptionally high because of their low activation energy and specific conformations for substrate recognition [2, 3]. Hence, enzymes have attracted constant attention in many fields including pharmaceuticals, food, fine chemicals, and energy [4-6].

However, free enzymes as used in **Chapter II,** are limited by several drawbacks such as their low thermal stability, complicated reusability, easy self-cleavage, and self-aggregation [1, 7]. The immobilization of enzymes onto solid supports is a promising method to overcome these disadvantages [1, 8], vastly improving their performance—comparable to the free enzymes in solution [1]. Therefore, the proper selection of supports is essential to ensure the complete use of these enzymes. Nanoparticles [9, 10], microspheres [11, 12], hydrogels [13-15], porous glass [16], and membranes [17, 18] are commonly used. Nanoparticles and microspheres have a high surface area effective for a large amount of immobilization; nevertheless, the reuse of them often relies on other separation processes like membrane filtration and centrifugation. Directly using microporous membranes as supports, often called as enzymatic membrane bioreactors (EMBRs), permits high surface area, easy reuse, low pressure drop, and relatively low diffusion resistance.

The important point on the enzyme immobilization is how to maintain their conformation and activity on the supports. Generally, enzyme immobilization onto membranes can be

achieved by three methods: (a) physical adsorption [19-23], (b) entrapment [24-26], and (c) covalent attachment. Although physical adsorption (via electrostatic, hydrophobic, or hydrophilic interaction) is a simple process, immobilized enzymes are easily eluted when they are utilized due to the relatively weak interactions. The entrapment technique retains the activity of the enzyme as no chemical reaction takes place between the membrane and the enzyme. However, it suffers in performance due to the diffusion barrier and enzyme leakage [27]. Covalent attachments simply form strong and stable linkages that prevent enzyme leakage, thereby giving rise to a robust biocatalyst. However, the formation of covalent bonds generally decreases enzyme activity and makes it difficult to efficiently immobilize a large amount of enzyme [28].

The utilization of spacer-arms between the membrane surfaces and enzymes provides considerable mobility to the reactive sites and consequently the immobilized enzymes, resulting in the improvement of the immobilization efficiency and enzyme activity. The commonly reported spacers are hydrazine [29] and diamine [30-33]. Following the introduction of enzymes, one method primarily activates carboxyl groups on the enzymes and then the active esters are conjugated with amino groups on the spacers. However, once the enzymes are activated, the amino groups in the enzymes competitively react with themselves on the membrane surface. This self-crosslinking between enzymes negatively affects their activity, and especially in the case of membranes, causes membrane fouling due to the aggregate formation or multilayer accumulation on/in the membrane [34]. Another commonly used method is inserting glutaraldehyde (GA) to conjugate amino groups on membrane surface and enzymes via the Schiff base reaction [20, 34-38]. However, GA also crosslinks enzymes each other and leads self-crosslinking. If the enzyme activity can be directly added to the end of the spacers on the membrane surfaces, enzyme immobilization efficiency can be improved by avoiding the above self-crosslinking. Although complicated, multi-step reactions were required. Sousa et al. immobilized pig liver esterase onto the surface of hollow fiber membranes using spacer molecules such as 1,4-butanediol diglycidyl ether and aminocaproic acid, which were activated to improve the enzyme activity [31]. Since

there are only a few reliable methods to immobilize enzymes on supports, only 20% of the industrial biocatalytic processes utilize immobilized enzymes [39].

In this study, we report a novel method via dicarboxylic acid halides to immobilize enzymes on commercial microporous membranes (Fig. III.1). Dicarboxylic acid halides with different molecular lengths are commercially available and exhibit a high reactivity with amino groups and hydroxyl groups, which are easily introduced onto membrane surfaces via plasma treatment, chemical treatment, polymer coating, and grafting. Trypsin and lipase were chosen as the enzyme model because they are commonly used for digestion of proteins and oils, respectively, as well as industrial production. Sebacoyl chloride (SC), a dicarboxylic acid halide, was used as a spacer and reacted with the surface of a commercial microfiltration membrane made from regenerated cellulose. The unreacted carboxylic end of SC was conjugated with trypsin via an active ester method. These surface initiated, sequential reactions occur on the membrane surface without self-crosslinking. Therefore, the enzyme molecules are expected to be efficiently immobilized on the membrane surface, largely keeping their molecular conformation and activity. The immobilization parameters were investigated for performance optimization, and the potential application of the resulting membranes was also demonstrated.
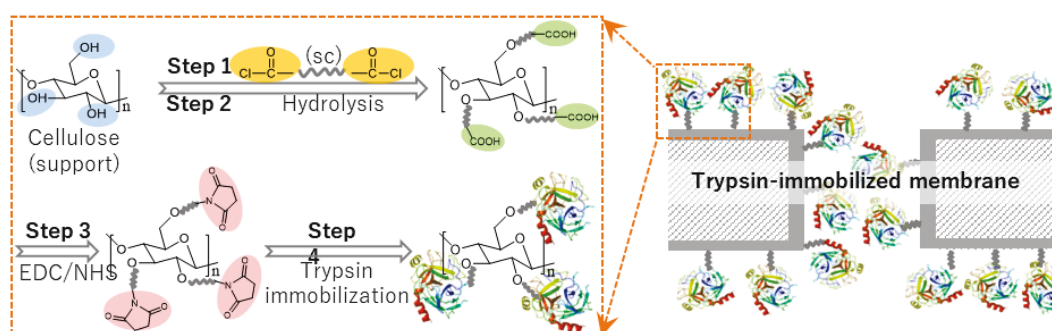
Fig. III.1 The schematic process for trypsin immobilization on regenerated cellulose membranes.

III.2 Experimental

III.2.1 Materials

Regenerated cellulose membranes with 0.2 mm pores were obtained from Merck Millipore (Darmstadt, Germany). Sebacoyl chloride (SC) and 1-(3-dimethylaminopropyl)-3-ethylcarbodiimide hydrochloride (EDC) were supplied by Tokyo Chemical Industry (Tokyo, Japan). N-Hydroxysuccinimide (NHS), p-nitrophenyl palmitate (p-NPP) and trichloroacetic acid were provided by Wako Pure Chemical Industries (Osaka, Japan). Benzoyl-*L*-arginine ethyl ester (BAEE) was obtained from Peptide Institute (Osaka, Japan). Fluorescein isothiocyanate-labeled albumin from bovine serum (FITC-BSA, 67 kDa), trypsin from bovine pancreas (24 kDa), and lipase from Candida rugosa were purchased from Sigma-Aldrich (St. Louis, MO, USA). Bicinchoninic acid (BCA) protein assay kit was purchased from Nacalai Tesque (Kyoto, Japan). Deionized water was produced in a Millipore Milli-Q water purification system. Other chemicals were purchased from Wako Pure Chemical Industries. All reagents were used as received without further purification.

III.2.2 Trypsin immobilization

A schematic representation of the enzyme immobilization process is shown in Fig. III.1. A regenerated cellulose membrane was immersed in n-hexane containing SC for 10 min and then washed in n-hexane to remove unreacted SC molecules (step 1). Following the evaporation of n-hexane, the membrane was submerged in deionized water for 30 min at 37°C to completely hydrolyze the acyl chloride groups on the membrane (step 2). The carboxylic groups on the SC-reacted membrane were conjugated with enzymes via an active ester method using EDC and NHS. To activate the carboxylic groups, the membrane was immersed into a 50 mM solution of phosphate buffered saline (PBS, pH 6.0) containing EDC (0.1 M) and NHS (0.1 M) with gentle shaking for 60 min at 25 °C and further washed with PBS (pH 7.6) three times (step 3). Next, the activated membrane was submerged in PBS (pH 7.6) containing trypsin or lipase and incubated in a shaker at 60 rpm for a given amount of time (step 4). Finally, the membrane was washed with PBS (pH 7.6) containing 3 M NaCl for 60 min followed by PBS (pH 7.6) for another 60 min to completely remove the physically

and loosely adsorbed enzyme molecules. The membrane was stored in PBS (pH 7.6) at 4 °C for further use.

III.2.3 Membrane characterization

To analyze the chemical property, attenuated total reflection Fourier transform infrared (ATR-FTIR) spectroscopy (Nicolet iS5, Thermo Fisher Scientific, Waltham, MA, USA) and X-ray photoelectron spectroscopy (XPS; JPS-9010 MC, JEOL, Tokyo, Japan) were performed. FTIR spectra recorded wavenumbers ranging between 1300–3500 cm^{-1}. Thirty-two scans were taken for each spectrum at a resolution of 2 cm^{-1}. The XPS spectra were recorded with the Al Kα radiation source at a take-off angle of 45 °C. The whole (0–1000 eV) and narrow spectra of all elements containing high resolutions were recorded. The hydrophilicity of the membrane surface was characterized based on the static contact angle measurement using a contact angle goniometer (Drop Master 300, Kyowa Interface Science, Saitama, Japan). A drop of Milli-Q water (4 mL) was released onto the membrane surface and the contact angle was measured using the images of the water drop on the membrane. At least six measurements were taken from different positions. The surface morphology of the membranes was observed by a field emission scanning electron microscope (FE-SEM; JSF-7500F, JEOL). The samples were freeze-dried (FD-1000, Tokyo Rikakikai, Tokyo, Japan) and then coated with a 5–10 nm osmium layer (Neco-STB, Meiwafosis, Tokyo, Japan). To verify the protein immobilization ability, FITC-BSA was immobilized onto the EDC/NHS activated membrane and the obtained membrane was observed by a confocal laser scanning microscope (CLSM; FV1000, Olympus, Tokyo, Japan). Pure water permeability was measured with a lab-made filtration cell (see Fig. III.2) in a gravity drive mode. The effective area of the used membrane was 3.14 cm^2.
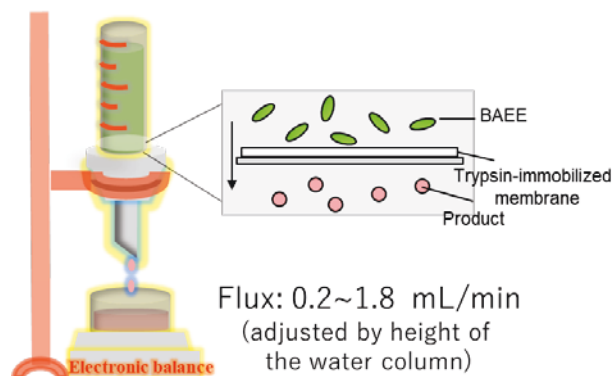
Fig. III.2 Experimental setup for the permeability measurement and activity determination in filtration mode for EMBRs.

III.2.4 Trypsin amount quantification

The membrane was analyzed regarding the amount of the immobilized trypsin via BCA assay [40, 41]. The membrane sample was immersed into BCA working solution, incubated for 30 min at 37 °C, and then agitated for 5 min at 25 °C. The absorbance of this solution at 562 nm was measured using a UV-vis spectrophotometer (V-630, Jasco, Tokyo, Japan). For calibration, free trypsin concentrations of 100, 200, 400, 600, 800, 1000, and 1500 ppm were used. The surface density (D) of the trypsin immobilized on the membrane was calculated from the equation below:

$$D \ (\mu g \ cm^{-2}) = \ A/S \qquad\qquad (\text{III.1})$$

where A (μg) represents the amount of the trypsin immobilized on the membranes, which can be obtained from the standard curve and S (cm^2) is the surface area of the membrane.

III.2.5 Activity determination

The trypsin activity was determined by measuring the kinetic hydrolysis of BAEE at 37 °C in a stirred cuvette reactor. Briefly, 75 mL of free trypsin or a trypsin-immobilized membrane (9 mm diameter) was added into a cuvette containing 3 mL of 0.086 mg mL^{-1} BAEE in 67 mM PBS (pH 7.6) and 125 mL of 1 mM HCl solution. The increase in absorbance at 253 nm (ΔAbs253 nm) was recorded for approximately 20 min by the UV-vis spectrometer. As an

index of enzymatic activity, a BAEE unit (U) was used, which is defined as the amount of trypsin required to produce a ΔAbs253 nm of 0.001 per minute with a pH 7.6 BAEE substrate at 25 °C in a reaction volume of 3.2 mL [42, 43]. We calculated the specific activity (*SA*) of the membrane at 37 °C as follows:

$$SA \ (\text{U} \ cm^{-2}) = \frac{1000 \ (\Delta\text{Abs}_{253nm(sample)} - \Delta\text{Abs}_{253nm(blank)})}{tS} \tag{III.2}$$

where t (min) referred to the operation time.

For the specific activity of free trypsin at 37 °C:

$$SA_{free} \ (\text{U} \ ug^{-1}) = \frac{1000 \ (\Delta\text{Abs}_{253nm(sample)} - \Delta\text{Abs}_{253nm(blank)})}{tA_{free}} \tag{III.3}$$

where A_{free} (µg) was the amount of free trypsin.

Meanwhile, the activity retention (R) was calculated as follows:

$$R \ (\%) = 100 \ \frac{SA/D}{SA_{free}} \tag{III.4}$$

Each result was obtained from the average of five parallel tests. The kinetic parameters were determined according to the Michaelis–Menten equation:

$$V = \frac{V_{max} \ [S]}{K_m + [S]} \tag{III.5}$$

where V (U) was the reaction rate, calculated from *SA*. V_{max} (U) was the maximum reaction rate at saturating BAEE concentration. [S] was the BAEE concentration. K_m was the Michaelis constant. V_{max} and K_m were determined using a Lineweaver– Burk plot.

The turnover number (K_{cat}) was calculated via the equation:

$$K_{cat} = \frac{V_{max}}{[E]} \tag{III.6}$$

where [E] is the enzyme concentration.

The method for activity determination of lipase was described as follows. 0.125g p-NPP was dissolved in 25 mL of EtOH and then mixed with an equal amount of 50 mM PBS (pH 7). The mixture was used as substrate solution. 125 µL of lipase solution or a lipase-immobilized membrane with 20 mm diameter was mixed with 2.5 mL of the substrate solution, and stirred at 37°C. After 10 min reaction, 2 mL of 0.5 M Na_2CO_3 was added to terminate the enzymatic reaction. The supernatant was diluted four times with deionized water and the absorbance was measured at 410 nm. Deionized water was used as the blank.

A p-NPP unit (U) was defined as the amount of lipase required to produce a ΔAbs_{410nm} of 0.001 per minute with a pH 7 p-NPP substrate at 37 ºC in a reaction volume of 2.625 mL. The specific activity (SA_{lipase}) was calculated as follows:

For immobilized lipase:

$$SA_{lipase} \ (U \ cm^{-2}) = \frac{1000 \ (\Delta Abs_{410nm(sample)} - \Delta Abs_{410nm(blank)})}{10 \ S_{lipase}} \qquad (III.7)$$

For free lipase:

$$SA_{free-lipase} \ (U/\mu g) = \frac{1000 \ (\Delta Abs_{410nm(sample)} - \Delta Abs_{410nm(blank)})}{t \ A_{free-lipase}} \qquad (III.8)$$

S $_{lipase}$ (cm^2) was the membrane area. A $_{free-lipase}$ (μg) was the amount of free lipase.

Meanwhile, the activity retention (R_{liapse}) was obtained:

$$R_{lipase} \ (\%) = 100 \cdot (SA_{lipase}/D_{lipase})/SA_{free-lipase} \qquad (III.9)$$

where D_{lipase} ($\mu g/cm^2$) was the density of lipase on the membrane.

III.2.6 Stability of the immobilized trypsin

The thermal resistance of immobilized trypsin and free trypsin was evaluated by measuring the relative activity at different catalytic temperatures. The specific activity at 37 °C was selected as the benchmark and the corresponding value was 100%. The relative activity was defined as:

$$Relative \ activity \ (\%) = \frac{100 SA_T}{SA_{37°C}} \qquad (III.10)$$

where SA_T was the value of SA performed at given temperature (T); $SA_{37°C}$ was the value of SA performed at 37 °C.

The continuous operation capability was studied by measuring the relative activity after incubation in a water bath at 37 °C for various periods of time. The initial specific activity at 37 °C was selected as the benchmark. The durability of the immobilized trypsin after repeated use was determined as follows: after one operation cycle for 20 min, the membrane was washed twice in 50 mM PBS (pH 7.6) and then soaked in a fresh reaction mixture to assay the enzymatic activity for ten cycles. The specific activity in cycle 1 was selected as the benchmark.

III.2.7 Potential application in enzymatic membrane bioreactors (EMBRs)

To use membranes in EMBRs, the effect of BAEE concentration in the soaking mode and the flow rate in the filtration mode on the activity of the trypsin-immobilized membrane were investigated to obtain a better performance in bioreactors. The apparatus and process for the filtration mode are shown in Fig. III.2. In order to demonstrate the potential application of the trypsin-immobilized membrane in a more practical situation, the catalytic performance against protein was investigated. BSA was chosen as a substrate model. Briefly, a 25 mm diameter membrane was immersed in 6 mL of BSA solution (5000 ppm) in 50 mM PBS (pH 7.6). After incubation at 37 °C for different time periods with stirring, the reaction was terminated by the addition of 1 mL trichloroacetic acid (50 wt%). The trichloroacetic acid denatured and precipitated BSA, leaving the peptide products in the solution. The solution was subsequently centrifuged at 8000 rpm for 3 min and the concentration of the peptides produced in the supernatant by the enzymatic reaction was quantified by measuring the absorbance at 280 nm.

III.3 Results and discussion

III.3.1 Membrane characterization

Firstly, the chemical properties of the modified membranes were analyzed by a combination of ATR-FTIR and XPS. Fig. III.3(A) shows the FTIR spectra of the membrane surfaces. A new peak appeared at 1740 cm^{-1} for the SC-immobilized membrane, which verified the presence of carboxyl groups. The peak at 1539 cm^{-1} existing in the spectrum of the trypsin-immobilized membrane was the characteristic peak of amino groups from trypsin. Table III.1 shows the chemical composition of the membrane surface measured by XPS. The C/O ratio increased along with the reaction process (pristine membrane: 1.32; SC-reacted membrane: 1.67; trypsin immobilized membrane: 2.25).

Theoretically, molecules of hydrolyzed SC and trypsin have higher C/O ratios than pristine cellulose membrane and thus, the increase in C/O ratio can be explained by the introduction of carboxyl acid groups on the SC-reacted membrane surface and trypsin on the trypsin-immobilized membrane surface. Additionally, the appearance of nitrogen on the

trypsin-immobilized membranes also demonstrated the presence of trypsin. The contact angle of the membrane surface, shown in Table III.1, was also changed by each modification process. After SC introduction, the contact angle value (30.7 °) became higher than that of the pristine membrane (20.4 °), which can be explained by the relative hydrophobicity of the long carbon chain of SC molecules. The trypsin immobilization further changed the contact angle to a more hydrophobic orientation (75.2 °), which corresponded to some hydrophobic chains in trypsin.

Fig. III.3(B) and (C) show the membrane surface morphologies observed by FE-SEM and CLSM, respectively. The SEM images in Fig. III.3(B) showed no obvious morphological change or pore blocking after the trypsin immobilization. Furthermore, the water permeability of the trypsin-immobilized membrane was measured to be around 85% of that of the pristine membrane, which indicated that the layer of immobilized trypsin on the membrane surfaces and inner pores was thin enough to not largely affect the permeability. It was consistent with previous studies in which very few enzyme molecules were immobilized [28, 41]. The CLSM images in Fig. III.3(C) revealed that the fluorescence from the immobilized FITC-BSA was uniformly distributed on the membrane surface, indicating that the presented method could be applied to uniformly immobilize various biomolecules.
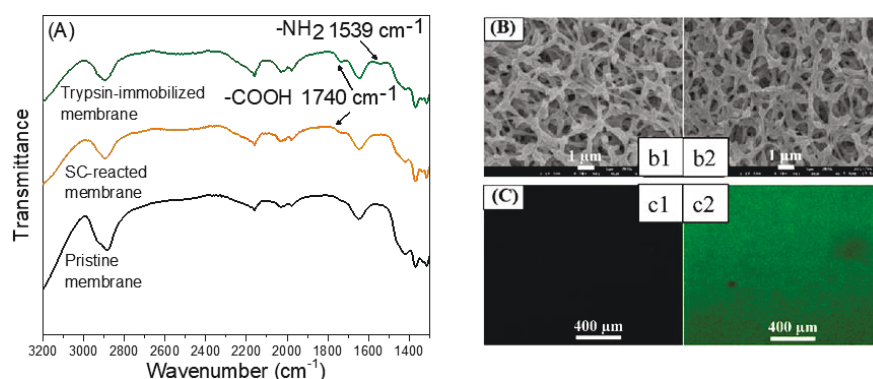

Fig. III.3 Characterization of the pristine and modified membrane. (A) The FTIR spectra of pristine, SC-reacted, trypsin-immobilized membranes. (B) Surfaces of the (b1) pristine membrane and (b2) trypsin-immobilized membrane. (C) CLSM images of the (c1) pristine membrane and (c2) FITC-BSA-immobilized membranes.

Table III.1 The chemical composition measured by XPS and the contact angle of pristine membrane, SC-reacted membrane and trypsin immobilized membranes.

Sample	Elemental ratio (rel. atom%)			C/O ratio	Contact angle (°)
	C 1s	O 1s	N 1s		
Pristine	56.86	43.14	0	1.32	20.4 ± 2
SC-reacted	62.51	37.49	0	1.67	30.7 ± 3
Trypsin-immobilized	64.50	28.60	6.89	2.25	75.2 ± 3

III.3.2 Trypsin immobilization

The pivotal parameters include reaction temperature, concentrations of SC and trypsin, and reaction time. In this section, the effects of these four factors on membrane performance were investigated. In order to calculate the activity retention (R) of immobilized trypsin, the specific activity of free trypsin (SA_{free}) was measured and the value was determined to be 2.256 U mg^{-1}. Table III.2 shows the effect of reaction temperature on trypsin immobilization. The surface density (D) and specific activity (SA) of the immobilized trypsin at 25 °C were six and two times higher than those at 4 °C respectively, due to the high reactivity between active ester and trypsin at high temperature. The value of D at 25 °C in this study was estimated to be 60 µg cm^{-2}, which was in good agreement with those reported values, ranging from several µg cm^{-2} to several tens µg cm^{-2} [41, 44-47]. Most of the previously reported values for SA were low such as 0.1 or 1 U cm^{-2}. However, in this study, SA reached to around 27 U cm^{-2} due to the high immobilization efficiency and uniform distribution of immobilized trypsin on the membrane surface. The R value of membranes modified at 4 °C was higher than that at 25 °C due to the better mobility of trypsin on the membranes owing to its low density. This corresponded to the rule reported by Koki et al [48]. The R value modified at 25 °C was around 20%, which was comparable to the previous reports [49, 50]. From the comprehensive analysis of D, SA and R at 25 °C supplemented with the nearly unchanged

water permeability result, we can conclude that the immobilization efficiency in this study was higher than other previously reported studies. The enzyme immobilization was usually performed at 4 °C to maintain the enzyme activity during the immobilization process [45, 48]. However, it needs a long reaction time such as 24 h [46]. Actually, the trypsin activity did not undergo a major change at 25 °C for several hours, which was verified in the following section. Although more high temperature may improve the immobilization efficiency, it affects the catalytic activity, as described the "Stability of the immobilized trypsin" section. Therefore, 25 °C was chosen for all further experiments.

Table III.2 Effect of reaction temperature on membrane performance factors including the surface density of immobilized trypsin (D), specific activity (SA), and activity retention (R)

Reaction temperature (°C)	D ($\mu g\ cm^{-2}$)	SA ($U\ cm^{-1}$)	R (%)
4	8 ± 2	9 ± 3	45 ± 2
25	60 ± 6	27 ± 2	20 ± 4

Fig. III.4(A) shows the effects of trypsin concentration on its immobilization. Increasing the trypsin concentration highly facilitated the reaction between trypsin and the membrane surface, thereby increasing D, which reached a maximum threshold of 75 $\mu g\ cm^{-1}$ at 10000 ppm of the trypsin concentration. However, SA almost achieved its maximum value at 7000 ppm and then nearly approached a plateau. Meanwhile, R decreased continuously from 30% at 100 ppm to 16% at 10000 ppm. This proved that "saturation region" existed for catalysis, implying that extremely high amounts of trypsin did not correlate to higher trypsin activity on the whole membrane. While the number of trypsin active sites on the membrane surface increased with its immobilized amount, the increasing trypsin density contrastingly hindered its activity. The balance of these two opposite phenomena resulted in a steady value for SA. The membrane with a trypsin concentration of 1000 ppm showed the best integrated performance and thus, this concentration was chosen for all following experiments.

Fig. III.4(B) and (C) show the effects of the reaction time and SC concentration on trypsin immobilization, respectively. Increasing the reaction time increased D and SA while decreasing R. The SA value reached its stable value at 180 min. Furthermore, increasing the SC concentration improved D (Fig. III.4(C)). The high SC concentration probably facilitated the introduction of carboxyl acid groups on the membrane surfaces. An extremely high acyl chloride concentration (2.0 wt%) was not so effective in improving trypsin immobilization because the carboxyl acid groups on the membrane reached saturation. Fig. III.5 summarizes the relationship between the surface density (D) and specific activity (SA). The "critical point" represents the optimum performance values for membranes. The corresponding values for D, SA, and R were around 36 µg cm^{-2}, 22 U cm^{-2}, and 26% respectively. From the results in Fig. 4, the "critical point" was obtained under optimum immobilization condition, which was decided as follows: 25 °C reaction temperature, 1000 ppm trypsin concentration, 180 min reaction time, and 1.0 wt% SC concentration. "Saturation region" represented membranes possessing the immobilized enzyme with the largest surface density and highest specific activity.

The kinetic parameters of trypsin were determined using Lineweaver–Burk plots (Fig. III.6) to evaluate the catalytic performance. The maximum reaction rate (V_{max}) and the turn over number (K_{cat}) of the immobilized trypsin were lower than that of the free trypsin because of the lower diffusion rate in the membrane pores, resulting in the decrease of the reaction rate of the immobilized trypsin in the pores. The Michaelis constant (K_m) were higher for the immobilized trypsin due to the introduction of stable covalent bonding and restriction of conformation change.
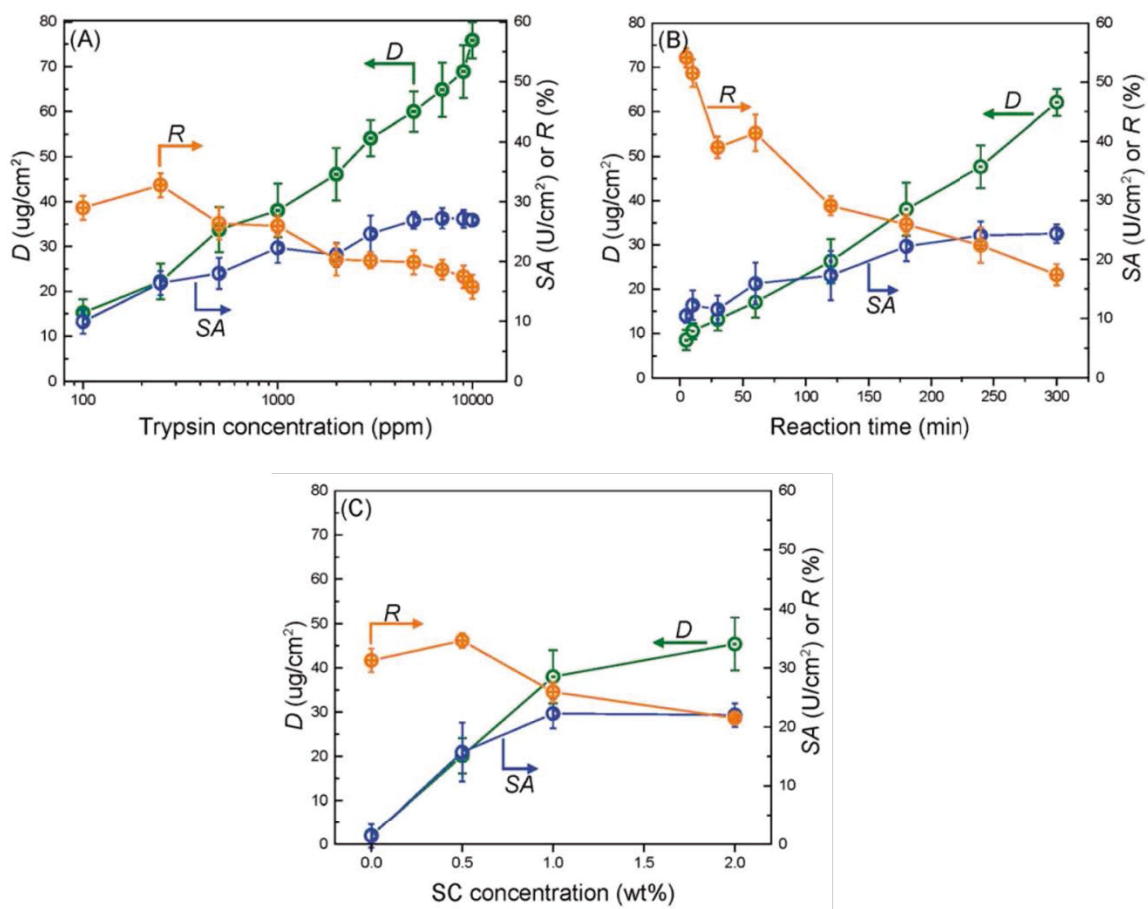
Fig. III.4 The effect of (A) trypsin concentration, (B) reaction time, and (C) SC concentration on membrane performance factors such as surface density of immobilized trypsin (*D*), specific activity (*SA*), and activity retention (*R*).
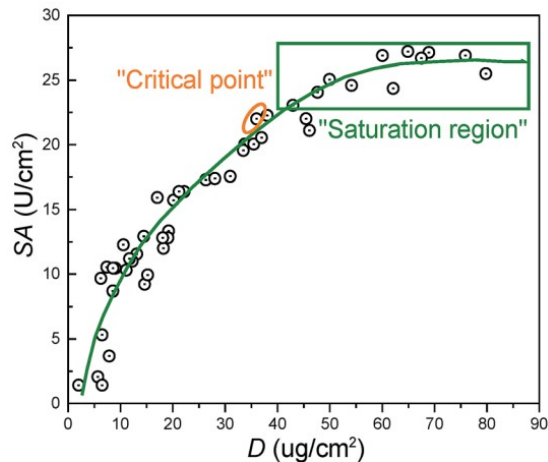
Fig. III.5 The relationship between the surface density (D) and specific activity (SA) of the immobilized trypsin on the membranes.
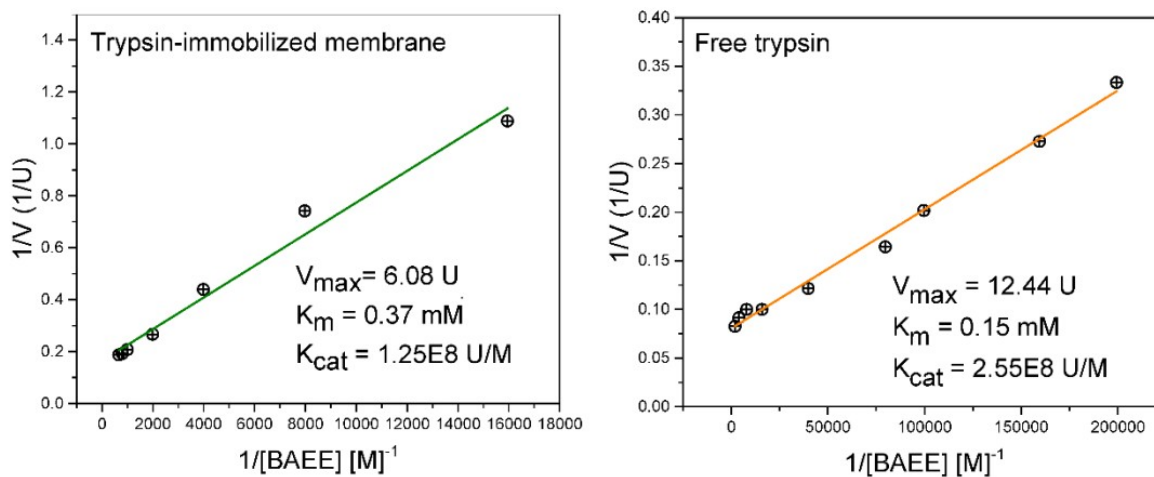
Fig. III.6 Lineweaver-Burk plots of the trypsin-immobilized membrane and free trypsin in the soaking mode for the kinetic parameter determination.

To demonstrate the applicability for various types of enzymes, lipase was also immobilized via the same method. Lipase-immobilized membranes were fabricated with the following condition: 25 ℃ reaction temperature, 1,000 ppm lipase concentration, 180 min reaction time,

and 1.0 wt % SC concentration. The values of D and SA were 18 µg/cm^2 and 25 U/cm^2 (1.39 U/µg). The value of SA_{free} was 1.17 U/µg. Using these values, R was calculated as 119 %. These data suggested this method could also improve the catalytic activity of lipase.

   Table III.3 lists various immobilized enzymes, particularly trypsin, that used polymeric membranes as supports and compared the related performance. The values of SA and R for immobilized trypsin in this work were higher than the trypsin in the other reports, while D was comparable. The immobilization method in this work could efficiently retain the enzymatic activity due to the prevention of self-crosslinking of enzymes, insertion of flexible spacers between enzymes and membrane, and uniform distribution of enzymes.

Table III.3 Comparison of the surface density (D), specific activity (SA), and activity retention (R) of various immobilized enzymes

Enzyme/membrane [a]	D (µg cm^{-2})	SA[b] (U cm^{-1})	R (%)	Ref.
Trypsin/cellulose	36	13.2	26	This study
Trypsin/cellulose	81	0.2	11	[50]
Trypsin/m-PE	No data	0.1	No data	[42]
Trypsin/PE	14	No data	25	[49]
Trypsin/PVDF	3	No data	No data	[28]
Lipase/cellulose	18	25	119	This study
Gox/cellulose	40	No data	19	[51]
Pig liver esterase/nylon	2	No data	22	[31]
Urease/ p(HEMA–GMA)	16	No data	27	[52]

[a] m-PE: modified polyethylene, PE: polyethylene, PVDF: polyvinylidene fluoride, p(HEMA−GMA): poly((2- hydroxyethyl methacrylate)-co-(glycidyl methacrylate)).

[b] All the values of SA here were measured at 25 °C.

III.3.3 Stability of the immobilized trypsin

The thermal resistance of the immobilized enzymes is one of the most important criteria in actual application [53]. Fig. III.7(A) shows the effect of the catalytic temperature on the relative activity. Generally, the effect of the thermal resistance of immobilized enzymes, especially for the covalently bound system, is higher than that of free enzymes [2]. The optimum temperature of free trypsin was observed to be about 37 ℃, whereas the immobilized trypsin was observed to be approximately 45 ℃. The increase in the optimum temperature indicates that the thermal resistance of trypsin was improved by the immobilization onto the membrane surfaces. The covalent bond formation between trypsin and the membrane surfaces suppressed the conformational change of trypsin, which resulted in a higher activation energy needed for the enzyme to reorganize itself into the proper conformation in order to bind to the substrate molecules [12].

The capability of the trypsin-immobilized membrane to continuously operate at 37 ℃ was investigated and the result is shown in Fig. III.7(B). At 37 ℃, the activity of free trypsin reduced to 20% of the initial value only during the 20 h incubation. However, the activity of trypsin-immobilized membrane kept the initial value even after the 24 days incubation, suggesting excellent durability over a long-term operation. The durability of the enzyme-immobilized membranes was reported to be not so effective in many previous studies. For example, a lipase immobilized membrane lost 20% of its original activity after storing at 4 ℃ for 15 days [36]. However, our immobilized enzyme showed better durability. Fig. III.7(C) shows the reusability. Its activity hardly decreased even after ten cycles. This result indicated no leakage and denaturation of the immobilized trypsin during repeated catalysis and washing.
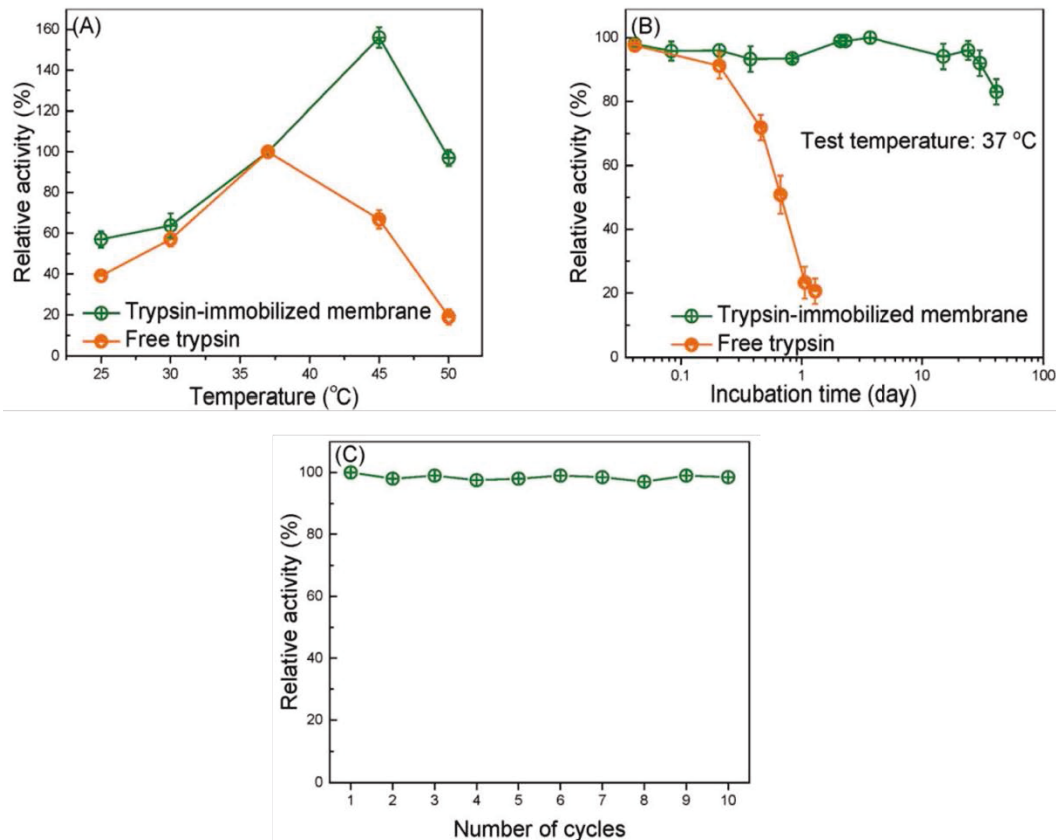
Fig. III.7 Evaluation of the stability of the immobilized trypsin (A) the effect of the catalytic temperature on the relative activity of the trypsin immobilized membrane and free trypsin. (B) Time courses of the relative activity of the trypsin-immobilized membrane and free trypsin at 37°C. (C) The relative activity of trypsin-immobilized membrane during ten operation cycles.

Fig. III.8 shows the thermal stability of the lipase including the effect of temperature on the activity, the continuous operation capacity, and the reusable performance. From Fig. III.8(A), the optimal catalytic temperature for lipase-immobilized membrane and free lipase was 45 °C and 37 °C, respectively, indicating the thermal stability of lipase was improved by the immobilization as the same as in the case of trypsin. Fig. III.8(B) exhibited the capacity

of continuous operation at 37 °C. We can see that the stability was improved after the immobilization. Fig. III.8(C) showed the lipase-immobilized membrane. The remained activity still can achieve to 45 % after the ten-cycle reaction.
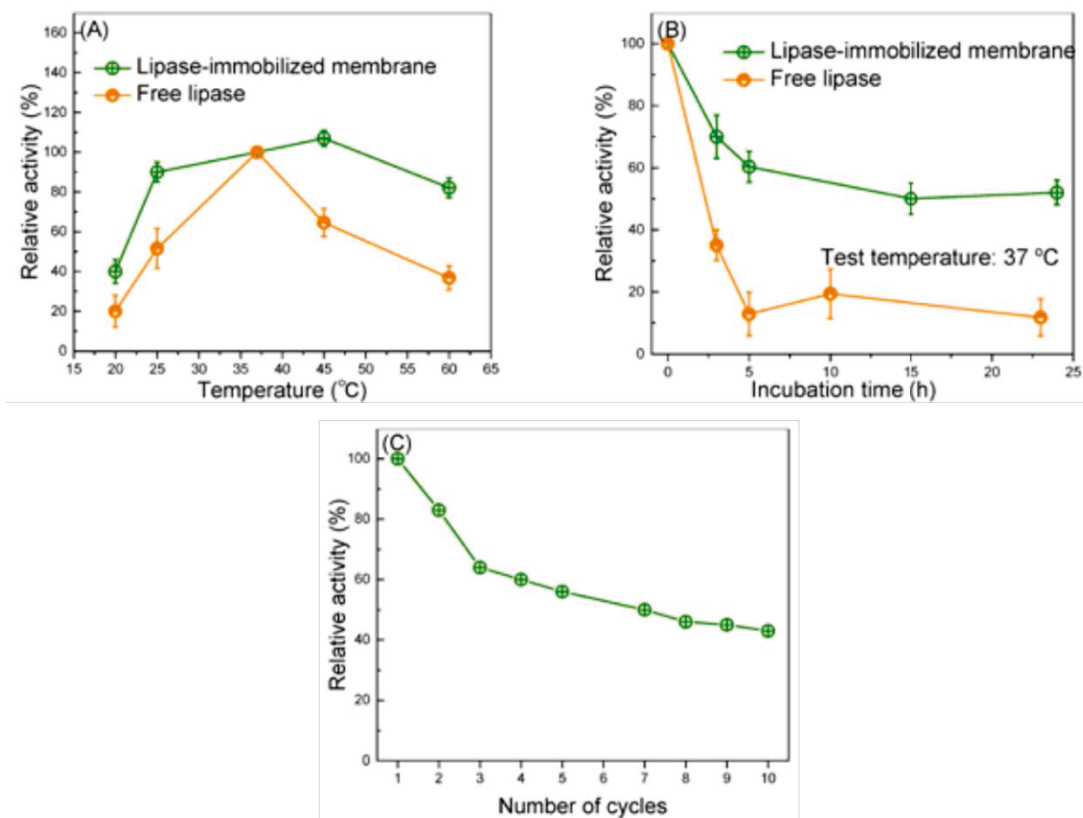
Fig. III.8 Evaluation of the stability of the lipase-immobilized membrane and free lipase. (A) The effect of the catalytic temperature on the relative activity of the lipase-immobilized membrane and free lipase. (B) Time courses of the relative activity of the lipase-immobilized membrane and free lipase at 37 °C. (C) The relative activity of lipase-immobilized membrane during ten operation cycles.

III.3.4 Potential application in enzymatic membrane bioreactors (EMBRs)

The application of the trypsin-immobilized membrane in EMBRs was investigated to demonstrate the potential for its practical application. We performed a continuous catalytic reaction under the filtration mode. Fig. III.9(A) shows the influence of the flow rate on the specific activity. The value of *SA* and *R* were surprisingly improved from 22 to 118 U cm^{-2} and from 26% to 145%, when the flow rate was increased from 0 to 1.52 mL min^{-1}. In the soaking mode (see Fig. III.10), *SA* increased with increasing the substrate concentration for the trypsin immobilized membrane, suggesting that the catalytic reaction at low substrate concentration was restricted by the diffusion of substrates [54], and especially the trypsin in the pores didn't react effectively. In the filtration mode, the convective flow in the membrane pores offered an enhanced mass transfer of substrates, which led to higher accessibility between substrates and immobilized trypsin on/in the membrane, and thus brought about much higher *SA* and *R* than the reported values. This high *R* value, 145%, means that immobilized trypsin has higher catalytic activity than the non-immobilized, native trypsin due to probably the stabilization of the molecular conformation by the immobilization onto the surface. The flow mode operation of the modified membranes was effective to enhance the catalytic activity as EMBRs.

Finally, we applied the modified membranes to catalyze BSA as a protein substrate model (Fig. III.9(B)). The amount of the peptide products was observed to continuously increase with the catalytic time. Furthermore, no obvious decrease in the reaction rate was observed during the second digestion run, suggesting good reusability of the modified membranes. This digestion ability was comparable to the pepsin membranes reported by Michiel, which required 30 h to obtain large amounts of products when BSA was used as a substrate [55]. In conclusion, the trypsin-immobilized membrane exhibits a great potential application in EMBRs.

The method presented in this study successfully immobilized a large amount of enzyme while effectively maintaining their catalytic activity by preserving their three-dimensional conformation. Besides enzyme immobilization, this method could also be applied to immobilize various biomolecules such as peptides, proteins, antibodies, and DNA onto various supports containing hydroxyl or amino groups. These composite materials have a

wide range of applications in separation, adsorption, catalysis, and sensors using their molecular recognition function.
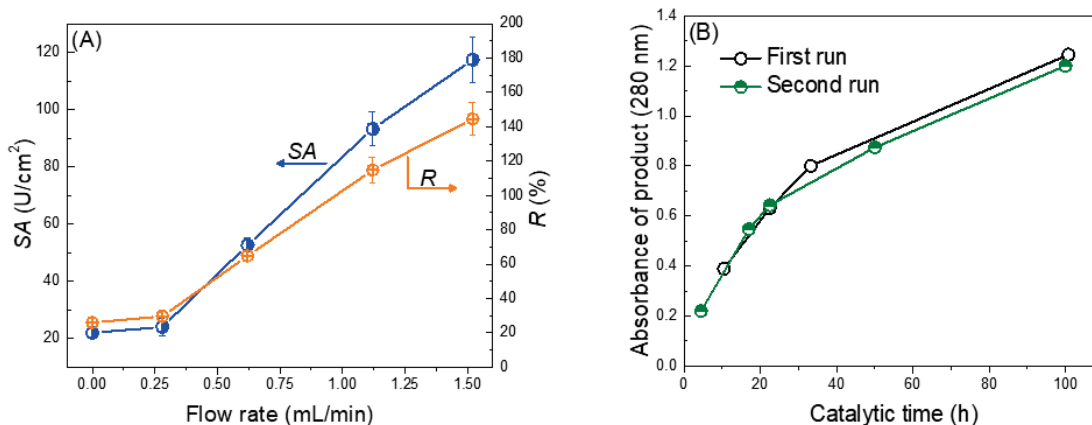
Fig. III.9 Demonstration of the trypsin-immobilized membrane as EMBRs. (A) Effect of the flow rate on the *SA* and *R* of the trypsin immobilized membrane in the filtration mode. The plot at 0 mL min^{-1} were estimated from the result of the soaking mode. (B) Digestion kinetics of BSA in the soaking mode at 37 °C.
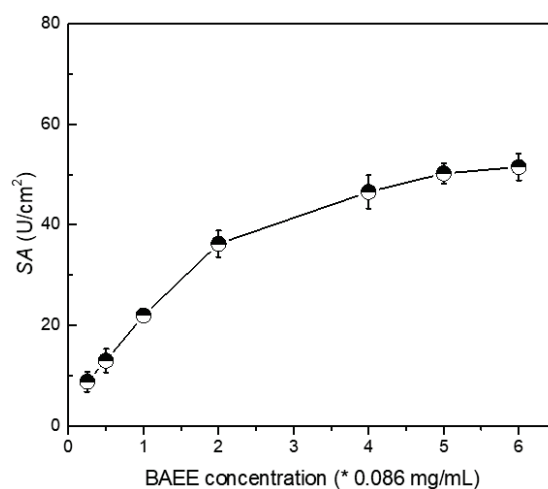
Fig. III.10 Effect of the substrate (BAEE) concentration on the enzymatic activity of the trypsin immobilized membrane.

III.4 Conclusions

Here, we presented a novel and facile strategy that used dicarboxylic acid halides as a functional spacer to immobilize enzymes onto porous membranes. The high reactive affinity between the acyl chlorides of the dicarboxylic acid halides and the hydroxyl groups on the membrane surface rapidly produced efficient introduction spacers on the membrane surfaces. During enzyme immobilization, the carboxyl groups on the ends of the spacers avoided the undesirable self-crosslinking of enzymes to ensure good catalytic activity and permeability. The optimum surface density of trypsin was reported to be 36 μg cm^{-2}, which showed a high specific activity of 22 U cm^{-2} and a high activity retention of 26%. In addition, the thermal stability, continuous operation capability, and reusability of the modified membranes were considered to be favorable for practical application. To demonstrate as EMBRs, the catalytic reaction in a filtration mode was attempted, and the resulted value of the activity retention was greatly improved to 145%, showing the catalytic activity of the immobilized trypsin was higher than that of non-immobilized, native trypsin. Furthermore, the efficient decomposition ability against BSA verified its excellent application potential in EMBRs. In addition, this method was effective for not only trypsin but also lipase, thus, it would be applicable to the immobilization of various kinds of enzymes.

Reference

[1] R.C. Rodrigues, C. Ortiz, A. Berenguer-Murcia, R. Torres, R. Fernandez-Lafuente, Modifying enzyme activity and selectivity by immobilization, Chem Soc Rev, 42 (2013) 6290-6307.

[2] P. Jochems, Y. Satyawali, L. Diels, W. Dejonghe, Enzyme immobilization on/in polymeric membranes: status, challenges and perspectives in biocatalytic membrane reactors (BMRs), Green Chemistry, 13 (2011) 1609-1623.

[3] M.B. Rao, A.M. Tanksale, M.S. Ghatge, V.V. Deshpande, Molecular and biotechnological aspects of microbial proteases, Microbiol Mol Biol R, 62 (1998) 597-+.

[4] S.M. Thomas, R. DiCosimo, A. Nagarajan, Biocatalysis: applications and potentials for the chemical industry, Trends Biotechnol, 20 (2002) 444-444.

[5] J.P. Rasor, E. Voss, Enzyme-catalyzed processes in pharmaceutical industry, Appl Catal a-Gen, 221 (2001) 145-158.

[6] A. Schmid, J.S. Dordick, B. Hauer, A. Kiener, M. Wubbolts, B. Witholt, Industrial biocatalysis today and tomorrow, Nature, 409 (2001) 258-268.

[7] Y.R. Qiao, M. Gumpertz, T. Van Kempen, Stability of pepsin (EC 3.4.23.1) during in vitro protein digestibility assay, J Food Biochem, 26 (2002) 355-375.

[8] P. Torres-Salas, A. del Monte-Martinez, B. Cutino-Avila, B. Rodriguez-Colinas, M. Alcalde, A.O. Ballesteros, F.J. Plou, Immobilized Biocatalysts: Novel Approaches and Tools for Binding Enzymes to Supports, Adv Mater, 23 (2011) 5275-5282.

[9] D.F.M. Neri, V.M. Balcao, F.O.Q. Dourado, J.M.B. Oliveira, L.B. Carvalho, J.A. Teixeira, Immobilized beta-galactosidase onto magnetic particles coated with polyaniline: Support characterization and galactooligosaccharides production, J Mol Catal B-Enzym, 70 (2011) 74-80.

[10] Y.H. Ren, J.G. Rivera, L.H. He, H. Kulkarni, D.K. Lee, P.B. Messersmith, Facile, high efficiency immobilization of lipase enzyme on magnetic iron oxide nanoparticles via a biomimetic coating, Bmc Biotechnol, 11 (2011).

[11] C. Chen, X.Y. Zhu, Q.L. Gao, F. Fang, L.W. Wang, X.J. Huang, Immobilization of lipase onto functional cyclomatrix polyphosphazene microspheres, J Mol Catal B-Enzym, 132 (2016) 67-74.

[12] M.Y. Arica, G. Bayramoglu, N. Bicak, Characterisation of tyrosinase immobilised onto spacer-arm attached glycidyl methacrylate-based reactive microbeads, Process Biochem, 39 (2004) 2007-2017.

[13] Y.C. Qian, P.C. Chen, G.J. He, X.J. Huang, Z.K. Xu, Preparation of Polyphosphazene Hydrogels for Enzyme Immobilization, Molecules, 19 (2014) 9850-9863.

[14] D. Kubac, A. Cejkova, J. Masak, V. Jirku, M. Lemaire, E. Gallienne, J. Bolte, R. Stloukal, L. Martinkova, Biotransformation of nitriles by Rhodococcus equi A4 immobilized in LentiKats (R), J Mol Catal B-Enzym, 39 (2006) 59-61.

[15] A.C. Pierre, The sol-gel encapsulation of enzymes, Biocatal Biotransfor, 22 (2004) 145-170.

[16] W. Limbut, P. Thavarungkul, P. Kanatharana, P. Asewatreratanakul, C. Limsakul, B. Wongkittisuksa, Comparative study of controlled pore glass, silica gel and Poraver((R)) for the immobilization of urease to determine urea in a flow injection conductimetric biosensor system, Biosens Bioelectron, 19 (2004) 813-821.

[17] S.V. Ebadi, A. Fakhrali, S.O. Ranaei-Siadat, A.A. Gharehaghaji, S. Mazinani, M. Dinari, J. Harati, Immobilization of acetylcholinesterase on electrospun poly(acrylic acid)/multi-walled carbon nanotube nanofibrous membranes, Rsc Adv, 5 (2015) 42572-42579.

[18] H. Kawakita, K. Sugita, K. Saito, M. Tamada, T. Sugo, H. Kawamoto, Optimization of reaction conditions in production of cycloisomaltooligosaccharides using enzyme immobilized in multilayers onto pore surface of porous hollow-fiber membranes, J Membr Sci, 205 (2002) 175-182.

[19] S.J. Bian, K. Gao, H.J. Shen, X.H. Jiang, Y.F. Long, Y. Chen, Organic/inorganic hybrid mesoporous silica membrane rapidly synthesized by a microwave-assisted method and its application in enzyme adsorption and electrocatalysis, J Mater Chem B, 1 (2013) 3267-3276.

[20] Z.G. Wang, J.Q. Wang, Z.K. Xu, Immobilization of lipase from Candida rugosa on electrospun polysulfone nanofibrous membranes by adsorption, J Mol Catal B-Enzym, 42 (2006) 45-51.

[21] C. Mateo, O. Abian, R. Fernandez-Lafuente, J.M. Guisan, Reversible enzyme immobilization via a very strong and nondistorting ionic adsorption on support-polyethylenimine composites, Biotechnol Bioeng, 68 (2000) 98-105.

[22] S. Sakai, Y.P. Liu, T. Yamaguchi, R. Watanabe, M. Kawabe, K. Kawakami, Immobilization of Pseudomonas cepacia lipase onto electrospun polyacrylonitrile fibers through physical adsorption and application to transesterification in nonaqueous solvent, Biotechnol Lett, 32 (2010) 1059-1062.

[23] Y.Y. Su, F. Peng, X.Y. Ji, Y.M. Lu, X.P. Wei, B.B. Chu, C.X. Song, Y.F. Zhou, X.X. Jiang, Y.L. Zhong, S.T. Lee, Y. He, Silicon nanowire-based therapeutic agents for in vivo tumor near-infrared photothermal ablation, J Mater Chem B, 2 (2014) 2892-2898.

[24] X.Y. Zhu, C. Chen, P.C. Chen, Q.L. Gao, F. Fang, J. Li, X.J. Huang, High-performance enzymatic membrane bioreactor based on a radial gradient of pores in a PSF membrane via facile enzyme immobilization, Rsc Adv, 6 (2016) 30804-30812.

[25] D.H. Chen, J.C. Leu, T.C. Huang, Transport and Hydrolysis of Urea in a Reactor-Separator Combining an Anion-Exchange Membrane and Immobilized Urease, J Chem Technol Biot, 61 (1994) 351-357.

[26] S. Gupta, Comparative study on hydrolysis of oils by lipase immobilized biocatalytic PS membranes using biphasic enzyme membrane reactor, J Environ Chem Eng, 4 (2016) 1797-1809.

[27] W.X. Zhang, A. Abbaspourrad, D. Chen, E. Campbell, H. Zhao, Y.W. Li, Q.N. Li, D.A. Weitz, Osmotic Pressure Triggered Rapid Release of Encapsulated Enzymes with Enhanced Activity, Adv Funct Mater, 27 (2017).

[28] S. Starke, M. Went, A. Prager, A. Schulze, A novel electron beam-based method for the immobilization of trypsin on poly(ethersulfone) and poly(vinylidene fluoride) membranes, React Funct Polym, 73 (2013) 698-702.

[29] C. Jolivalt, S. Brenon, E. Caminade, C. Mougin, M. Pontie, Immobilization of laccase from Trametes versicolor on a modified PVDF microfiltration membrane: characterization of the grafted support and application in removing a phenylurea pesticide in wastewater, J Membr Sci, 180 (2000) 103-113.

[30] S. Georgieva, T. Godjevargova, M. Portaccio, M. Lepore, D.G. Mita, Advantages in using non-isothermal bioreactors in bioremediation of water polluted by phenol by means of immobilized laccase from Rhus vernicifera, J Mol Catal B-Enzym, 55 (2008) 177-184.

[31] H.A. Sousa, C. Rodrigues, E. Klein, C.A.M. Afonso, J.G. Crespo, Immobilisation of pig liver esterase in hollow fibre membranes, Enzyme Microb Tech, 29 (2001) 625-634.

[32] A. De Maio, M.M. El-Masry, M. Portaccio, N. Diano, S. Di Martino, A. Mattei, U. Bencivenga, D.G. Mita, Influence of the spacer length on the activity of enzymes immobilised on nylon/polyGMA membranes Part 1. Isothermal conditions, J Mol Catal B-Enzym, 21 (2003) 239-252.

[33] S. Georgieva, T. Godjevargova, D.G. Mita, N. Diano, C. Menale, C. Nicolucci, C.R. Carratelli, L. Mita, E. Golovinsky, Non-isothermal bioremediation of waters polluted by phenol and some of its derivatives by laccase covalently immobilized on polypropylene membranes, J Mol Catal B-Enzym, 66 (2010) 210-218.

[34] D.Y. Koseoglu-Imer, N. Dizge, I. Koyuncu, Enzymatic activation of cellulose acetate membrane for reducing of protein fouling, Colloid Surface B, 92 (2012) 334-339.

[35] O. Barbosa, C. Ortiz, A. Berenguer-Murcia, R. Torres, R.C. Rodrigues, R. Fernandez-Lafuente, Glutaraldehyde in bio-catalysts design: a useful crosslinker and a versatile tool in enzyme immobilization, Rsc Adv, 4 (2014) 1583-1600.

[36] J. Zhu, G. Sun, Lipase immobilization on glutaraldehyde-activated nanofibrous membranes for improved enzyme stabilities and activities, React Funct Polym, 72 (2012) 839-845.

[37] S. Tembe, B.S. Kubal, M. Karve, S.F. D'Souza, Glutaraldehyde activated eggshell membrane for immobilization of tyrosinase from Amorphophallus companulatus: Application in construction of electrochemical biosensor for dopamine, Anal Chim Acta, 612 (2008) 212-217.

[38] S.L. Chen, X.J. Huang, Z.K. Xu, Effect of a spacer on phthalocyanine functionalized cellulose nanofiber mats for decolorizing reactive dye wastewater, Cellulose, 19 (2012) 1351-1359.

[39] A.J.J. Straathof, S. Panke, A. Schmid, The production of fine chemicals by biotransformations, Curr Opin Biotech, 13 (2002) 548-556.

[40] P.K. Smith, R.I. Krohn, G.T. Hermanson, A.K. Mallia, F.H. Gartner, M.D. Provenzano, E.K. Fujimoto, N.M. Goeke, B.J. Olson, D.C. Klenk, Measurement of Protein Using Bicinchoninic Acid, Anal Biochem, 150 (1985) 76-85.

[41] A. Schulze, D. Breite, Y. Kim, M. Schmidt, I. Thomas, M. Went, K. Fischer, A. Prager, Bio-Inspired Polymer Membrane Surface Cleaning, Polymers-Basel, 9 (2017).

[42] M. Ghasemi, M.J.G. Minier, M. Tatoulian, M.M. Chehimi, F. Arefi-Khonsari, Ammonia Plasma Treated Polyethylene Films for Adsorption or Covalent Immobilization of Trypsin: Quantitative Correlation between X-ray Photoelectron Spectroscopy Data and Enzyme Activity, J Phys Chem B, 115 (2011) 10228-10238.

[43] G.W. Schwert, Y. Takenaka, A Spectrophotometric Determination of Trypsin and Chymotrypsin, Biochim Biophys Acta, 16 (1955) 570-575.

[44] A. Kumari, S. Datta, Phospholipid bilayer functionalized membrane pores for enhanced efficiency of immobilized glucose oxidase enzyme, J Membr Sci, 539 (2017) 43-51.

[45] D. Saeki, S. Nagao, I. Sawada, Y. Ohmukai, T. Maruyama, H. Matsuyama, Development of antibacterial polyamide reverse osmosis membrane modified with a covalently immobilized enzyme, J Membr Sci, 428 (2013) 403-409.

[46] M.Y. Arica, S. Senel, N.G. Alaeddinoglu, S. Patir, A. Denizli, Invertase immobilized on spacer-arm attached poly(hydroxyethyl methacrylate) membrane: Preparation and properties, J Appl Polym Sci, 75 (2000) 1685-1692.

[47] R. Sternberg, D.S. Bindra, G.S. Wilson, D.R. Thevenot, Covalent Enzyme Coupling on Cellulose-Acetate Membranes for Glucose Sensor Development, Anal Chem, 60 (1988) 2781-2786.

[48] K. Itoyama, H. Tanibe, T. Hayashi, Y. Ikada, Spacer Effects on Enzymatic-Activity of Papain Immobilized onto Porous Chitosan Beads, Biomaterials, 15 (1994) 107-112.

[49] K. Yamada, T. Nakasone, R. Nagano, M. Hirata, Retention and reusability of trypsin activity by covalent immobilization onto grafted polyethylene plates, J Appl Polym Sci, 89 (2003) 3574-3581.

[50] A.H.M. Cavalcante, L.B. Carvalho, M.G. Carneiro-da-Cunha, Cellulosic exopolysaccharide produced by Zoogloea sp as a film support for trypsin immobilisation, Biochem Eng J, 29 (2006) 258-261.

[51] U. Bora, P. Sharma, K. Kannan, P. Nahar, Photoreactive cellulose membrane - A novel matrix for covalent immobilization of biomolecules, J Biotechnol, 126 (2006) 220-229.

[52] M.Y. Arica, Epoxy-derived pHEMA membrane for use bioactive macromolecules immobilization: Covalently bound urease in a continuous model system, J Appl Polym Sci, 77 (2000) 2000-2008.

[53] T.C. Cheng, K.J. Duan, D.C. Sheu, Application of tris(hydroxymethyl)phosphine as a coupling agent for beta-galactosidase immobilized on chitosan to produce galactooligosaccharides, J Chem Technol Biot, 81 (2006) 233-236.

[54] C. Garcia-Galan, A. Berenguer-Murcia, R. Fernandez-Lafuente, R.C. Rodrigues, Potential of Different Enzyme Immobilization Strategies to Improve Enzyme Performance, Adv Synth Catal, 353 (2011) 2885-2904.

[55] M.J.T. Raaijmakers, T. Schmidt, M. Barth, M. Tutus, N.E. Benes, M. Wessling, Enzymatically Active Ultrathin Pepsin Membranes, Angew Chem Int Edit, 54 (2015) 5910-5914.

Chapter IV Polyketone-based membrane support improves the organic solvent resistance of laccase catalysis

IV.1 Introduction

Enzymes contribute to all *in vivo* biological transformations such as decomposition, synthesis, and modification of specific molecules, which makes them indispensable biocatalysts in all living organisms [1]. Due to their exquisite and intriguing nature, significant investigations have been carried out on the application of enzymes in food, pharmaceutical, biomedical, biofuel, and environmental production industries [2]. Enzymes have evolved to work in cellular aqueous media because native protein structure can be maintained by an intricate balance of noncovalent interactions in water. The addition of organic solvents may disrupt these forces, which may lead to the conformational changes and as a result, enzymes have become intolerant of harsh, organic solvents [3]. Also, the great potential of enzyme catalysts for various organic reactions is limited in aqueous media as a consequence of the poor water solubility of most organic compounds, undesirable hydrolytic side reactions, unfavorable thermodynamic equilibria, and difficulties in product recovery [4]. Significant effort has been extended from both academia and industry to address these limitations and to explore the possibilities of enzyme-catalyzed reactions in organic solvents [5]. Fortunately, although activity is suppressed, some enzymes such as thermolysin [6], engineered proteases [7], lipase [8], and laccase [9] still can work in organic solvents for successful peptides synthesis, for asymmetric (trans)esterifications, and for the coupling of phenols. Furthermore, using protein engineering via physical treatment [10], chemical modification [11], and, more recently, evolutionary molecular engineering [12], the resistance of enzymes against organic solvents has been improved. Unfortunately, these methods must confront the formidable drawbacks of complex modification and expense.

Another complementary and facile way to cope with the insufficient organic solvent resistance of free enzymes as well as the general hindrances of non-reusability and instability

is immobilizing them onto solid supports, which is referred to as the enzyme immobilization process [3, 13]. For this approach, various support systems such as particles, hydrogels, and membranes are available. Among them, polymeric microporous membranes are the most promising candidates since they present easier reusability than particles, lower diffusion barriers than hydrogels, and more readily tunable characteristics than ceramic membranes [14]. Composites obtained by coupling the intrinsic separation ability of membranes with the catalytic activity of enzymes can serve as enzymatic membrane reactors (EMRs) [15]. Until now, most EMR applications involving organic solvents have been biphasic membrane bioreactors, for example, lipase immobilized clay composite membranes for the hydrolysis of olive oil [16]. Such heterogeneous biocatalysis often suffers from the inherently low catalytic rates attributed to the high diffusional barriers of substrates and the transfer for products between two phases. Since pure organic solvents usually have high toxicity toward most enzymes such as laccase, protease and lipase [17], a homogeneous aqueous-organic solvent system can present new possibilities to broaden the potential applications of enzymes by providing both a high mass transfer rate and adequate retention of enzyme activity, thus resulting in high overall reaction rates [18]. Thus far, however, only a few studies have been reported [19]. Iborra et al. immobilized chymotrypsin onto gelatin-α-alumina dynamic membranes, and successfully used these EMRs for peptide synthesis in water-dimethyl sulfoxide (DMSO) solvents [20]. One important hindrance is the lack of robust supporting membranes in organic media.

Ideal supporting membranes for organic solvent-involved EMRs should have the advantages of broad organic solvent resistance and easy enzyme immobilization. Cellulose-based membranes are the most popular natural supports that are used to immobilize enzymes due to the high density of hydroxyl groups, which can serve as useful tethers for the enzyme molecules [21]. The cellulose acetate (CA) membrane is the first reported polymeric membrane able to function in non-aqueous solvents [22]. The regenerated cellulose (RC) membrane is another promising candidate due to its similar outstanding organic solvent-resistance. However, biodegradability via cellulase and poor acid-alkali stability of cellulose materials limit their applicability [23]. The other reported membrane materials utilized for

biocatalysis (whole-cell MBR or free enzyme) in organic media include polyimide [24], polypropylene [25], and polyamide [26], all of which have shown potential for use in EMRs. Moreover, in consideration of the organic solvent-resistance, reports of organic solvent nanofiltration (OSN) membranes [27] made from polyacrylonitrile, polybenzimidazole, and poly(ether-ether-ketone) have proven to be viable possible candidates for EMRs applications. However, applications of all the above candidates are considerably hampered either by the difficulty of introducing reactive groups for enzyme immobilization or by inadequate membrane stability when exposed to harsh organic solvents. Here, a type of microporous membrane, referred to as hydroxylated polyketone (PK-OH), was developed as a novel platform for enzyme immobilization. PK-OH membranes are based on a novel aliphatic polyketone polymer with strong organic solvent-resistance and can be easily fabricated using a simple phase separation process [28] followed by post-modification of the surface ketone groups to hydroxyl groups.

In this work, the enzyme was immobilized on PK-OH, as well as on contrastive RC, via carboxylation of the membrane surface and an active ester reaction [29] which was described in **Chapter III**. Laccase was selected as a model enzyme due to its great potential for use in industry, such as in the decomposition of micropollutants [30]. The mechanism of the high immobilization density of novel PK-OH was investigated in detail. The activities of laccase after immobilization in various media, either in batch or filtration mode were significantly improved. The excellent reusability, stability and durability of this enzyme further demonstrated the potential of PK-OH in EMRs application. This work may open totally new research areas for the usage of polymeric EMRs in homogeneous aqueous-organic solvents including bioremediation and organic synthesis.

IV.2 Experimental

IV.2.1 Materials

Polyketone (PK) polymer (Molecular weight: 200,000 g/mol) was kindly provided by Asahi Kasei in Japan. Regenerated cellulose (RC) membranes with 0.2 μm pores were obtained from Merck Millipore (Darmstadt, Germany). Laccase from *Trametes*

versicolor (powder, light brown, $\geq$ 0.5 U/mg), 2,2'-azino-bis(3-ethylbenzothiazoline-6-sulfonic acid) (ABTS), 2,4,6-trichlorophenol (TCP), bisphenol A (BPA), and fluorescein isothiocyanate labeled bovine serum albumin (FITC-BSA), Bradford reagent for protein assay kit were obtained from Sigma-Aldrich (St. Louis, MO, USA). Polytetrafluoroethylene syringe filter with a pore size of 0.45 µm was purchased from Membrane Solutions (Texas, USA). Dialysis tubing was obtained from Thermo Fisher Scientific (Waltham, USA). Fluorescein 5-isothiocyanate, sebacoyl chloride (SC) and 1-(3-dimethylaminopropyl)-3-ethylcarbodiimide hydrochloride (EDC) were supplied by Tokyo Chemical Industry (Tokyo, Japan). Ultrapure water was produced using a Milli-Q water purification system (Millipore, Bedford, MA, USA). Resorcinol, sodium tetrahydroborate (NaBH$_4$), N-hydroxysuccinimide (NHS), sodium dihydrogenphosphate (NaH$_2$PO$_4$), disodium hydrogenphosphate (Na$_2$HPO$_4$), bovine serum albumin (BSA), sodium dodecyl sulfate (SDS) and all other organic solvents including hexane, methanol (MeOH), ethanol (EtOH), n-propanol (PA), dimethyl sulfoxide (DMSO), acetone, and dimethylformamide (DMF) were purchased from Wako Pure Chemical Industries (Osaka, Japan). All reagents were used as received without further purification and the purity specifications are listed in Table IV.1.

Table IV.1 The purity of reagents used in this work.

Reagents	Purity
MeOH, PA	$\geq$ 99.7 %
EtOH, Acetone, DMF	$\geq$ 99.5 %
DMSO, resorcinol, NaH$_2$PO$_4$, Na$_2$HPO$_4$	$\geq$ 99.0 %
ABTS, TCP, EDC, NHS	$\geq$ 98.0 %
BPA	$\geq$ 97.0 %
Hexane	$\geq$ 96.0 %
SC, Fluorescein 5-Isothiocyanate, SDS, NaBH$_4$	$\geq$ 95.0 %

IV.2.2 Preparation of PK-OH membranes and laccase immobilization

The fabrication process of laccase-immobilized PK-OH membranes is described in Scheme IV.1. First, porous PK membranes were prepared via a non-solvent induced phase separation (NIPS) method described in our previous report [28]. Briefly, PK powder was dissolved in a resorcinol/water solution (65/35 wt.%) to form a 10 wt.% PK dope solution. After degassing, the polymer solution was cast on a clean glass plate. Subsequently, the glass plate was immersed in a MeOH/water (35/65 wt.%) coagulation bath for 20 min. Subsequently, the formed PK membranes were washed in acetone and hexane for 20 min each. To obtain PK-OH membranes, a pristine PK membrane was immersed in a 0.5 wt.% $NaBH_4$ aqueous solution for 5 min to reduce the ketone groups on the membrane surface to hydroxyl groups as outlined in our previous study [31]. Furthermore, the membrane was washed thoroughly using water, acetone, and hexane, and was finally air dried for storage.

Laccase was covalently immobilized using a strategy described in our previous work [29]. Briefly, the pristine PK-OH membrane ($24.53\ cm^2$) was immersed in a 1 wt.% SC hexane solution to introduce carboxyl groups (referred to as PK-COOH). Subsequently, after the activation of the carboxyl groups with EDC and NHS (referred to as PK-NHS), the membrane was immersed in 5 mL of 50 mmol/L phosphate buffered saline (PBS) solution (pH 7.6) containing 5 g/L laccase. Finally, the membrane was washed with a 2 mL of 3 wt.% NaCl aqueous solution for 1 h and 2 mL of 0.3 wt.% SDS aqueous solution for another 1 h to remove the physically adsorbed laccase. The obtained membranes (referred to as PK-OH-laccase) were stored in a PBS solution (pH 7.6) at 4 ºC until further use. The PK immobilizing laccase using the same procedure will be referred to here as PK-laccase. For comparison, physically laccase-adsorbed membranes: PK-P-laccase and PK-OH-P-laccase, were prepared only by immersing the PK and PK-OH membranes into a 5 g/L laccase solution and then using a PBS solution for washing and storing.
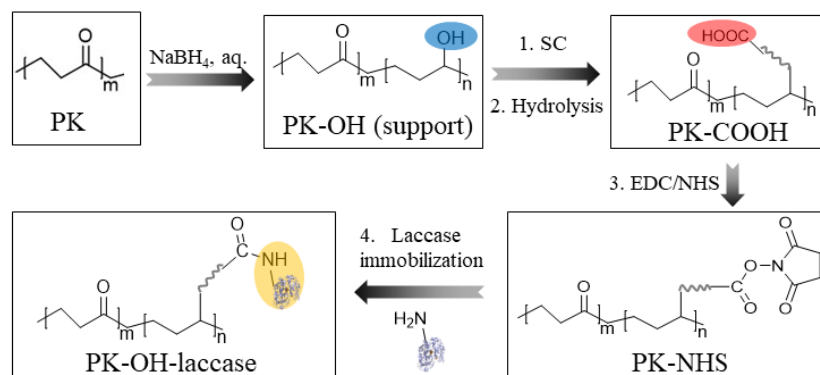
Scheme IV.1 Schematic process for the reduction of PK to PK-OH and the covalent immobilization of laccase on PK-OH.

IV.2.3 Membrane characterizations

The chemical properties of the membrane were analyzed via attenuated total reflection Fourier-transform infrared (ATR-FTIR) spectroscopy (Nicolet iS5, Thermo Fisher Scientific, Waltham, MA, USA) and X-ray photoelectron spectroscopy (XPS; JPS-9010 MC, JEOL, Tokyo, Japan). The surface morphology was observed using field emission scanning electron microscopy (FE-SEM; JSF-7500F, JEOL). Before analysis, each sample was freeze-dried (FD-1000, Tokyo Rikakikai, Tokyo, Japan) and osmium coated (Neco-STB, Meiwafosis, Tokyo, Japan). The hydrophilicity of the membrane was characterized using the static contact angle, which was accomplished via the use of a contact angle goniometer (Drop Master 300, Kyowa Interface Science, Saitama, Japan). The detailed conditions for the above measurements were the same as those previously reported [29]. In addition, fluorescein labeled laccase (FTIC-laccase) was immobilized on the membrane using the same method employed for laccase, in order to visualize the interaction between laccase and the membranes. FTIC-laccase was prepared using a procedure similar to one found in the literature [32]. Specifically, 0.2 M NaH_2PO_4 and 0.2 M Na_2HPO_4 solutions were first prepared and mixed to produce 100 mL of buffer at pH 8.6. Next, 0.01 g fluorescein 5-isothiocyanate and 0.1 g laccase were added. After stirring for 3 h at 25 °C, the product was dialyzed in a buffer, pH 7.4, for 72 h via a dialysis bag with a molecular weight cut-off that ranged from 6000-8000. The final product was obtained after filtering with a 0.45 µm filter,

and it was then stored in a refrigerator for further use. FITC-BSA, as a protein model, was used simultaneously, to study the universality of the interaction between protein and the membrane. Subsequently, the immobilized FTIC-laccase and FITC-BSA were analyzed using confocal laser scanning microscopy (CLSM; FV1000, Olympus, Tokyo, Japan). The pure water permeability was measured using a lab-made filtration cell in gravity drive mode [29] to detect any pore blocking caused by the immobilization of laccase. To be specific, gravity-driven filtration (10 cm water column) was used, and the membrane area was 4.9 cm^2. Milli-Q water at pH 8 was used for determination. The mean pore size of the membrane was measured using a liquid-liquid porometer (LLP-1100A, Porous Materials, Ithaca, NY, USA).

IV.2.4 Enzyme amount quantification

Laccase concentration was measured using the Bradford assay with BSA as a standard protein (Fig. IV.1). We added 0.5 mL of a protein solution to 1.0 mL of Bradford working reagent, and incubated the combination for 5 min. The absorbance was recorded at a wavelength of 595 nm using a UV-Vis spectrophotometer (V-630, Jasco, Tokyo, Japan). PBS solution was used as the blank sample for the laccase solution before and after immobilization. A 3 wt.% NaCl aqueous solution was the blank for the washing solution. The immobilized amount of laccase ($A_{laccase}$) was determined as shown in equation (IV.1).

$$A_{laccase} = (C_b - C_a) V_b - C_w V_w \qquad \text{(IV.1)}$$

The immobilized density is shown in equation (IV.2).

$$Density \ (\mu g/cm^2) = A_{laccase}/A_{membrane} \qquad \text{(IV.2)}$$

In equation (1), C_b, C_a, and C_w (ppm) are the concentrations of the laccase solution before immobilization, after immobilization and after washing, respectively. V_b and V_w (mL) are the volumes for laccase immobilization and washing, respectively. In equation (IV.2), $A_{membrane}$ (cm^2) is the area of the supporting membrane.

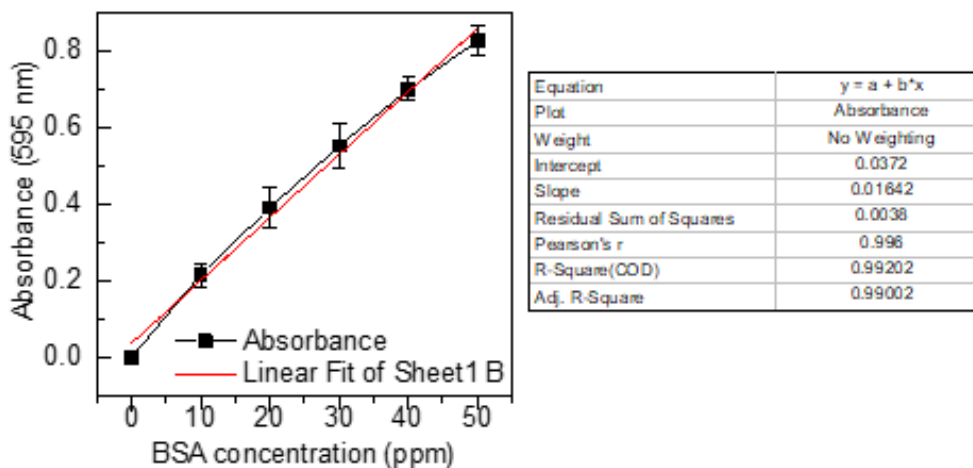| Equation	y = a + b*x
Plot	Absorbance
Weight	No Weighting
Intercept	0.0372
Slope	0.01642
Residual Sum of Squares	0.0038
Pearson's r	0.996
R-Square(COD)	0.99202
Adj. R-Square	0.99002

Fig. IV.1 Standard curve of BSA for Bradford assay determination. All the experiments were repeated three times to prevent the experiment errors.

IV.2.5 Batch activity determination

The activities of laccase in aqueous or aqueous-organic solvents were determined by monitoring the oxidation rate of ABTS to $ABTS^+$. 150 µL free enzyme (250 ppm) or a laccase immobilized membrane with a diameter of 9 mm was added into the 3 mL solution (0.5 mM ABTS at pH 5.5 in given types of media) and allowed it to react for 5 min at 20 °C. The increase in absorbance at 420 nm (ΔAbs_{420nm}; extinction coefficient $\varepsilon_{420} = 36.0$ mM^{-1} cm^{-1}) was recorded using a UV-Vis spectrometer. The cuvette used had an effective length of 1 cm. One enzyme unit (U) was defined as the amount of enzyme needed to catalyze 1µM of ABTS substrate per minute. The specific activity of the free and immobilized laccase was calculated as shown in equation (IV.3).

$$\textbf{\textit{Specific activity}} \, (\textbf{U/mg}) = \ \textbf{1000} \cdot \textbf{V} \cdot (\Delta A_{sample} - \Delta A_{blank}) / \, (\varepsilon_{420} \cdot t \cdot A_{laccase})$$

$$(IV.3)$$

where ΔA_{sample} and ΔA_{blank} are the change in absorbance of the sample and blank at 420 nm; V (mL) is the volume of the reaction solution, and here the value is 3; t (min) is the reaction time.

In addition, the activity retention was defined as the actual activity of the immobilized laccase divided by the theoretical activity of the immobilized laccase. It can be calculated in equation (IV.4).

$$Activity\ retention\ (\%) =\ 100 \cdot Specific\ activity_{immobilized}\ /$$
$$Specific\ activity_{free} \qquad\qquad (IV.4)$$

where *Specific activity_immobilized* and *Specific activity_free* are the specific activities of the immobilized and free laccase, respectively.

Furthermore, the kinetic parameters including V_{max} (the maximum reaction activity), K_m (the Michaelis-Menten constant), K_{cat} (the turnover number of the enzyme) and K_{cat}/K_m (the catalytic efficiency) were determined from the Michaelis-Menten equation using different concentrations of ABTS (from 0.05 to 5.0 mM) solution as substrates in aqueous and aqueous-organic solvents.
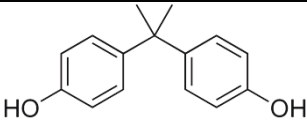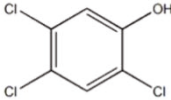
IV.2.6 Batch oxidation of TCP and BPA

Laccase has a great capability to detoxify phenolics, such as pesticides (i.e., TCP) and plasticisers (i.e., BPA) in contaminated effluents. These compounds have a significant impact on human health [33]. In this portion of the study, TCP and BPA were chosen as targets, and the related properties are listed in Table IV.2. Adsorption is the most common way to remove them from water. Usually, organic solvents are used to regenerate adsorbents [34], which cause the organic solvents to become highly concentrated with micropollutants. To promote further biodegradation, the catalysis of laccase in organic solvent-included media should be developed and investigated. Additionally, a higher substrate concentration can efficiently improve the conversion rate, the application of which has appeared in no other reports. In consideration of the limited water solubility of BPA and TCP (< 0.5 g/L), an aqueous media containing 20 vol% DMSO was used to achieve a high concentration of 1.4 g/L. The degradation ability was tested using both free and immobilized laccase.

Either 53 μL of free laccase (5000 ppm) or a laccase immobilized membrane with a diameter of 25 mm was added into solutions that contained 10 mL of either a TCP or a BPA solution. To eliminate the adsorption removal mechanism, another laccase immobilized

membrane was heated at 80 °C for 30 min to deactivate the laccase, and was used as the blank. UV-Vis spectrophotometry was used to qualitatively detect the products. In addition, for BPA, 3 g/L ABTS was added to enhance the catalysis. The change in TCP or BPA concentration was analyzed via high-performance liquid chromatography (HPLC) utilizing a Shim-pack GIST C18 column (4×250 mm, Shimadzu GLC, Tokyo, Japan) and a UV detector (SPD-20A, Shimadzu, Kyoto Japan). The wavelengths for the detections of TCP and BPA detection were 298 and 280 nm, respectively. Isocratic elution was performed by pumping acetonitrile and water (50:50 v/v) at a flow rate of 0.6 mL/min at 40 °C. The assay solution for TCP was diluted 11-fold with DMSO. Before analysis, the solution was filtered with a Nylon membrane (0.22 μm pore size) to remove impurities for a final analysis volume of 30 μL.

Table IV.2 Physicochemical properties of micropollutants.

Name	BPA	TCP
Structure		
Molecular weight (g/mol)	228.3	197.4
Log D	3.32	3.69
Water solubility (g/L)	0.3	0.5
PKa	9.6	6.23

IV.2.7 Enzymatic membrane bioreactors filtration performance

To investigate the potential of PK-OH-laccase for use as a practical EMR, the catalytic activity of PK-OH-laccase in filtration mode was adopted using a dead-end membrane filtration apparatus shown in Fig. IV.2. The flow rate of the substrate solution was adjusted from 0 to 3 mL/min using a syringe pump. The flow rate of 0 mL/min refers to the batch

mode. The effect of the flow rate on the activities of laccase was determined by comparing the activity in batch mode ($Activity_{batch}$) with that in filtration mode ($Activity_{filtration}$). The relative activity was defined as shown in equation (IV.5).

$$Relative\ activity\ (\%) = 100 \cdot Activity_{filtration} / Activity_{batch}$$

(IV.5)

In addition, the reusability, stability, and durability of immobilized laccase, which are essential criteria in practical applications, all were tested towards ABTS. The reusability was also measured towards TCP and BPA. After one cycle of catalysis, PK-OH-laccase was washed with MeOH for 10 min before being reused.
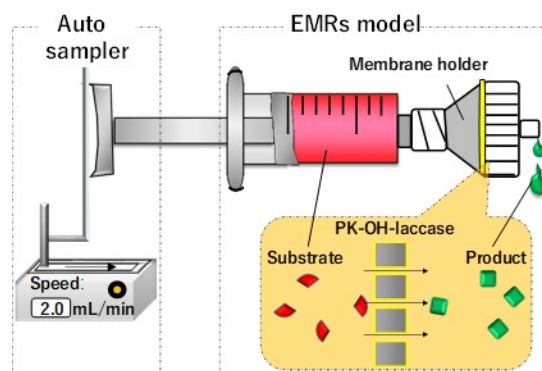
Fig. IV.2 Devices for determining the activity of the membranes in the filtration mode of EMRs.

IV.3 Results and Discussion

IV.3.1 Membrane characterization

First, the chemical properties of the fabricated membranes were evaluated by measuring the FTIR and XPS spectra. The FTIR spectrum (Fig. IV.3(a)) of PK-OH consisted of a very strong peak at 3300 cm^{-1}, ascribed to the hydroxyl groups (-OH), whereas this hydroxyl peak was largely reduced in the spectrum of PK-COOH, indicating sufficient conversion of the hydroxyl groups. However, the characteristic carbonyl peaks associated with newly generated carboxylic ester groups and carboxylic acid groups of a modified SC molecule layer at around 1720 cm^{-1} could

not be observed with PK-COOH, because of the overlap of the strong absorbance of the ketone groups at approximately 1690 cm^{-1} from the membrane matrix. The subsequent EDC-NHS activation of PK-COOH caused little change in the FTIR spectrum, but the following laccase immobilization resulted in the reappearance of a strong peak at 3300 cm^{-1}, coming from the N-H stretch of the amines of laccase [35]. In addition, a new and small peak at 1539 cm^{-1}, ascribed to amide II, was also seen with the obtained PK-OH-laccase, and was attributed to the peptide bond of laccase itself. A characteristic amide I peak at approximately 1670 cm^{-1} was not found due to the existence of a strong ketone peak at approximately 1690 cm^{-1}. Furthermore, the XPS spectra indicated the appearance of a nitrogen signal after the immobilization of laccase (Fig. IV.3(b) and Table IV.3). The nitrogen signal can be attributed to the immobilized laccase, since just after the EDC/NHS activation (i.e. PK-NHS), the membrane showed no signal for nitrogen. Meanwhile, most of nitrogen came from the peptide bonds indicted by the nitrogen peak-split result in Fig. IV.4. The reduction in the degree of the surface ketone groups was measured to be 47 % based on the curve-fitting analysis of the carbon peak-spilt result (Fig. IV.3(c) and (d)). The observed changes in surface chemistry were consistent with the contact angle measurements of water droplets on the membranes under air. PK-OH showed an even higher hydrophilicity compared to the pristine hydrophilic PK membrane due to the presence of the hydroxyl groups, while PK-OH-laccase became less hydrophilic than PK-OH due to the introduction of laccase which contains hydrophobic portions (Table IV.3). In addition, the membrane permeability of PK-OH-laccase was 89.0 % of the permeability of PK-OH and the average pore size was barely changed (Table IV.3). As shown in Fig. IV.3(e) and (f), the FE-SEM surface images of the two membranes are similar and consist of fiber-like porous structures. These results indicate the successful surface modifications (i.e. hydroxylation and enzyme immobilization) without obvious changes in the pore structure.
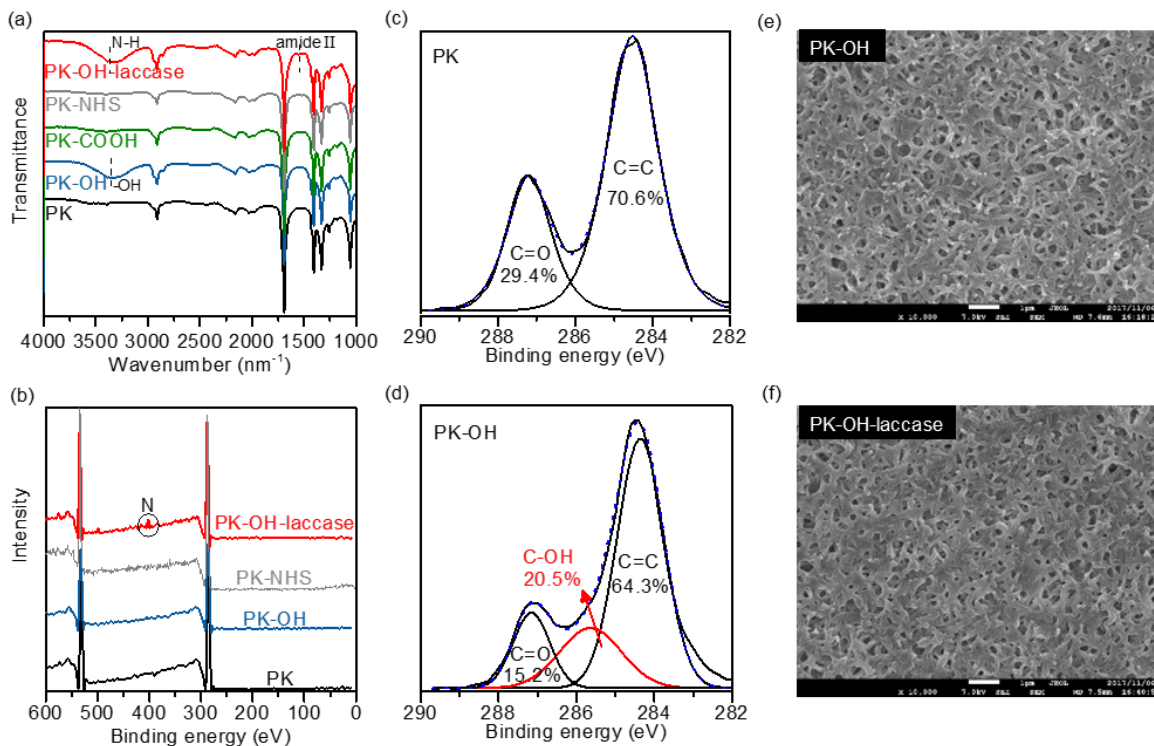
Fig. IV.3 Characterization of the pristine and modified membranes. (a) FTIR, (b) XPS spectra. XPS peak-split analysis of carbon in (c) PK and (d) PK-OH membranes. SEM images of (e) PK-OH and (f) PK-OH-laccase membrane surface.

Table IV.3 Elemental ratio of membranes evaluated using XPS data, water contact angles, and water permeabilities of the fabricated membranes. All the experiments were repeated three times to prevent the experiment errors.

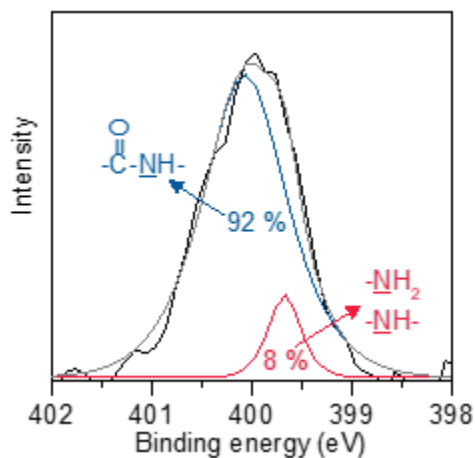| Membranes	Elemental ratio (relative atom%)			Contact angle (°)	Permeability (LMH/0.01 bar)	Pore size (nm)
	C	O	N			
PK	76.9 ± 0.2	23.1 ± 0.2	0	48.0 ± 2.2	21.6 ± 1.3	62 ± 5
PK-OH	76.7 ± 0.3	23.3 ± 0.3	0	27.7 ± 1.2	22.7 ± 4.1	65 ± 4
PK-NHS	78.1 ± 0.2	21.9 ± 0.2	0	No data	No data	No data
PK-OH-laccase	71.0 ± 0.3	23.6 ± 0.3	5.4 ± 0.2	36.3 ± 1.5	20.2 ± 0.5	61 ± 3

Fig. IV.4 The XPS peak-split analysis of the nitrogen peak on PK-OH-laccase. Black line was the measured nitrogen result. The blue line, red line and grey line represented the nitrogen from peptide bonds, amino bonds and the fitting result of both, respectively.

IV.3.2 Catalytic activity of laccase in an aqueous solvent

To evaluate the superiority of PK-OH as a support, a RC membrane was used as a control. Similar to PK-OH, the RC membrane is another competitive substrate due to its high resistance to organic solvents, a significant number of hydroxyl groups, and a highly porous membrane structure. Table IV.4 displays the catalytic activity of the laccase immobilized membranes. As shown, PK-OH-laccase demonstrated a much better comprehensive performance than RC-laccase in terms of laccase density, specific activity, and activity retention. The immobilization density of PK-OH-laccase (462 µg/cm^2) was higher that of previously reported membranes such as polyvinylidene fluoride (20–250 µg/cm^2) [36], and polyethersulfone (50–130 µg/cm^2) [37]. It would be reasonable to assume that the mixed surface chemistry of PK-OH, i.e., approximately 50/50 ketone/hydroxyl groups, was mainly responsible for the achieved high enzyme immobilization amount. Compared with the chemistry of RC, which has a main chain that is rich in hydroxyl groups, the ketone groups of PK-OH were speculated to facilitate enzyme immobilization via adsorption. The pristine PK

membrane was found to contain a lot of ketone groups that can be used for effective enzyme immobilization solely by physical adsorption in the absence of covalent-bonding via spacers (SC in this work). The obtained PK-P-laccase membrane showed a high enzyme density (403 μg/cm^2) similar to PK-OH-laccase, however, a relatively low activity retention (7.7%), which may have been caused by the lack of a flexible spacer between the membrane and the laccase. On the other hand, direct adsorption, rather than covalent attachment, may more easily change the enzyme conformation. Meanwhile, the RC-laccase may have shown the lowest activity retention because of the worst distribution of laccase on RC, which was caused by the lack of adsorption during immobilization.

Table IV.4 Performances of free laccase, PK-OH-laccase, RC-laccase, and PK-P-laccase in aqueous solution. All the experiments were repeated three times to prevent the experiment errors.

	Density (μg/cm^2)	Specific activity (U/mg)	Activity retention (%)
Free laccase	No data	360 ± 20	No data
PK-OH-laccase	462 ± 20	44 ± 3	12.2 ± 0.2
RC-laccase	281 ± 11	14 ± 2	3.9 ± 0.1
PK-P-laccase	403 ± 31	28 ± 6	7.7 ± 0.2
RC-P-laccase	0	0	No data

PK-OH-laccase and RC-laccase indicated covalently attached laccase on PK-OH and RC membrane, respectively. PK-P-laccase and RC-P-laccase were physical adsorption of laccase on PK-OH and RC membrane, respectively.

As shown in Table IV.5 and in Fig. IV.5(a), PK-OH-laccase showed values for V_{max} and K_{cat} were higher than that of RC-laccase due to a higher laccase density, which suggests a great number of available active sites for catalysis. However, the K_m of PK-OH-laccase was offset by the higher laccase loading as well as by its smaller pore size (pore size of RC-laccase: 153 ± 5 nm), which indicated higher diffusion resistance. As

a consequence, the K_{cat}/K_m of the two was comparable. In addition, the immobilization obviously altered neither the optimal operation pH nor the temperature of free laccase and PK-OH-laccase (Fig. IV.6).

Overall, the comparison between PK-P-laccase, PK-OH-laccase and RC-laccase with decreasing numbers of ketone groups and an increasing number of hydroxyl groups implies that both physical adsorption and covalent-bond reactions contribute to enzyme immobilization. The spacer-tethered enzymes with restricted conformational transition were considered to maintain activity more easily by preventing fatal denaturation.

Table IV.5 Kinetic parameters of free laccase, PK-OH laccase and RC-laccase in water. All the experiments were repeated three times to prevent the experiment errors.

	V_{max} (μmol min^{-1})	K_m (μM)	K_{cat} (μmol min^{-1} mg^{-1})	K_{cat}/K_m (L min^{-1} mg^{-1})
Free laccase	7.7 ± 0.8	32.6 ± 3.0	205.0 ± 21.1	6.3 ± 1.2
PK-OH-laccase	13.6 ± 0.4	193.0 ± 25.0	46.2 ± 8.5	0.2 ± 0.1
RC-laccase	3.2 ± 0.5	61.8 ± 1.2	17.9 ± 4.8	0.3 ± 0.1
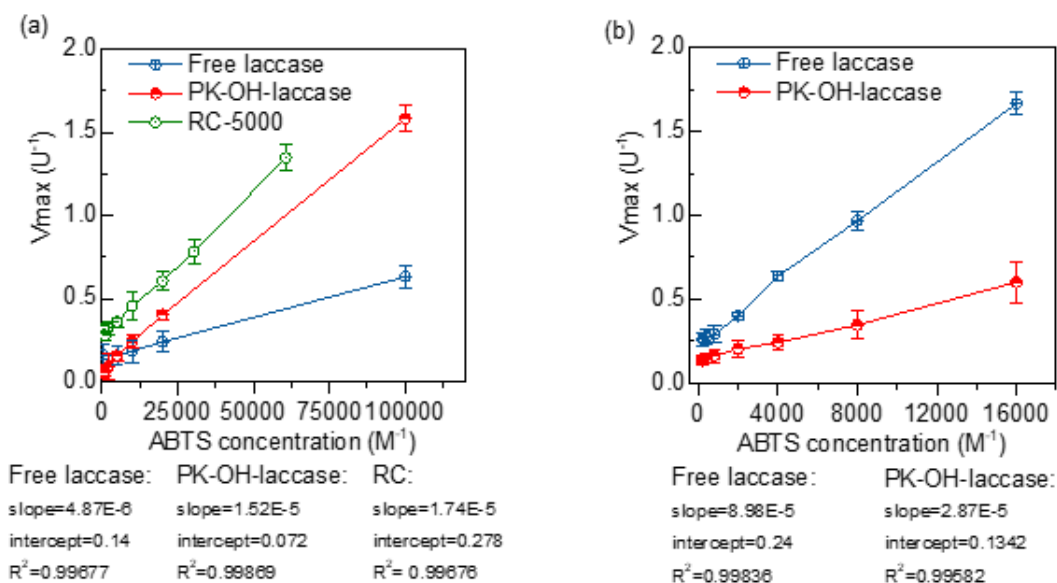
Fig. IV.5 Line weaver-Burk plots of free laccase and PK-OH-laccase measured in (a) aqueous medium and (b) 20 vol% DMSO for kinetic parameter determination. All the experiments were repeated three times to prevent the experiment errors.

Fig. IV.6 Effect of temperature and pH on the activity of free and immobilized laccase toward ABTS. The specific activity at 20 °C and pH 5.5 was considered to be the standard and its value was 100%. All the experiments were repeated three times to prevent the experiment errors.

The enzyme density can be facilely adjusted by using different enzyme concentrations in the preparation process (step 4 in Scheme IV.1). The relationship between enzyme densit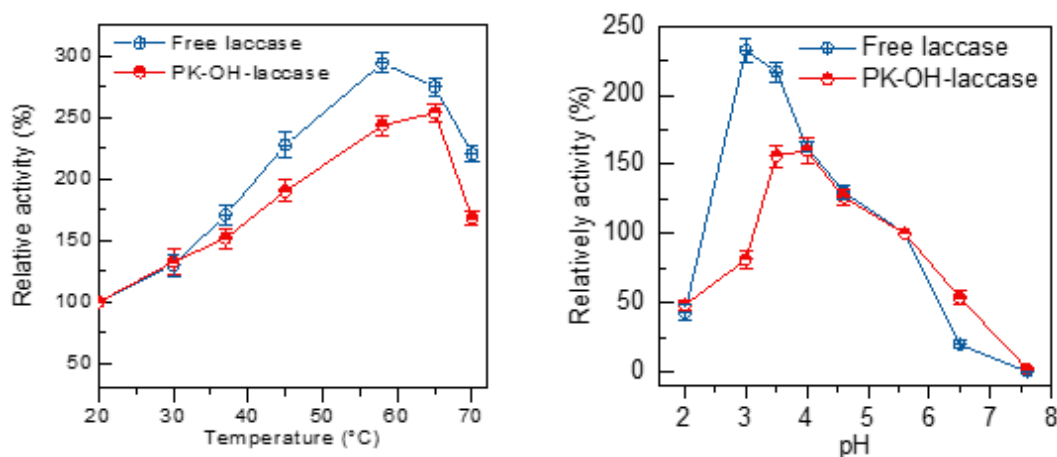y and catalytic activity was investigated (Table IV.6). By increasing laccase concentration (100-5000 ppm) for immobilization, the density and total activity of immobilized enzymes was also increased, whereas the specific activity and activity retention was decreased and approached a saturated value at 5000 ppm. This tendency is in line with other reports [29, 38]. This phenomenon was expected and can be explained by enzyme density that was too high, which restricted the enzyme flexibility and mobility necessary for catalysis. However, to guarantee a high level of removal efficiency of target pollutants in practical EMR applications, high levels of enzyme density with high total activity is favorable, which is why 5000 ppm laccase was chosen for the PK-OH-laccase in this work.

Table IV.6 Performances of immobilized laccase with different laccase concentration during immobilization. All the experiments were repeated three times to prevent the experiment errors.

Laccase concentration in step 4 (ppm)	Density ($\mu g/cm^2$)	Specific activity (U/mg)	Activity retention (%)	Activity (U)
5000	462 ± 20	44 ± 3	12.2 ± 0.2	12.5 ± 0.1
1000	279 ± 12	45 ± 5	12.6 ± 0.2	7.7 ± 0.2
500	184 ± 11	50 ± 4	14.2 ± 0.4	5.7 ± 0.1
100	25 ± 5	71 ± 5	20.1 ± 0.5	1.1 ± 0.1

Protein immobilization using FTIC-laccase was further carried out to visualize the proposed adsorption effect on enzyme immobilization. The fluorescence of FITC was

observed using CLSM. Fig. IV.7(a)–(c) show the physical adsorption of FITC-laccase on the membranes. The RC membrane showed very little adsorption (Fig. IV.7(a)), while the PK membrane adsorbed a significant amount of laccase, and the amount on PK-OH was intermediate (Fig. IV.7(b) and (c)). These results indicate that the attractive force of PK was much stronger than that of either PK-OH or RC. Most of the adsorbed macromolecules could be washed out by solvent rinsing as shown in Fig. IV.7(a')-(c'). Fig. IV.7(d)–(f) show the covalent attached FITC-laccase on the membrane surface. The strong intensity observed for PK was actually caused by physical adsorption since there were no reactive sites on the surface of PK for covalent-bond attachment. In addition, with the help of the hydroxyl groups, more FITC-laccase can be immobilized via covalent bonds on the PK-OH and RC membranes compared to the corresponding physical adsorption, and these bonds remained stable after thorough solvent washing as shown in Fig. IV.7(d') and (e'). This demonstrated the excellent stability and thus the working feasibility of the PK-OH-laccase in organic solvents. In addition, FTIC-BSA was used as another model and the properties of BSA and laccase proved to be similar (see Table IV.7). The same tendency (see Fig. IV.8) of FTIC-BSA with FTIC-laccase is reflective of universal interactions between proteins and membranes.

Mateo et al. reported that the electrostatic interaction between enzymes and support surfaces improved the immobilization efficiency [39]. Therefore, it can be speculated that the attraction between laccase and ketone groups existed and was expected to assist in the immobilization of laccase onto hydrophilic PK-OH. On the contrary, numerous studies on the design of surfaces that resist protein adsorption have verified that without other attraction forces between protein and surface, hydroxyl groups can efficiently repel protein efficiently due to high levels of hydration of hydroxyl groups [40].
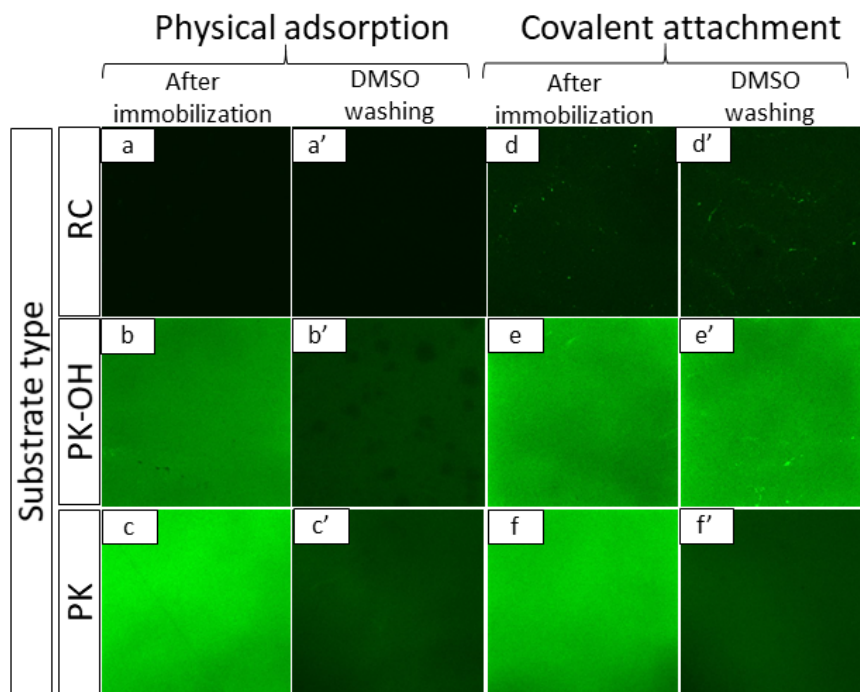
Fig. IV.7 CLSM images of the surfaces of RC, PK-OH, and PK membranes either adsorbing or covalently immobilizing FTIC-laccase.

Table IV.7 The pI, Mw and molecular size of laccase and BSA

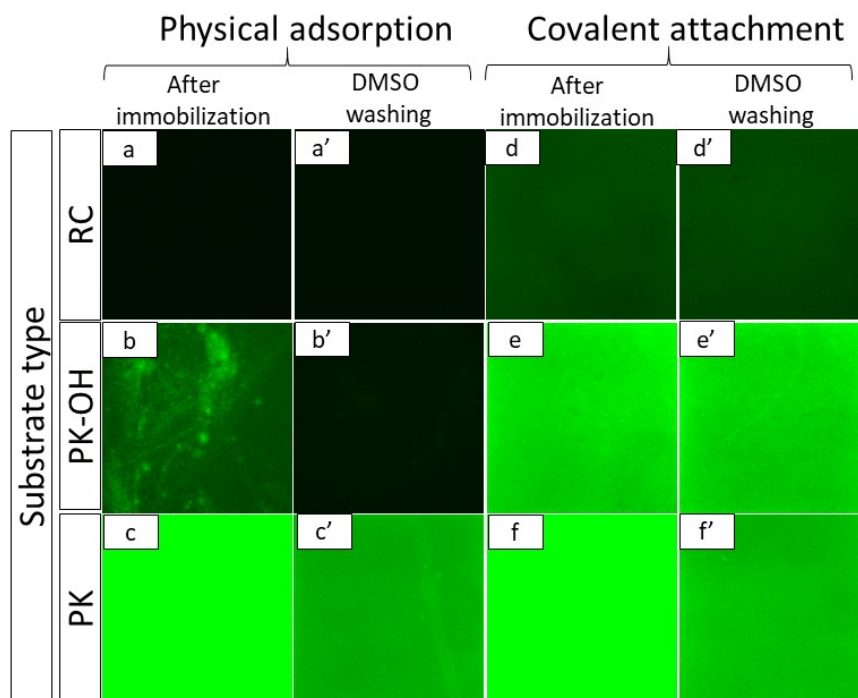|	pI	Mw	Size
BSA	4.7	66.5 KDa	$5 \times 7 \times 5$ nm
Laccase	3 ~ 5 [1]	63.0 KDa	$7 \times 5 \times 5$ nm [2]

Fig. IV.8 CLSM images of the surface of RC, PK-OH, and PK membrane adsorbing or covalently immobilizing FTIC-BSA.

Fig. IV.9 shows the proposed mechanism for the immobilization process. The attraction forces of the ketone groups on PK-OH, which are expected to be mainly hydrogen bonds, promoted the adsorption of laccase. The adsorbed laccase easily reacted with the carboxyl groups of the SC molecules (Fig. IV.9(a)). Furthermore, the hydroxyl groups of RC repelled the migration of laccase to the membrane surface (Fig. IV.9(b)). Thus, higher amounts of laccase were immobilized in a better distribution, which contributed to the high activity retention of PK-OH-laccase. This attraction force appeared to exist between many types of proteins and PK-OH, showing no restrictions for the types of immobilized enzymes unlike other methods, such as layer-by-layer, which requires corresponding charges for the electrostatic attraction [33]. Therefore, the PK-OH membrane is expected to be the most promising support for enzyme immobilization for applications in aqueous-organic solvents.
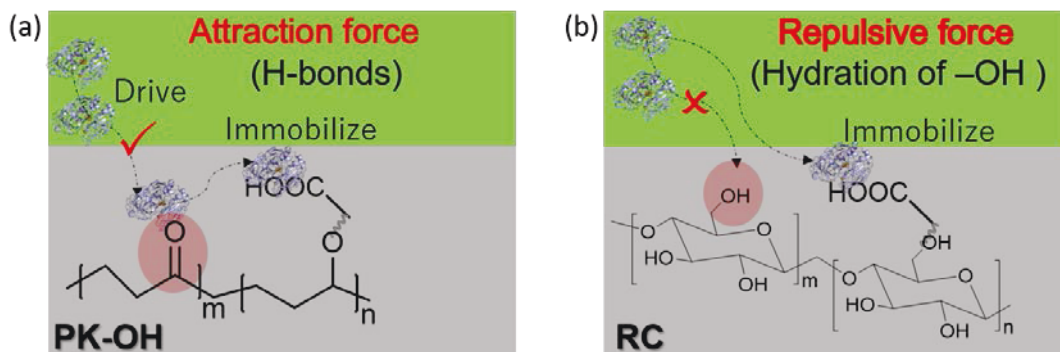
Fig. IV.9 Comparison of the protein immobilization process between the (a) PK-OH and (b) RC membranes.

IV.3.3 Catalytic activity of laccase in aqueous-organic solvents

To display the catalytic activity of laccase in harsh environments, several types of aqueous-organic solvents containing 20 vol% organic solvents were employed for ABTS catalysis (Fig. IV.10(a)). To eliminate the effect of pH, the final pH of all the solutions was maintained at 5.5. The organic solvents utilized here can be roughly divided into alcohols and non-alcohols. The values of the logarithm partition coefficient in the octanol-water system (logP) are shown in Table IV.8. The activity sequence of free laccase for aqueous-alcohol solvents was MeOH > EtOH > PA, which implied that higher hydrophobicity (higher logP) led to lower enzyme activity. This tendency was in agreement with other reports [9]. However, for aqueous non-alcoholic solvents, there was no relationship between logP and enzyme activity due to an entirely different mechanism [41]. The low activity of laccase in aqueous-DMF may be attributed to the strong ripping force of water around an enzyme, which is necessary for catalysis. This work focused on the immobilization of laccase on PK-OH membranes with the overall aim of improving its activity in aqueous-organic solvents. The results demonstrated the superior resistance of immobilized laccase toward organic solvents. Moreover, the activity of immobilized laccase was 1.2–3.5 times higher than the activity of free laccase. This may be due to the hydrophilicity of the PK-OH membrane assisting with the preservation of water molecules around laccase, which provided a much better microenvironment for conformation maintaining. The results were similar to those for the

chitosan-immobilized laccase [42] and nylon-immobilized cytochrome *c* [43]. At the same time, the kinetic parameters of immobilized and free laccase were measured in 20 vol% DMSO, as shown in Fig. IV.5(b) and in Table IV.9. The K_m of PK-OH-laccase (213.9 µM) was lower than that of free laccase (370.0 µM), suggesting a higher level of substrate affinity for immobilized laccase. This opposes to the trend in an aqueous solution environment (see Table IV.5), which is natural and comfortable for the free enzyme. In addition, the K_{cat}/K_m values of immobilized and free laccase approximated in 20 vol% DMSO, while the difference between them was approximated 30-fold in an aqueous solution. This indicates that the protection of the enzyme by membrane immobilization helps improve catalytic activity retention against harsh organic solvent condition. The activity improvement indicated that the PK-OH membrane was an appropriate support matrix for applications in aqueous-organic solvents.

The other advantage of applying mixed solvents to enzyme catalysis was the use of flexibly adjusted ratios of aqueous and organic solvents. This provides various solvent properties, which helps to regulate the product properties in organic synthesis [44, 45]. Since DMSO is widely utilized as a solvent in biological areas, it was used as a model organic solvent. Fig. IV.10(b) shows the effect of the DMSO concentration on catalytic activity. Increasing the DMSO concentration reduced the activity of free laccase. However, immobilization onto the PK-OH membrane alleviated this decrease, particularly for a 30 vol% DMSO content, due to a better microenvironment for the immobilized laccase.
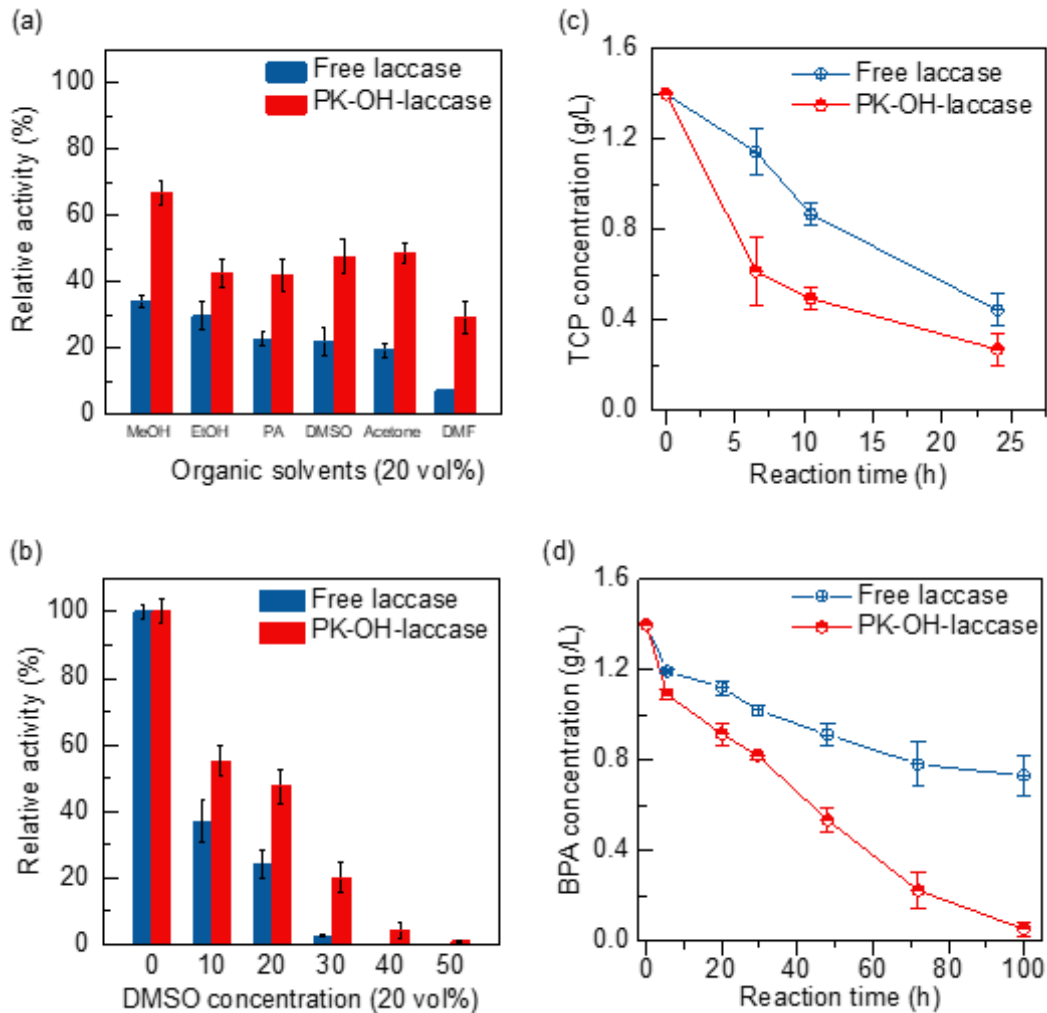
Fig. IV.10 Catalytic activity of PK-OH-laccase in homogeneous aqueous-organic solvents. The activity of free enzyme and PK-OH-laccase in an aqueous PBS solution was considered the standard (100 %) for evaluation. (a) Effects of the type of organic solvents on catalytic activity. (b) Effect of DMSO concentration on the catalytic activity. Time dependence of (c) TCP and (d) BPA removal percentages during the catalytic reaction using free laccase and PK-OH-laccase in 20 vol% DMSO at 20 ºC. All experiments were repeated three times to prevent the experiment errors.

Table IV.8 LogP of the solvents used in this study.

	H$_2$O	MeOH	EtOH	n-PA	DMSO	Acetone	DMF
logP*	No data	−0.74	−0.32	0.34	−1.35	−0.24	−0.46

*logP is the logarithm partition coefficient in the octanol-water system.

Table IV.9 Kinetic parameters of free laccase and PK-OH laccase in 20 vol% DMSO.

	V$_{max}$	K$_m$	K$_{cat}$	K$_{cat}$/K$_m$
	(μmol min^{-1})	(μM)	(μmol min^{-1} mg^{-1})	(L min^{-1} mg^{-1})
Free laccase	4.2 ± 0.8	370.0 ± 3.0	111.1 ± 21.1	0.3 ± 0.1
PK-OH-laccase	7.5 ± 0.5	213.9 ± 1.2	25.5 ± 4.8	0.1 ± 0.1

In practice, the product of TCP via laccase catalysis is light pink, presenting a peak maxima at 277 nm (Fig. IV.11), which is presumably attributed to the harmless dichloro-1,4-benzoquinone product [33]. Through the calculation (HPLC results in Fig. IV.12), Fig. IV.10(c) shows that the immobilized laccase had a removal percentage that was 1.6 ~ 1.9 times higher than that of free laccase due to the better protection of the immobilized laccase against DMSO. Meanwhile, the deactivated PK-OH-laccase can not remove TCP, which led us to believe that the improved removal ability came from the enhanced catalysis after immobilization. Another phenolic substrate, BPA, identified as an endocrine disruptor, is an important industrial chemical, mainly in the manufacture of polycarbonates, epoxy resins, and polyester resins [46]. The catalytic process appears in Fig. IV.13. For individual ABTS, or ABTS and its product, a peak developed at 4.3 min (Fig. IV.13(a) and (b)). After adding BPA, a peak at 15.2 min emerged, and was precisely identified as BPA (Fig. IV.13(c) and (d)). In Fig. IV.13(e) and (f), the product obtained using BPA catalysis appears at 5.0–6.0 min. Notably, we focused on the decreasing area of the BPA peak for calculating the removal rate. Fig. IV.10(d) displays the time

dependence of the BPA concentration during catalysis using laccase, and the catalytic percentage of PK-OH-laccase was 1.2 ~ 2.0 times higher than that of free laccase. Meanwhile, the blank deactivated PK-OH-laccase showed no ability to remove BPA. The above results showed the improved organic solvent resistance of laccase catalysis is surely achieved by using a polyketone based membrane support.
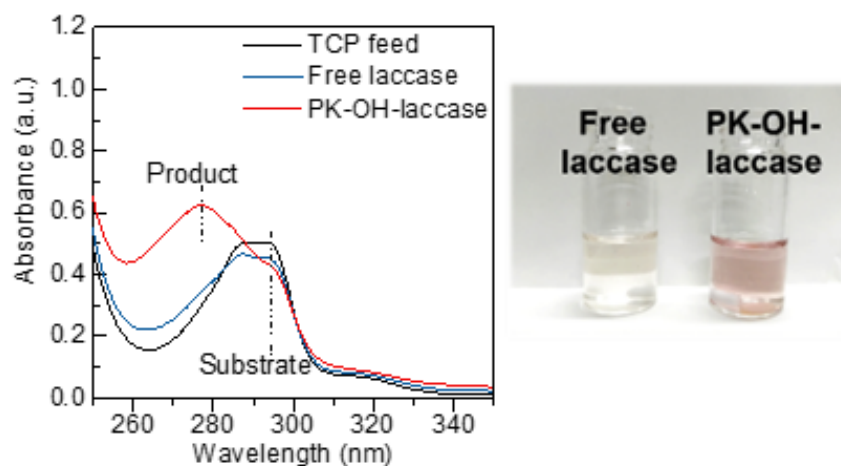

Fig. IV.11 UV spectra and photo of TCP and its pink product formed by laccase catalysis.
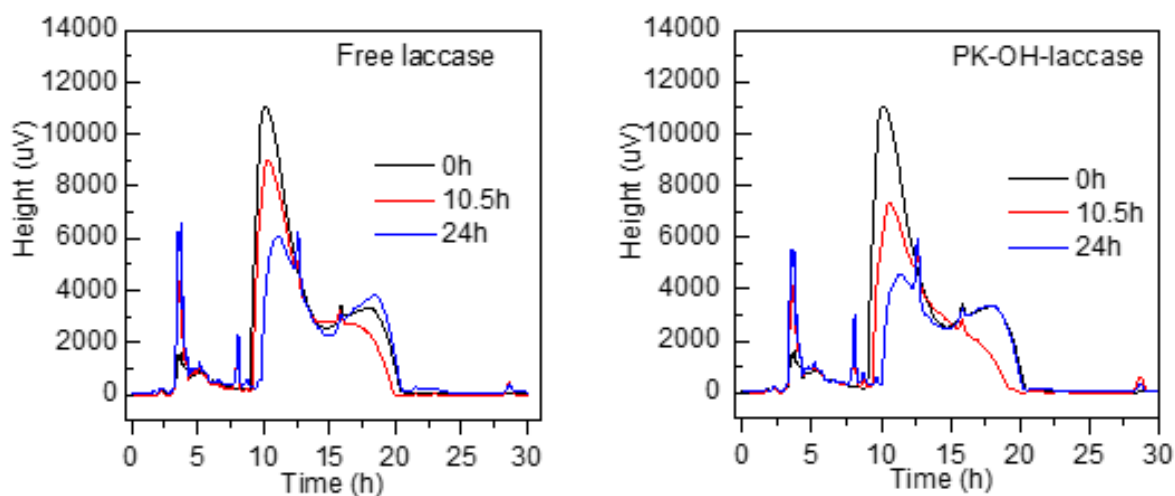

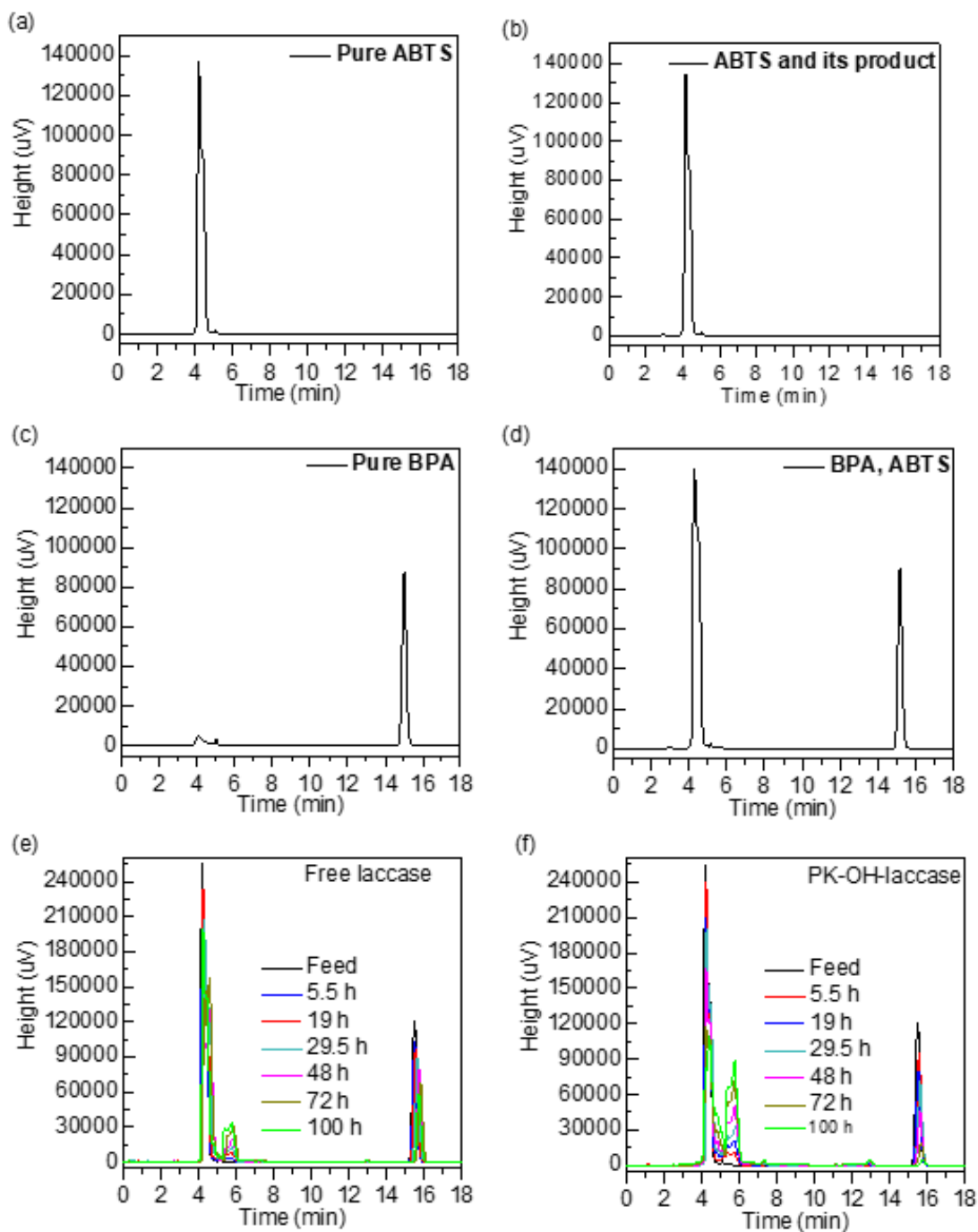Fig. IV.12 Time dependence of the degradation of TCP using free laccase and PK-OH-laccase.

Fig. IV.13 HPLC of (a) pure ABTS, (b) ABTS and its product, (c) pure BPA, and (d) the mixture of BPA and ABTS. Time dependence of the degradation of BPA using (e) free laccase and (f) PK-OH-laccase.

IV.3.4 Potential applications for enzymatic membrane bioreactors (EMRs)

Given that the convection transfer was the better application for the membrane, the continuous flow reactor was further developed in this direction. The performance of PK-OH-laccase as an EMR in aqueous-organic solvents was analyzed using ABTS in 20 vol% DMSO as a substrate. Fig. IV.14(a) shows the effect of the permeate flux on the relative activity of PK-OH-laccase. When the permeate flux increased from 0 to 2 mL/min, the relative activity gradually increased to 240 %. When it increased from 2 to 3 mL/min, however, the relative activity decreased. This observation was attributed to the trade-off between the higher level of mass transfer efficiency and lower residence time [47]. In actual applications, the best activity can be obtained by optimizing the permeate flux according to the properties of substrates.

Furthermore, satisfactory reusability, stability and durability are essential criteria for EMRs in practical applications. Fig. IV.14(b) shows the relative activity during the ten cycles of repeat catalytic reaction. PK-OH-laccase obviously maintained its catalytic activity during the ten cycles. In addition, the immobilized laccase maintained almost its entire initial activity after storage for 40 days at 4 °C. This level of storage stability is higher than previously reported result [33]. Fig. IV.14(c) presents the relative activity during 48 h of continuous catalysis. Free laccase lost 8 % of its initial activity after 50 h of incubation at 20 °C, while the immobilized version maintained its entire level of initial activity. These results were consistent with an earlier report by Susann [48]. The improved durability came from restriction to the unfolding movements of the immobilized enzyme, which helped the enzymes maintain their activity. These above results allowed reuse of the membrane for the decompositions of TCP and BPA. Fig. IV.14(d) showed the loss of PK-OH-laccase decomposition ability towards TCP and BPA in the second and third cycles. Product accumulation in the membrane coming from the high catalytic efficiency may be the main reason. Nevertheless, based on these results, it can be concluded that PK-OH-laccase provides a possibility acting as an EMR in aqueous-organic solvents.
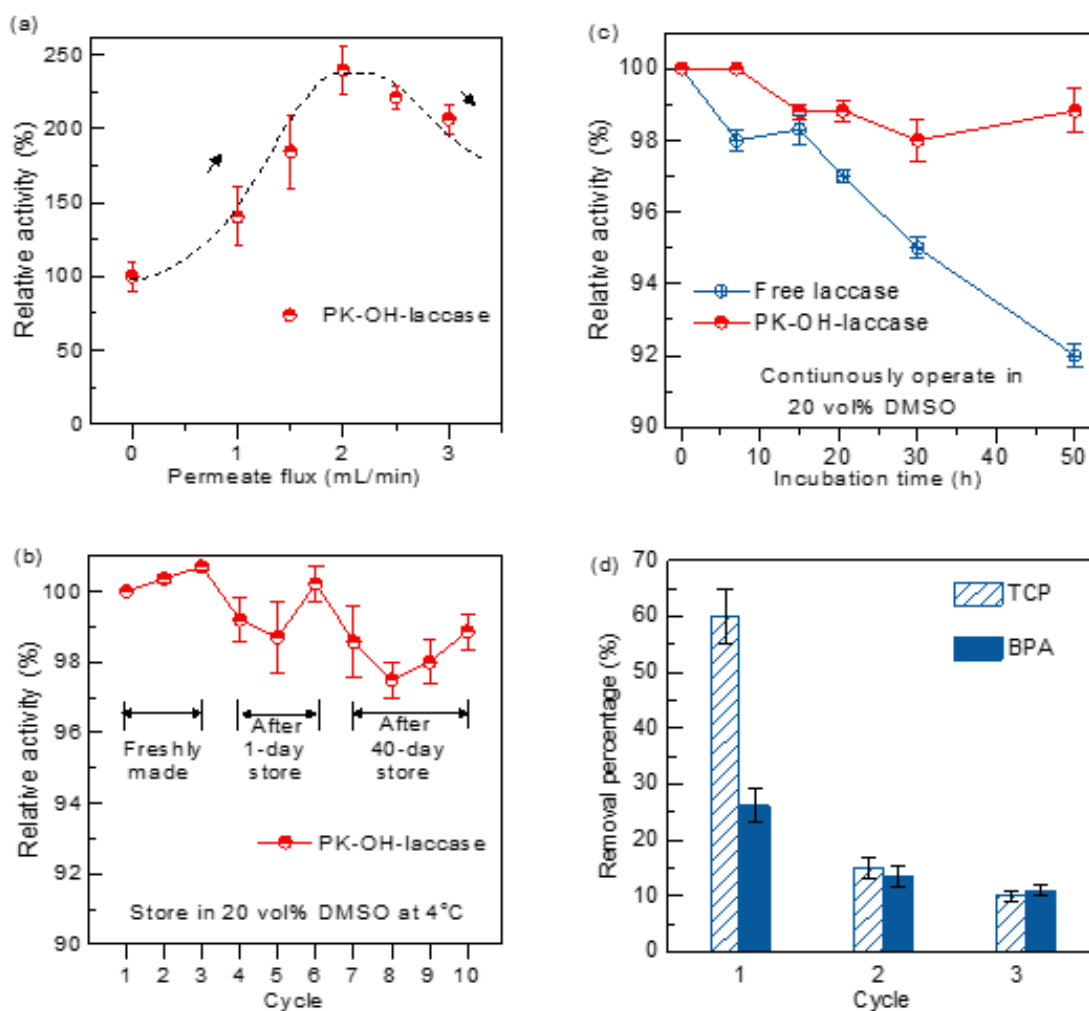
Fig. IV.14 PK-OH-laccase as an EMR in 20 vol% DMSO. (a) Effect of the filtration rate on the relative activity. The relative activity normalized with the activity at a flow rate of zero. (b) Relative activity of PK-OH-laccase for ten repeated cycles of catalysis towards ABTS. The results of the first three cycles were obtained shortly following the preparation of PK-OK-laccase. Cycles 4–6 and 7–10 were carried out after PK-OH-laccase was kept in storage at 4 °C, for 1 and 40 days, respectively. (c) Time dependence of the relative activity towards ABTS during 48 h of continuous operation and the relative activity normalized with the initial specific activity. (d) The removal percentages of micropollutants by PK-OH-laccase in three cycles. For TCP, one cycle was 5.5 h, and for BPA, one cycle was 6.5 h. All the experiments were repeated three times to prevent the experiment errors.

IV.4 Conclusions

Employing green enzyme catalysis in various organic reactions is a very intriguing proposition because of the plausibility of many industrial applications. Enzyme immobilization is considered effective in improving enzyme tolerance to harmful organic solvents and enabling continuous enzymatic membrane reactor (EMR) mode for operations that incorporates separation functions. In this study, novel hydroxylated aliphatic polyketone (PK-OH) membranes with strong solvent resistance and ease of manufacture and functionalization were employed as robust polymeric supports for efficient laccase immobilization. On the membrane surface, the presence of many polar ketone groups facilitated enzyme enrichment by physical adsorption and then effective covalent bonding with adjacent hydroxyl groups, leading to significantly improved immobilization density than conventional solvent-resistant regenerated cellulose (RC) membranes. Compared with free laccase, immobilized laccase showed great organic solvent tolerance and maintained high activity during long storage times even in harsh DMSO aqueous solutions. Furthermore, high-concentration phenolic compounds were more efficiently degraded far beyond the level of water solubility when the proposed system was operated. To the best of our knowledge, this study provides the first useful insights in engineering enzyme-immobilized membranes for use as potential EMRs in the removal of concentrated micropollutants in homogeneous aqueous-organic solutions. In the future, more efficient and enzyme-friendly immobilization strategies will be explored to improve activity retention after immobilization for higher cost-effectiveness, and to develop optimal membrane operation parameters and cleaning strategies that will further improve reusability and sustainability.

Reference

[1] S. Shoda, H. Uyama, J. Kadokawa, S. Kimura, S. Kobayashi, Enzymes as green catalysts for precision macromolecular synthesis, Chem Rev, 116 (2016) 2307-2413.

[2] H.E. Schoemaker, D. Mink, M.G. Wubbolts, Dispelling the myths - biocatalysis in industrial synthesis, Science, 299 (2003) 1694-1697.

[3] V. Stepankova, S. Bidmanova, T. Koudelakova, Z. Prokop, R. Chaloupkova, J. Damborsky, Strategies for stabilization of enzymes in organic solvents, ACS Catal, 3 (2013) 2823-2836.

[4] A.M. Klibanov, Improving enzymes by using them in organic solvents, Nature, 409 (2001) 241-246.

[5] G. Carrea, S. Riva, Properties and synthetic applications of enzymes in organic solvents, Angew Chem Int Ed, 39 (2000) 2226-2254.

[6] K. Nakanishi, Y. Kimura, R. Matsuno, Kinetics and equilibrium of enzymatic-synthesis of peptides in aqueous organic biphasic systems - thermolysin-catalyzed synthesis of N-(benzyloxycarbonyl)-L-aspartyl-L-phenylalanine methyl-ester, Eur J Biochem, 161 (1986) 541-549.

[7] R.D. Kidd, P. Sears, D.H. Huang, K. Witte, C.H. Wong, G.K. Farber, Breaking the low barrier hydrogen bond in a serine protease, Protein Sci, 8 (1999) 410-417.

[8] R. Chenevert, N. Pelchat, F. Jacques, Stereoselective enzymatic acylations (transesterifications), Curr Org Chem, 10 (2006) 1067-1094.

[9] J. Rodakiewicz-Nowak, S.M. Kasture, B. Dudek, J. Haber, Effect of various water-miscible solvents on enzymatic activity of fungal laccases, J Mol Catal B: Enzym., 11 (2000) 1-11.

[10] K. Griebenow, A.M. Klibanov, Can conformational changes be responsible for solvent and excipient effects on the catalytic behavior of subtilisin Carlsberg in organic solvents?, Biotechnol Bioeng, 53 (1997) 351-362.

[11] R.K. Singh, M.K. Tiwari, R. Singh, J.K. Lee, From protein engineering to immobilization: promising strategies for the upgrade of industrial enzymes, Int J Mol Sci, 14 (2013) 1232-1277.

[12] J.D. Bloom, F.H. Arnold, In the light of directed evolution: pathways of adaptive protein evolution, Proc Natl Acad Sci USA, 106 (2009) 9995-10000.

[13] R.C. Rodrigues, C. Ortiz, A. Berenguer-Murcia, R. Torres, R. Fernandez-Lafuente, Modifying enzyme activity and selectivity by immobilization, Chem Soc Rev, 42 (2013) 6290-6307.

[14] J.Q. Luo, A.S. Meyer, R.V. Mateiu, D. Kalyani, M. Pinelo, Functionalization of a membrane sublayer using reverse filtration of enzymes and dopamine coating, ACS Appl Mater Inter, 6 (2014) 22894-22904.

[15] L. Girono, E. Drioli, Biocatalytic membrane reactors: applications and perspectives, Trends Biotechnol, 18 (2000) 339-349.

[16] G. Pugazhenthi, A. Kumar, Enzyme membrane reactor for hydrolysis of olive oil using lipase immobilized on modified PMMA composite membrane, J Membr Sci, 228 (2004) 187-197.

[17] N. Doukyu, H. Ogino, Organic solvent-tolerant enzymes, Biochem Eng J, 48 (2010) 270-282.

[18] G.R. Castro, T. Knubovets, Homogeneous biocatalysis in organic solvents and water-organic mixtures, Crit Rev Biotechnol, 23 (2003) 195-231.

[19] G.M. Rios, M.P. Belleville, D. Paolucci, J. Sanchez, Progress in enzymatic membrane reactors - a review, J Membr Sci, 242 (2004) 189-196.

[20] P. Lozano, T. De Diego, M.P. Belleville, G.M. Rios, J.L. Iborra, A dynamic membrane reactor with immobilized alpha-chymotrypsin for continuous kyotorphin synthesis in organic media, Biotechnol Lett, 22 (2000) 771-775.

[21] K. Labus, I. Gancarz, J. Bryjak, Immobilization of laccase and tyrosinase on untreated and plasma-treated cellulosic and polyamide membranes, Mat Sci Eng C-Mater, 32 (2012) 228-235.

[22] S. Sourirajan, Separation of hydrocarbon liquids by flow under pressure through porous membranes, Nature, 203 (1964) 1348-1349.

[23] A.F. Che, X.J. Huang, Z.K. Xu, Polyacrylonitrile-based nanofibrous membrane with glycosylated surface for lectin affinity adsorption, J Membr Sci, 366 (2011) 272-277.

[24] R. Valadez-Blanco, A.G. Livingston, Enantioselective whole-cell biotransformation of acetophenone to S-phenylethanol by Rhodotorula glutinis. Part II. Aqueous-organic systems: emulsion and membrane bioreactors, Biochem Eng J, 46 (2009) 54-60.

[25] M. Indlekofer, M. Funke, W. Claassen, M. Reuss, Continuous enantioselective transesterification in organic-solvents - use of suspended lipase preparations in a microfiltration membrane reactor, Biotechnol Progr, 11 (1995) 436-442.

[26] A.I. Ruiz, A.J. Malave, C. Felby, K. Griebenow, Improved activity and stability of an immobilized recombinant laccase in organic solvents, Biotechnol Lett, 22 (2000) 229-233.

[27] P. Marchetti, M.F.J. Solomon, G. Szekely, A.G. Livingston, Molecular separation with organic solvent nanofiltration: a critical review, Chem Rev, 114 (2014) 10735-10806.

[28] M. Yasukawa, S. Mishima, M. Shibuya, D. Saeki, T. Takahashi, T. Miyoshi, H. Matsuyama, Preparation of a forward osmosis membrane using a highly porous polyketone microfiltration membrane as a novel support, J Membr Sci, 487 (2015) 51-59.

[29] C. Liu, D. Saeki, H. Matsuyama, A novel strategy to immobilize enzymes on microporous membranes via dicarboxylic acid halides, RSC Adv, 7 (2017) 48199-48207.

[30] R. Xu, C.L. Chi, F.T. Li, B.R. Zhang, Laccase-polyacrylonitrile nanofibrous membrane: highly immobilized, stable, reusable, and efficacious for 2,4,6-trichlorophenol removal, ACS Appl Mater Inter, 5 (2013) 12554-12560.

[31] L. Cheng, A. R. Shaikh , L.F. Fang , S. Jeon , C.J. Liu , L. Zhang , H.C. Wu , D.M. Wang , H. Matsuyama, Fouling-resistant and self-cleaning aliphatic polyketone membrane for sustainable oil–water emulsion separation, ACS Appl Mater Inter, 10 (2018) 44880-44889.

[32] Z.A. Yi, L.P. Zhu, Y.Y. Xu, X.N. Gong, B.K. Zhu, Surface zwitterionicalization of poly(vinylidene fluoride) porous membranes by post-reaction of the amphiphilic precursor, J Membr Sci, 385 (2011) 57-66.

[33] R. Sarma, M.S. Islam, A.F. Miller, D. Bhattacharyya, Layer-by-layer-assembled laccase enzyme on stimuli-responsive membranes for chloro-organics degradation, ACS Appl Mater Inter, 9 (2017) 14858-14867.

[34] A. Alsbaiee, B.J. Smith, L.L. Xiao, Y.H. Ling, D.E. Helbling, W.R. Dichtel, Rapid removal of organic micropollutants from water by a porous beta-cyclodextrin polymer, Nature, 529 (2016) 190-194.

[35] X.T. Cao, J.Q. Luo, J.M. Woodley, Y.H. Wan, Bioinspired multifunctional membrane for aquatic micropollutants removal, ACS Appl Mater Inter, 8 (2016) 30511-30522.

[36] J.W. Hou, G.X. Dong, Y. Ye, V. Chen, Enzymatic degradation of bisphenol-A with immobilized laccase on TiO_2 sol-gel coated PVDF membrane, J Membr Sci, 469 (2014) 19-30.

[37] J.W. Hou, G.X. Dong, Y. Ye, V. Chen, Laccase immobilization on titania nanoparticles and titania-functionalized membranes, J Membr Sci, 452 (2014) 229-240.

[38] C. Chao, J.D. Liu, J.T. Wang, Y.W. Zhang, B. Zhang, Y.T. Zhang, X. Xiang, R.F. Chen, Surface modification of halloysite nanotubes with dopamine for enzyme immobilization, ACS Appl Mater Inter, 5 (2013) 10559-10564.

[39] C. Mateo, R. Torres, G. Fernandez-Lorente, C. Ortiz, M. Fuentes, A. Hidalgo, F. Lopez-Gallego, O. Abian, J.M. Palomo, L. Betancor, B.C.C. Pessela, J.M. Guisan, R. Fernandez-Lafuente, Epoxy-amino groups: A new tool for improved immobilization of proteins by the epoxy method, Biomacromolecules, 4 (2003) 772-777.

[40] I. Banerjee, R.C. Pangule, R.S. Kane, Antifouling coatings: recent developments in the design of surfaces that prevent fouling by proteins, bacteria, and marine organisms, Adv Mater, 23 (2011) 690-718.

[41] Y.Y. Wan, R. Lu, L. Xiao, Y.M. Du, T. Miyakoshi, C.L. Chen, C.J. Knill, J.F. Kennedy, Effects of organic solvents on the activity of free and immobilised laccase from Rhus vernicifera, Int J Biol Macromol, 47 (2010) 488-495.

[42] W.Y. Yang, D.Y. Min, S.X. Wen, L. Jin, L. Rong, M. Tetsuo, C. Bo, Immobilization and characterization of laccase from Chinese Rhus vernicifera on modified chitosan, Process Biochem, 41 (2006) 1378-1382.

[43] R. Vazquezduhalt, K.M. Semple, D.W.S. Westlake, P.M. Fedorak, Effect of water-miscible organic-solvents on the catalytic activity of cytochrome-c, Enzyme Microb Tech, 15 (1993) 936-943.

[44] A.L. Gutman, E. Meyer, E. Kalerin, F. Polyak, J. Sterling, Enzymatic resolution of racemic amines in a continuous reactor in organic-solvents, Biotechnol Bioeng, 40 (1992) 760-767.

[45] R. Ikeda, H. Uyama, S. Kobayashi, Novel synthetic pathway to a poly(phenylene oxide). Laccase-catalyzed oxidative polymerization of syringic acid, Macromolecules, 29 (1996) 3053-3054.

[46] Y.Q. Huang, C.K.C. Wong, J.S. Zheng, H. Bouwman, R. Barra, B. Wahlstrom, L. Neretin, M.H. Wong, Bisphenol A (BPA) in China: a review of sources, environmental levels, and potential human health impacts, Environ Int, 42 (2012) 91-99.

[47] J.W. Hou, G.X. Dong, B. Luu, R.G. Sengpiel, Y. Ye, M. Wessling, V. Chen, Hybrid membrane with TiO_2 based bio-catalytic nanoparticle suspension system for the degradation of bisphenol-A, Bioresource Technol, 169 (2014) 475-483.

[48] S. Schachschal, H.J. Adler, A. Pich, S. Wetzel, A. Matura, K.H. van Pee, Encapsulation of enzymes in microgels by polymerization/cross-linking in aqueous droplets, Colloid Polym Sci, 289 (2011) 693-698

Chapter V Organic liquid mixture separation using an aliphatic polyketone-based organic solvent reverse osmosis (OSRO) membrane

V.1 Introduction

Approximately 10 to 15% of the world's total energy consumption is expended on industrial chemical separations [1], and more than 80% of the associated separation energy is consumed by the energy-intensive distillation process and similar thermally driven separation processes relying on liquid-to-vapor phase change [2, 3]. As motivated by the great success of membrane desalination replacing thermal desalination [4], the emerging membrane-based organic solvent separations processes may dramatically reduce the energy consumption (possibly down to one-tenth of the energy consumed by thermal approaches), carbon dioxide emission, and carbon footprint by directly separating organic liquids without phase change [3, 5]. The first challenge is to fabricate robust membranes with the required molecular selectivity, permeability, and area ($>10,000$ m^2). To date, organic solvent nanofiltration (OSN) membranes with a molecular weight cutoff (MWCO) above 200 Da have been commercialized and are widely used for separating solutes from solvents [6-8]. However, OSN is not suitable for separating frequently encountered small molecules of similar size with molecular weight (M_w) lower than 100 Da, such as alcohol/alkane mixtures. Organic solvent reverse osmosis (OSRO) membranes that can differentiate between similar molecules with small differences in kinetic diameter are highly desired [2, 3].

While the original OSRO concept was investigated by Sourirajan in 1970 using integrally skinned asymmetric cellulose acetate membranes to separate alcohols from cyclic hydrocarbons and alkyl aromatics, the development of OSRO membranes still remains at an early stage. Organic solvents can cause cellulose acetate membranes to swell or collapse [9]. Therefore, the development of stable and scalable OSRO membranes are in demand. Organic solvent-resistant membranes made from polyacrylonitrile, cellulose acetate butyrate, and

aromatic polyamide were subsequently developed; however, the separation factor (lower than 3.0) of these membranes was not satisfactory [10-12]. Moreover, a perfluorodioxole copolymer membrane prepared on a polytetrafluoroethylene support was able to separate highly polar solvents, such as N-methyl pyrrolidone, from toluene at a low permeability of 0.026 LMH bar^{-1}, however, it did not exhibit selectivity toward smaller molecules such as methanol (MeOH) and toluene [13]. In another study, a silica-zirconia membrane exhibited a 70% rejection and a 0.03 LMH bar^{-1} flux for hexane/ethanol (EtOH) mixture at 60 °C [14]. The recently developed carbon molecular sieve (CMS) membranes by Lively et al. achieved a separation factor of 4.5 towards *para*-xylene and *ortho*-xylene mixture by OSRO process [15].

Herein, we report a polyketone (PK)-based thin-film composite (TFC) membrane possessing potential in OSRO separation of organic liquid mixtures. A defect-free polyamide layer could be formed on a non-swelling PK support using a reliable and scalable interfacial polymerization (IP) process similarly used for the mass production of desalination TFC RO membranes [16]. The chemistry of the support membrane is crucial for determining the organic solvent resistance of the TFC composites and the properties of the synthesized polyamide layer [17, 18]. PK is a thermoplastic alternating copolymer of carbon monoxide and ethylene, containing CH$_2$CH$_2$CO repeat units [19]. The compact, semi-crystalline crystal structure of PK due to polar carbonyl groups facilitates strong intramolecular and intermolecular interactions, resulting in an over 30% higher solvent resistance than that of nylon [20]. The chemical bonds formed between the amine groups of polyamide and the ketone groups of PK, as well as other strong physical interactions are believed to further improve solvent resistance [21, 22]. Of note, the microporous supports prepared from polysulfone, chemically cross-linked polyimide, polybenzimidazole, and polyacrylonitrile can undergo varying degrees of organic solvent swelling, which can decrease the separation ability of the formed TFC membranes in organic liquids [6, 23-25]. To our knowledge, this is the first attempt to use a TFC membrane fabricated via IP reaction to achieve the separation of organic liquid mixtures based on OSRO.

Several binary organic liquid mixtures were separated using the developed PK-based OSRO membrane (PK-RO), and an outstanding separation factor of 38.0 was achieved for MeOH and heptane mixtures, along with a flux of 5 LMH under 3 MPa. Moreover, PK-RO outperformed the commercial OSN and RO membranes in terms of separation factor and stability.

V.2 Experimental

V.2.1 Materials

Polyketone (PK) polymer with an M_w of 200,000 g mol^{-1} was kindly provided by Asahi Kasei Co. (Japan). Resorcinol, MeOH, acetone, and hexane (FUJIFILM Wako Pure Chemical Co., Osaka, Japan) were used to fabricate the PK support membrane. 1,3,5-benzenetricarbonyl trichloride (TMC), 10-camphorsulfonic acid (CSA) (Tokyo Chemical Industry, Japan), 1,3-phenylene diamine (MPD), sodium dodecyl sulfate (SDS), and triethyl amine (TEA) (FUJIFILM Wako Pure Chemical Co.) were used in the interfacial polymerization (IP) reaction to fabricate the polyamide layer on the PK support.

Sodium chloride (NaCl) (FUJIFILM Wako Pure Chemical Co.) was used to evaluate salt rejection in an aqueous solution. Milli-Q water (Merck Millipore Co., Germany) was used for this study. All other organic solvents to investigate OSRO performance, including polar protic solvents (ethanol (EtOH), propanol, isopropanol, butanol, and pentanol); polar aprotic solvents (acetonitrile (AcN), acetone, and tetrahydrofuran (THF)); and non-polar solvents (toluene, heptane, pentane, and benzene) were purchased from TCI Co. (Japan).

One commercial RO membrane (SWC5, Nitto, Osaka, Japan) and two OSN membranes with an MWCO of 150 Da (Duramem 150) and 200 Da (Duramem 200) (Evonik, Essen, Germany) were used for comparison.

V.2.2 Polyketone-based reverse osmosis (PK-RO) membrane preparation

First, the porous PK support membrane was fabricated using the non-solvent induce phase separation process [21]. The PK polymer was dissolved in a resorcinol/water (65/35 wt%) solution to form a 14 wt% PK casting solution. After degassing, the homogenous solution

was cast using a 400-µm-thick casting knife on a non-woven fabric that was tightly attached on a clean glass plate. Subsequently, the plate was immersed into a coagulation bath of MeOH/water (35/65 wt%) for 20 min. The formed membrane was washed in acetone and hexane for 20 min each. Finally, the membrane was air dried and stored for further use.

The IP reaction was conducted on the top of the PK support. Briefly, an aqueous solution containing 2 wt% MPD, 2 wt% TEA, 4 wt% CSA, and 0.25 wt% SDS was gradually poured on the top of the PK support and gently removed after soaking for 5 min. Then, a 0.15 wt% TMC hexane solution was rapidly poured on the membrane to allow IP reaction to occur for 2 min. After removing the hexane solution, the membrane was heated at 100°C in an oven for 5 min, and immersed in Milli-Q water for 12 h to completely remove residual unreacted monomers. The final membrane was preserved in Milli-Q water prior to use.

V.2.3 Membrane characterization

Membrane surface and cross-sectional morphologies were observed using a field scanning electron microscope (FE-SEM; JSF-7500, JEOL, Tokyo, Japan). The samples were freeze-dried using a vacuum freeze dryer (FDU-1200; Tokyo Rikakikai, Tokyo, Japan) and coated with Pt/Pd using an ion-sputter apparatus (E-1010; Hitachi High-Technologies Corporation, Tokyo, Japan) before observation. The chemical composition of the membrane surface was analyzed by X-ray photoelectron spectroscopy (XPS, JPS-9010MC, JEOL).

A soak test was performed to evaluate membrane stability in solvents. Three aggressive soak liquids (toluene, acetone, and THF) were used. PK-RO and SWC5 membranes were soaked in the corresponding solvents for 1 day before obtaining digital photographs.

V.2.4 Organic solvent separation test

Reverse osmosis filtration tests were performed at 25±2 °C using a cross-flow filtration apparatus as shown in Fig. V.1. The membrane, with an effective surface area of 8.04 cm^2, was placed into a stainless steel cell. The feed solution was fed into the cell at a cross-flow rate of 9.9 mL/min using a dual pump (KP-21 series; FLOM Co., Japan). Milli-Q water, NaCl aqueous solution, pure organic liquids, or organic liquid mixtures were used as feed solutions,

as required. The applied pressure was adjusted using a backpressure valve in the range of 1–3 MPa. During filtration, the feed side near the membrane surface was magnetically stirred at 200 rpm to minimize concentration polarization. The concentrate was recycled into the feed solution. A large volume of the feed solution was used and often replenished to maintain a constant feed concentration. The permeate was collected in a sealed flask as a function of time and weighted. The flux (J_v; L·m^{-2}·h^{-1}, LMH) was calculated according to Eq. (V.1):

$$J_v = \frac{M}{A \times t \times \rho} \tag{V.1}$$

where M (g) is the mass of the accumulated permeate, A (m^2) is the effective membrane area, t (h) is the filtration time, and ρ (g/L) is the density of the permeate.

In the case of NaCl aqueous solution, NaCl rejection (R; %) was calculated according to Eq. (V.2):

$$R = (1 - \frac{C_p}{C_f}) \times 100 \tag{V.2}$$

where C_p and C_f are the molar concentrations of NaCl in the permeate and feed solution, respectively.

Only binary organic liquid mixtures were used in this study. The major constituent of the mixture was the solvent and the minor constituent was the solute. The mixture was noted as *AxBy* according to their compositions. *A* is the solvent (*x* wt%), *B* is the solute (*y* wt%). MeOH and toluene were abbreviated as "M" and "T", respectively. The other organic liquids are denoted by their full names. For example, the solution with 90 wt% MeOH and 10 wt% toluene was denoted as M90T10. The solution with 90 wt% acetone and 10 wt% toluene was denoted as Acetone90T10. The separation performance of the OSRO membrane toward organic liquid mixtures was evaluated via separation factor (α), defined by Eq. (V.3) as:

$$\alpha = \frac{[C_{solvent}/C_{solute}]_{permeate}}{[C_{solvent}/C_{solute}]_{feed}} \tag{V.3}$$

where $C_{solvent}$ and C_{solute} represent molar fractions of the solvent and solute, respectively.

Effective pressure ΔP_{eff} (kPa) was calculated according to Eq. (V.4) as follows:[14]

$$\Delta P_{eff} = \Delta P - \sigma \Delta \pi \tag{V.4}$$

where ΔP and Δπ are differences in the applied pressure and osmotic pressure, respectively. σ represents the reflection coefficient. Herein, considering the high rejection of solute as will be shown in the result part, σ value was estimated as 1.

   Δπ (kPa) was calculated using the van't Hoff equation (Eq. V.5):[13]

$$\Delta\pi = RT \left(\sum C_{i,f} - \sum C_{i,p} \right) \tag{V.5}$$

where $C_{i,f}$ and $C_{i,p}$ are the molar concentrations of the rejected component i in the feed and permeate, respectively. R is the gas constant and T is the absolute temperature (K).

The procedure for the membrane test is described herein. Firstly, the membrane integrity was confirmed by NaCl rejection in aqueous solution as follows: a pre-filtration step was performed for each membrane for 1 h at 2 MPa using Milli-Q water as the feed. Thereafter, the NaCl rejection was measured using a 0.2 wt% NaCl aqueous solution as the feed at 2 MPa. The NaCl concentration was determined from conductivity of the solution (B-771, Horiba, Kyoto, Japan). The membranes with an NaCl rejection above 96% were stored in a cell and continuously used in the following steps. Otherwise, the membrane was discarded and a new piece was tested. Then, Milli-Q water was fed again at 2 MPa for 1 h to wash the test unit. Secondly, the membrane was compacted by MeOH as described in the following steps: Milli-Q water in the cell was replaced with MeOH, and the filtration was continued for 2 h at 1 MPa to balance membrane permeability. Then, the membrane was pre-compacted by filtrating MeOH at 3 MPa for several hours until the flux stabilized. Finally, the membrane was ready for various tests.

To test the resistance of the membrane to MeOH, the MeOH flux was initially measured at an applied pressure of 3 MPa, then at 2 MPa, and finally at 1 MPa. Thereafter, the pressure was increased to 2 MPa and 3 MPa; finally, the MeOH flux was measured again.

For performance in aqueous media, the water flux and NaCl rejection were measured following the above-mentioned compaction scheme. For the water flux, Milli-Q water was used to clean the test unit for 1 h at 3 MPa. Subsequently, the water flux was measured at 1–3 MPa. The NaCl rejection rate was determined at 1–3 MPa by introducing 0.2 wt% NaCl aqueous solution as the feed. After completing the test, the unit was washed with Milli-Q water.

For flux determination of pure organic liquids, the cell was initially cleaned with MeOH and then replaced by the desired organic liquid for 1 h. Flux measurement was performed at an applied pressure of 3 MPa until a stable value was achieved. For performance measurements in organic liquid mixtures, the cell was initially cleaned with MeOH and subsequently replaced by the solvent (the major constituent of mixtures). After obtaining a stable flux, the desired organic liquid mixture was fed into the test unit. For the determination of the separation factor, at least 20 g permeate was collected as a sample. The composition of the sample was analyzed using a GC-2014 gas chromatograph equipped with an auto injector (Shimadzu, Japan). The mixture was separated using a Porapak-Q column (Waters Co., Ltd., MA, USA). High purity helium (99.999%) was used as the carrier gas (Taiyo Nippon Sanso Co., Japan). The injection port, oven temperature, and detector temperatures were set at 210 °C, 200 °C, and 200 °C respectively, with the column flow rate of 30 mL min^{-1}. The test time for one sample was 20 min and the volume of the injected sample was 1 μL. A chromatopac integrator (C-R8A; Shimadzu, Japan) was used as the data acquisition system. All measurements were based on at least two membrane samples, and the average values were reported.

After filtering the mixture, the test unit was sequentially cleaned with MeOH and Milli-Q water for 2 h each before rendering the unit for testing new membranes.

To test the long-term filtration performance of PK-RO in organic liquid mixtures, filtration tests were conducted using M90T10 and Acetone90T10 as the feed solutions at 3 MPa for 120 h. For comparison, the performance of commercial RO membrane (SWC5) was also measured.
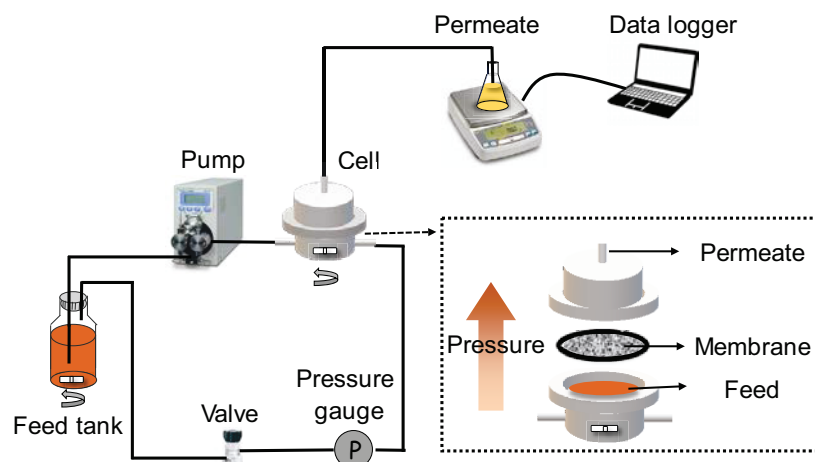
Fig. V.1 A schematic diagram of a lab-scale cross-flow membrane test unit.

V.3 Results and discussion

V.3.1 Membrane characterization

As shown in Fig. V.2(A), the top surface of the PK support had an average pore size of approximately 300 nm and its cross-section consisted of fibrils. Moreover, a non-porous layer was formed on the top surface of PK-RO. As shown in Fig. V.2(B), a nitrogen peak was observed in XPS for PK-RO, which confirmed the presence of a polyamide layer. As reported in our previous study, a pinhole-free polyamide layer can be successfully formed on the PK membrane by virtue of the Paal-Knorr Pyrrole reaction between amine monomers and PK [21]. The chemical bond between polyamide and the PK support might confer high chemical resistance to PK-RO [22]. A cross-section image of PK-RO showed that the thickness of polyamide layer was around 100 nm, which is similar to that of commercial RO membranes, ranging from 100 to 200 nm. Table V.1 shows the elemental content of membrane surfaces. These values of PK-RO were similar to those of the commercial RO membrane SWC5. The N/O ratio indicates the degree of cross-linking of the polyamide layer [26]; similar N/O ratios suggest that both the PK-RO and SWC5 surfaces were cross-linked to a comparable degree.

Membranes fabricated from 1,3-phenylene diamine (MPD) and 1,3,5-benzenetricarbonyl trichloride (TMC) typically exhibit a sodium chloride (NaCl) rejection of higher than 90%

133

and often higher than 99%, along with water permeability of 1–10 LMH bar^{-1} [16]. As shown in Fig. V.3, the PK-RO showed a NaCl rejection above 97% and water permeability around 0.5 LMH bar^{-1}. This result suggests that the PK-RO membrane is available as a RO membrane in aqueous media. Moreover, the linear increase in water flux and slight increase in the NaCl rejection along with pressure confirmed the defect-free ability. The overlap of fluxes and pressure curves with the increase and decrease of pressure indicated the steady state of the membrane in water.

The stability of PK-RO in three aggressive organic solvents (toluene, acetone, and tetrahydrofuran (THF)) and its comparison with SWC5 was investigated by digital microscopy, as shown in Fig. V.4. None of the solvents caused a visible change to PK-RO, thereby proving its good stability in the tested solvents. In contrast, the polyamide layer of SWC5 had obviously dropped off due to dissolvability of the support membrane in these solvents. Therefore, PK-RO can be a promising OSRO membrane to be potentially used for the separation of organic liquids.
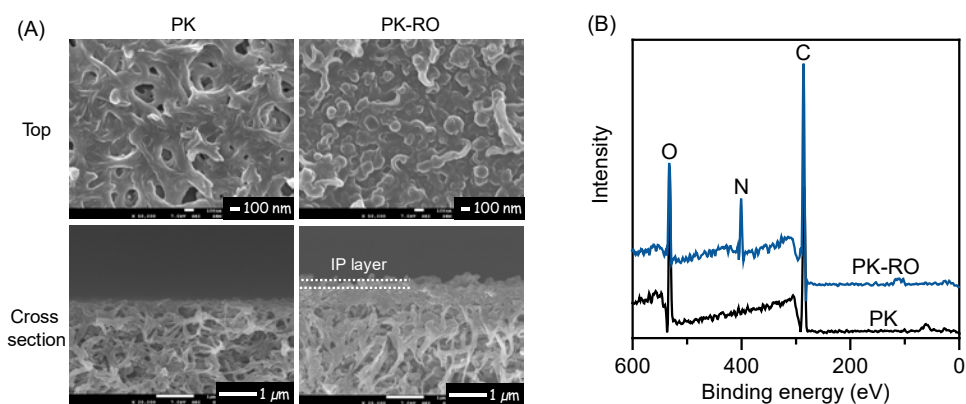

Fig. V.2 (A) SEM images of the top surfaces and cross-sections of PK and PK-RO membranes. The polyamide layer formed by interfacial polymerization (IP layer) is marked in the figure. (B) XPS spectra of PK and PK-RO membranes.

Table V.1 Elemental content of PK, PK-RO, and SWC5 membranes surface analyzed by XPS.

Membrane	Elemental ratio (relative atom%)			N/O ratio
	C	O	N	
PK	71.3	28.7	0	0
PK-RO	74.4	13.0	12.6	0.97
SWC5[*]	74.2	13.3	12.5	0.94

[*] SWC5 is a commercial RO membrane provided by Nitto, Osaka, Japan
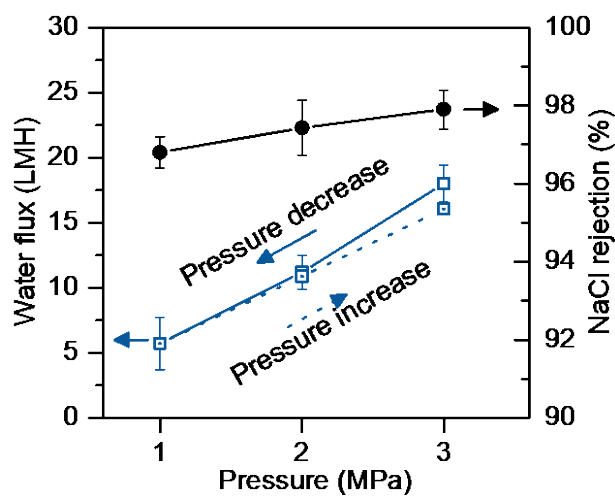

Fig. V.3 The effect of applied pressure on water flux and NaCl rejection of the PK-RO membrane. The feed solution was 34 mmol L-1 NaCl. The membrane was pre-compacted by methanol filtration at 3 MPa. The fluxes were initially tested at 3 MPa, then at 2 MPa, and finally at 1 MPa. After the above test, the pressure was increased to 2 and 3 MPa again, and the fluxes were re-measured.
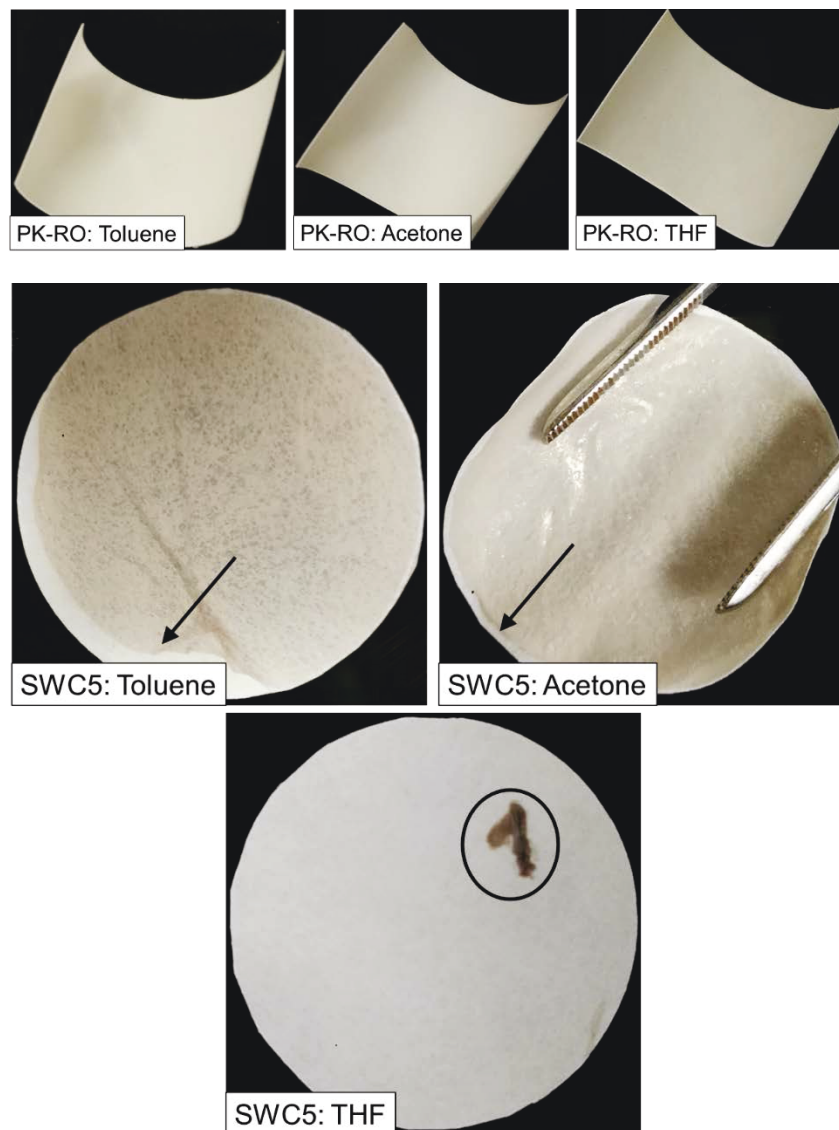
Fig. V.4 The digital photos of membranes after immersion in each solvent for 1 day.

V.3.2 Single-component organic liquid filtration

MeOH is a highly versatile chemical that is used in various industries ranging from pharmaceutical to paint. In many cases, MeOH forms a homogeneous solution with other organic substances such as alcohols and aromatic compounds. The separation and recycling of MeOH from different mixtures is required for its reuse. Therefore, MeOH was chosen as the main liquid for this work. Membrane compaction must be considered when using

polymeric membranes under high pressure [7], so MeOH filtration was conducted using the test unit shown in Figure 2 at 3 MPa to test membrane compaction. As shown in Fig. V.5(A), MeOH permeability decreased by 50% during the first 5 h, and subsequently remained stable at 0.5 LMH bar^{-1}. This decline in permeability was presumably due to compaction of the support and the selective layer [7, 27]. The MeOH permeability of PK-RO is slightly lower, yet adequate, than that of most OSN membranes (1–50 LMH bar^{-1}) [7, 28-30]. In addition, after compaction, MeOH flux was linear with applied pressure over the range 1 to 3 MPa, and the overlap of the fluxes with the pressure curves was confirmed by the increase and decrease of pressures (see Fig. V.5(B)), suggesting that PK-RO remained in a stable state in MeOH after compaction up to 3 MPa.

PK-RO can potentially be used for the filtration of various organic liquids, and therefore, the permeabilities of several other liquids were measured. The selected liquids have different physicochemical properties as shown in Table V.2. The permeabilities were analyzed using the transport model proposed for the OSN membrane [7]. In this model, the permeability (LMH bar^{-1}) of the organic liquid through the nanofilm was calculated according to the following equation (V.6):

$$\text{Permeability} = K \, \frac{\delta_p}{\eta d_m^2} \tag{V.6}$$

where K is a constant of the nanofilm, and δ_p, η, and d_m are the Hansen solubility parameter due to dipole forces (Pa$^{0.5}$), viscosity (Pa s), and molar diameter (m) of the organic liquid, respectively. As shown in Fig. V.6, this model explained well the permeabilities of liquids expect MeOH. The higher permeability of MeOH than that expected from the model is probably due to the similar δ_p value of MeOH to that of the polyamide layer, as well as the small size of MeOH (Table V.2). It is presumed that the contribution of the dipolar force and molecular size to permeability in the RO filtration is higher than that in the NF filtration. It is worth noting that the zero flux of hexane and toluene were due to their much lower δ_p value than that of the polyamide layer. Because the permeabilities of small polar molecules are higher than that of large non-polar molecules, PK-RO is expected to efficiently separate small polar molecules from large non-polar ones. On the other hand, a stable permeability

was obtained for all the tested liquids over at least 12 h, suggesting the robust stability and no swelling of PK-RO in these liquids.
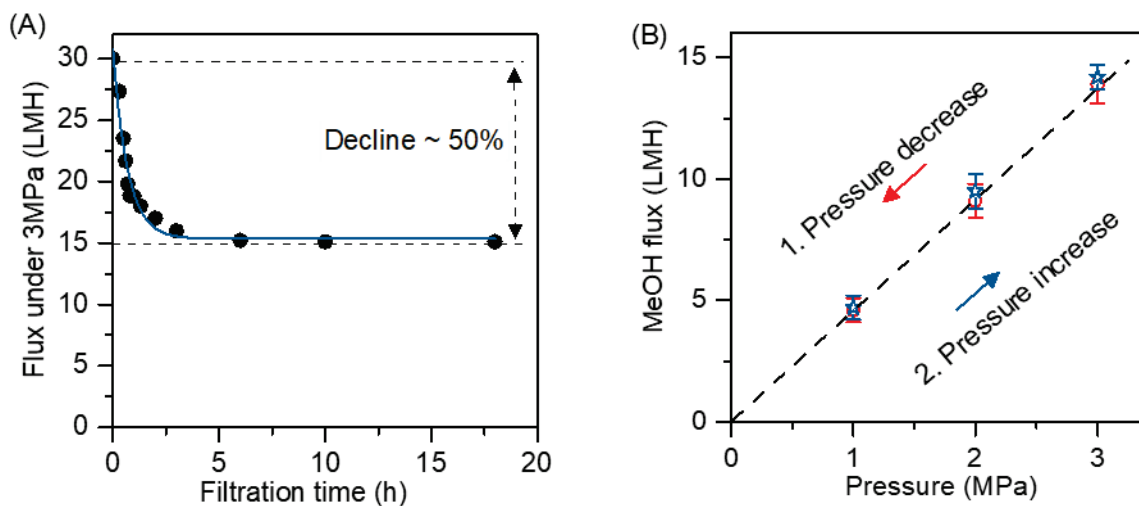

Fig. V.5 (A) Time course of methanol flux through the PK-RO membrane at 3 MPa. (B) Methanol flux as a function of pressure. The pressure was initially decreased from 3 to 1 MPa and subsequently increased from 1 to 3 MPa.

Table V.2 Physiochemical properties of organic liquids and the polyamide layer.

Solvent	M_w (g mol^{-1})	Molar diameter (d_m) (nm) [7]	Viscosity (η) (mPa s) [31]	Hansen solubility parameter (δ_p) * (MPa$^{0.5}$) [7]
MeOH	32.04	0.51	0.54	12.3
AcN	41.05	0.55	0.34	18.0
EtOH	46.07	0.57	1.08	8.8
Acetone	58.08	0.62	0.32	10.4
THF	72.11	0.62	0.46	5.7
Hexane	86.18	0.75	0.29	0.0
Toluene	92.14	0.70	0.56	1.4
Polyamide layer [32]	No data	No data	No data	11.9

*Hansen solubility parameter due to dipole forces, indicating polarity. A high δ_p value means high polarity of the organic liquid.
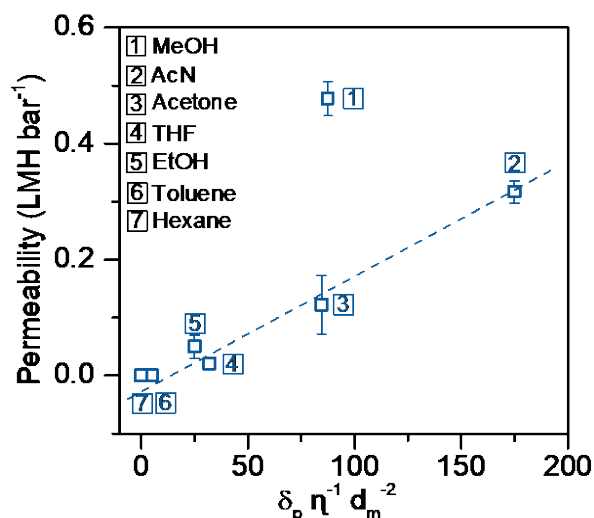
Fig. V.6 Permeabilities (liter m^{-2} h^{-1} bar^{-1}, LMH bar^{-1}) of various organic liquids tested at 3 MPa. The permeabilities were analyzed using the transport model proposed for OSN membranes.[7] The dotted line was the smoothed line of the permeabilities of all organic liquids, except MeOH. MeOH, AcN, THF, and EtOH are methanol, acetonitrile, tetrahydrofuran, and ethanol, respectively.

V.3.3 Separation of toluene from MeOH solution

The permeation of organic liquid mixtures through membrane is generally much more complex than that of a single organic liquid, because of the high number of interactions between them. In this section, the flux and separation factor of mixtures were investigated. On the above discussion, PK-RO is expected to exhibit an efficient separation of large non-polar molecules from small polar ones. The mixture of MeOH and toluene is widely encountered in the pharmaceutical and fine chemical industries. However, their separation using thermal methods such as distillation are not preferred due to the high operating cost and also the formation of azeotropic mixtures. MeOH is a small polar molecule, whereas toluene is a large non-polar molecule (Table. V.2). Thus, PK-RO was used to separate toluene from MeOH solution first.

In this study, the mixture was noted as *AxBy* according to the compositions. *A* is the solvent of *x* wt%, *B* solute of *y* wt% as defined in experimental section of the supporting information. A mixture of 90 wt% MeOH and 10 wt% toluene (M90T10) was used as a feed solution. If each component permeates through the membrane independently, the separation factor should be infinity, because the permeability of toluene through PK-RO at 3 MPa was zero (Fig. V.6). However, as shown in Fig. V.7, the separation factor was not infinity. This is because the interaction between toluene and MeOH causes toluene to transport along with MeOH.

Based on the non-equilibrium thermodynamic model, the volume flux (J_v) and molar solute flux (J_s) through a membrane were calculated as follows:[14]

$$J_v = L_p(\Delta P - \sigma \Delta \pi) \tag{V.7}$$

$$J_s = P(C_m - C_p) + (1 - \sigma)\bar{C}J_v \tag{V.8}$$

where L_p is the solvent permeability coefficient; ΔP and $\Delta \pi$ are the differences in applied pressure and osmotic pressure, respectively; σ represents the reflection coefficient; P is the diffusivity of the solute; C_m and C_p are the molar concentrations of the solute in the feed and permeate, respectively; and $\bar{C}$ is the mean log solute concentration on both sides of the membrane.

The effect of applied pressure on the flux and separation factor was studied and showed in Fig. V.7(A). The flux of mixture did not increase linearly with applied pressure, while it increased linearly for pure MeOH and water, as shown in Fig. V.5(B) and Fig. V.3, respectively. This phenomenon was caused by high osmotic pressure, resulting from the high concentration of toluene (86700 ppm) in the feed. The effective pressure (ΔP_{eff}), as described in Eq. (V.4), was estimated by reducing osmotic pressure from applied pressure (see Table V.3). As shown in Fig. V.8, the mixture flux increased linearly with the effective pressure, as indicated in Eq. (V.7). It is worth noticing that the toluene flux was greater than zero when the effective pressure was zero (Fig. V.8). This was due to toluene diffusion through the membrane, as indicated in Eq. (V.8). In addition, the toluene flux increased with the effective pressure, suggesting that the convection transport of toluene occurs along with

MeOH. Because the increase in MeOH flux with pressure was much higher than that of toluene, the highest separation factor (8.4) was obtained at the highest pressure of 3 MPa.

The component ratio of organic liquid mixtures varies in the actual application. Thus, it is necessary to investigate performance under different ratios of the feed solution. Fig. V.7(B) shows the flux and separation factor as a function of MeOH fraction (wt%) in feed. Because the osmotic pressure decreased with an increase in the MeOH fraction, the effective pressure (ΔP_{eff}) increased for the MeOH fraction when a constant pressure of 3 MPa was applied on the feed solution; this resulted in the high flux of MeOH. The increase in ΔP_{eff} also led to an increase in the separation factor because of the above-mentioned reason in Fig. V.7(A).

The performance of PK-RO was compared with that of commercial membranes (OSN membrane: Duramem 150 and Duramem 200; RO membrane: SWC5). As shown in Fig. V.9, two types of OSN membranes showed similar separation factor around 2.0, due to their larger pore size than the PK-RO membrane. Although SWC5 and PK-RO have a similar polyamide layer, SWC5 showed a lower separation factor of 4.8 than PK-RO. This may have been caused by the swelling of SWC5 in M90T10. PK-RO outperformed other membranes in the highest separation factor.
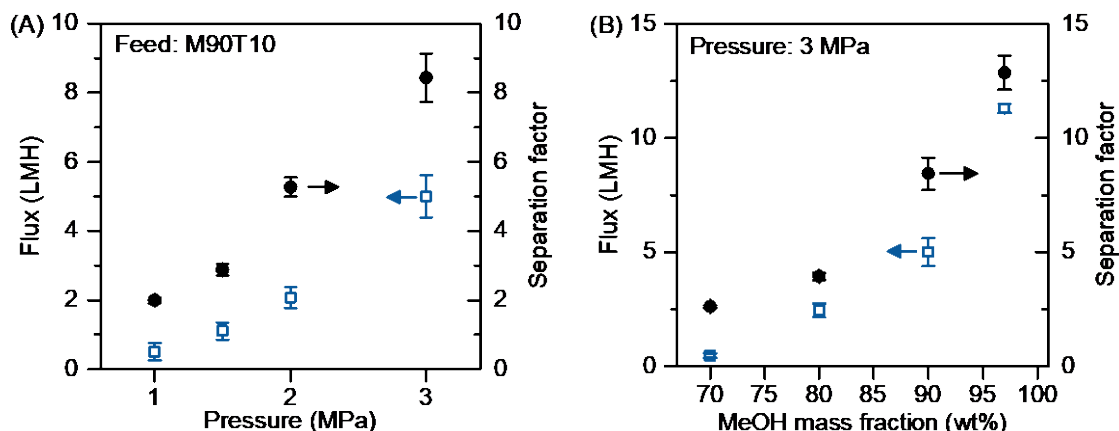

Fig. V.7 Fluxes and separation factors (A) at different applied pressures for M90T10, and (B) at different MeOH mass fractions in the feed solution at 3 MPa.

Table V.3 Estimated osmotic pressure under different applied pressures.

Pressure (MPa)	Rejection (%)	Estimated osmotic pressure* (kPa)	Effective pressure (MPa)
1	47	1061	-0.061
1.5	63	1420	0.080
2	80	1801	0.199
3	87	1957	1.043

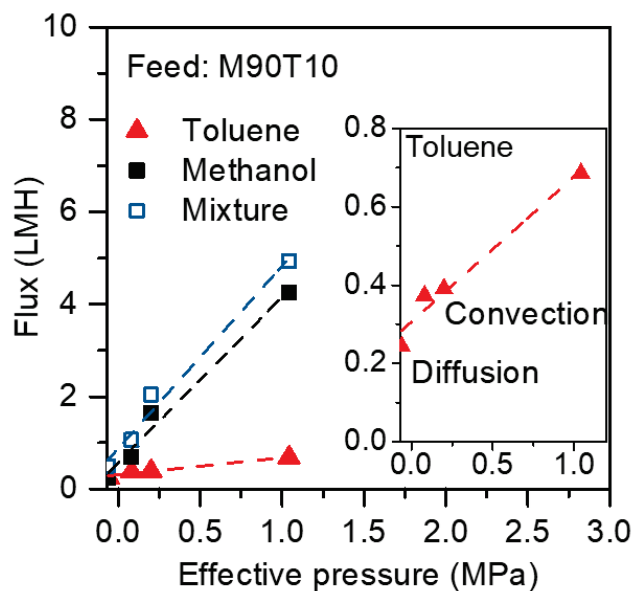* Osmotic pressure was estimated via van't Hoff equation shown in Eq. (S5).

Fig. V.8 The respective fluxes of toluene, methanol and the total flux of mixture as a function of effective pressure. The feed solution was M90T10, and the effective pressures were shown in Table V.3.
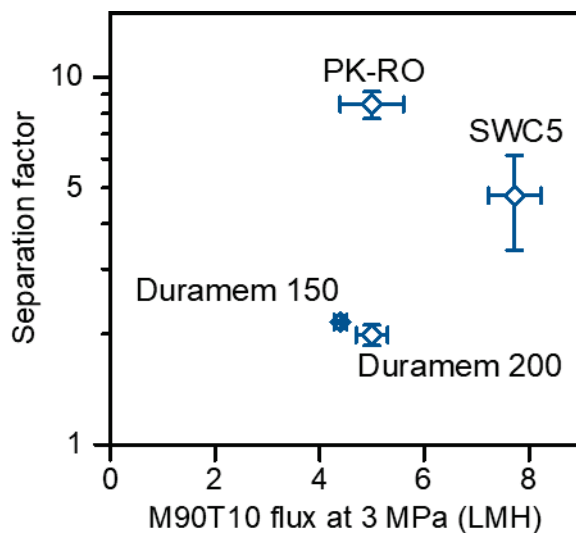
Fig. V.9 Fluxes and separation factors of PK-RO and commercial membranes. The feed was M90T10 and the applied pressure was 3 MPa.

V.3.4 Separation of other mixtures

Toluene was successfully separated from MeOH solution using OSRO because of its lower polarity and larger size than MeOH. Similarly, the separation of other organic molecules with lower polarity and/or larger size than MeOH can be promising. Some solutes and MeOH mixtures were investigated and the results are shown in Fig. V.10(A). Aliphatic alcohols, aliphatic alkanes, and aromatic compounds were chosen for this study. As shown in Fig. V.10(a1), all mixtures showed similar fluxes because the solvents for all mixtures were MeOH. As shown in Fig. V.10(a2) and (a3), the separation factor increased with the molecular weight and decreased with δ_p of the solutes. These results indicate that a higher separation factor would be expected for a solute with larger size and lower polarity. For example, the highest separation factor of 38.0 was obtained for a mixture of M90heptane10.

For more applications, OSRO membranes are required to preserve their separation characteristics in polar aprotic liquids, because the swelling of many OSN membranes in polar aprotic liquids has been reported [23]. EtOH, AcN, acetone, and THF were chosen as the solvents in this study, while toluene was selected as the solute. As shown in Fig. V.10(b1), the flux decreased with the molecular weight of the solvent, confirming that the flux depends

on the permeability of the solvent (Fig. V.6). A high separation factor can be expected for a small, highly polar solvent molecule. The separation factor decreased with the molecular weight as shown in Fig. V.10(b2) and increased with δ_p of the solvents, except AcN as shown in Fig. V.10(b3). These results further confirm that the important factors in separation of organic liquids are size and polarity. The separation factors were at least above 2.5, showing adequate separation of toluene from polar solvents by PK-RO.

V.3.5 Filtration stability

For practical application, the high performance of a membrane over a long term guarantees its continued use. The stability of PK-RO was evaluated in M90T10 (Fig. V.11(A)) and Acetone90T10 (Fig. V.11(B)) mixtures. The stable flux and separation factor were obtained by filtration over 120 h for both mixtures, suggesting PK-RO is stable in polar protic solvents and polar aprotic solvents. However, SWC5 showed gradually decreased separation factor in M90T10 and no separation ability in M70T30, acetone90T10 and ACN90T10, as shown in Fig. V.12. The excellent solvent resistance of the PK-RO membrane endows its applicability across various mixtures.
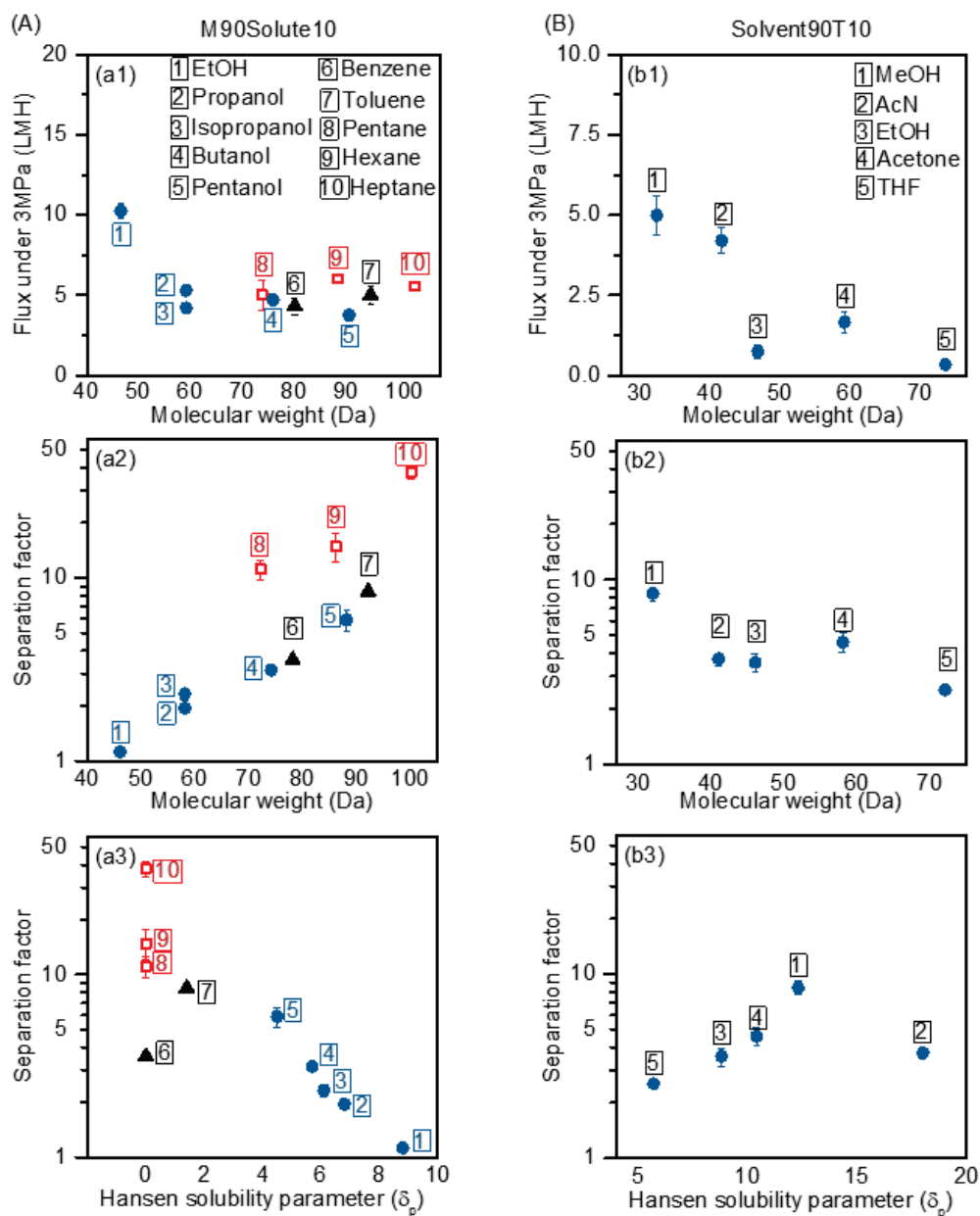
Fig. V.10 Separation performance of PK-RO for various organic liquid mixtures. (A) 90 wt% MeOH and 10 wt% solute (M90solute10) systems: (a1) fluxes vs. molecular weight, (a2) separation factors vs. molecular weight, (a3) separation factors vs. Hansen solubility parameter. (B) 90 wt% solvent and 10 wt% toluene (Solvent90T10) systems: (b1) fluxes vs. molecular weight, (b2) separation factors vs. molecular weight, (b3) separation factors vs. Hansen solubility parameter.
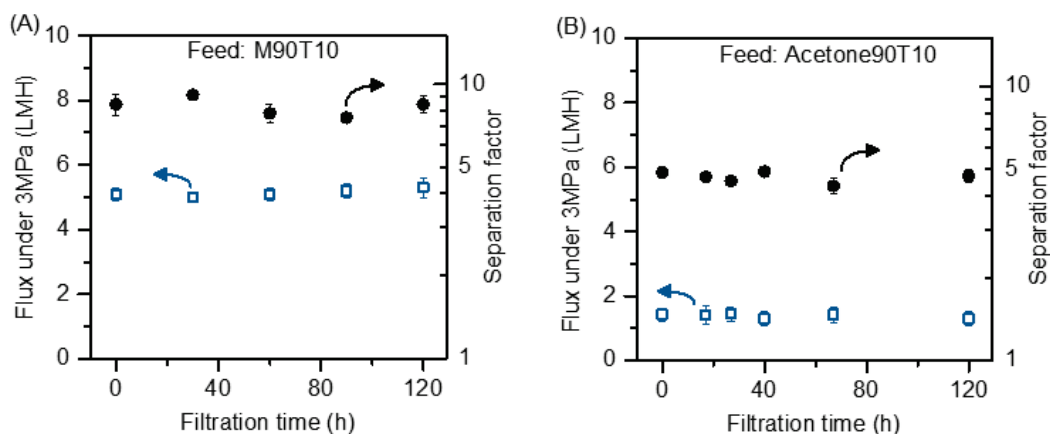
Fig. V.11 PK-RO stability in the filtration of (A) M90T10 and (B) Acetone90T10 mixture.
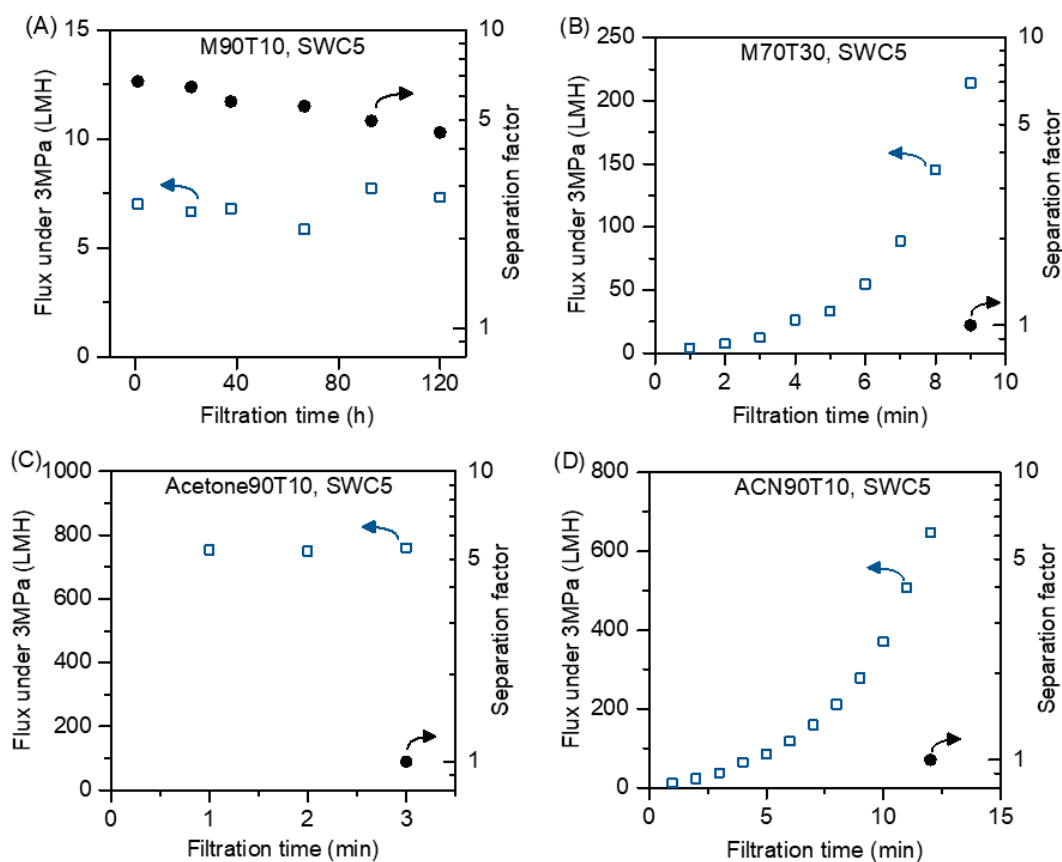

Fig. V.12 The stability of SWC5 in the filtration of (A) M90T10, (B) M70T30, (C) Acetone90T10, (D) AcN90T10 mixtures.

V.4 Conclusions

The separation of organic liquid mixtures is required for many industrial applications. Separation by membrane is preferred due to its low energy consumption. However, the membrane must exhibit high resistance to organic liquids to apply OSRO. In this work, an OSRO membrane with a PK membrane as the support and a selective polyamide layer formed by interfacial polymerization (IP) was used to separate organic liquid mixtures. The obtained membrane, PK-RO, exhibited excellent selectivity for large, non-polar organic liquids (aliphatic alkanes, aromatic compounds, and aliphatic alcohols) from small, polar liquids (MeOH, EtOH, AcN, acetone, and THF) with high fluxes. The highest separation factor of 38.0 was obtained for a mixture of heptane and methanol. The efficient separation was primarily attributed to the difference in the molecular size and polarity. PK-RO provided superior stability and separation factor than the commercial membranes. To our knowledge, this is the first study in which an OSRO membrane was fabricated using IP. This work can bring about a revolutionary change for the OSRO separation of organic liquid mixtures without phase change. In addition, the fabrication of the PK-RO membrane can be easily scaled up using the well-established IP procedure.

Reference

[1] D.S. Sholl, R.P. Lively, Seven chemical separations to change the world, Nature, 533 (2016) 316-316.

[2] R.P. Lively, D.S. Sholl, From water to organics in membrane separations, Nat Mater, 16 (2017) 276-279.

[3] B. Liang, X. He, J. Hou, L. Li, Z. Tang, Membrane Separation in Organic Liquid: Technologies, Achievements, and Opportunities, Adv Mater, (2018) 1806090.

[4] A.G. Fane, R. Wang, M.X. Hu, Synthetic Membranes for Water Purification: Status and Future, Angew Chem Int Edit, 54 (2015) 3368-3386.

[5] G. Belfort, Membrane Filtration with Liquids: A Global Approach with Prior Successes, New Developments and Unresolved Challenges, Angew Chem Int Edit, 58 (2019) 1892-1902.

[6] P. Marchetti, M.F.J. Solomon, G. Szekely, A.G. Livingston, Molecular Separation with Organic Solvent Nanofiltration: A Critical Review, Chem Rev, 114 (2014) 10735-10806.

[7] S. Karan, Z.W. Jiang, A.G. Livingston, Sub-10 nm polyamide nanofilms with ultrafast solvent transport for molecular separation, Science, 348 (2015) 1347-1351.

[8] G.H. Zhu, F.Y. Zhang, M.P. Rivera, X.X. Hu, G.Y. Zhang, C.W. Jones, R.P. Lively, Molecularly Mixed Composite Membranes for Advanced Separation Processes, Angew Chem Int Edit, 58 (2019) 2638-2643.

[9] J. Kopecek, S. Sourirajan, Performance of porous cellulose acetate membranes for the reverse osmosis separation of mixtures of organic liquids, Ind Eng Chem Process Des Develop, 9, (1970) 5-12.

[10] H. Nomura, S. Yoshida, M. Seno, H. Takahashi, T. Yamabe, Permselectivities of Some Aromatic-Compounds in Organic Medium through Cellulose-Acetate Membranes by Reverse-Osmosis, J Appl Polym Sci, 22 (1978) 2609-2620.

[11] W.J. Adam, B. Luke, P. Meares, The Separation of Mixtures of Organic Liquids by Hyperfiltration, J Membr Sci, 13 (1983) 127-149.

[12] Y. Fang, S. Sourirajan, T. Matsuura, Reverse osmosis separation of binary organic mixtures using cellulose acetate butyrate and aromatic polyamide membraes, J Appl Polym Sci, 44, (1992) 1959-1969.

[13] J. Chau, P. Basak, K.K. Sirkar, Reverse osmosis separation of particular organic solvent mixtures by a perfluorodioxole copolymer membrane, J Membr Sci, 563 (2018) 541-551.

[14] T. Tsuru, M. Miyawaki, T. Yoshioka, M. Asaeda, Reverse osmosis of nonaqueous solutions through porous silica-zirconia membranes, AIChE J, 52 (2006) 522-531.

[15] D.Y. Koh, B.A. McCool, H.W. Deckman, R.P. Lively, Reverse osmosis molecular differentiation of organic liquids using carbon molecular sieve membranes, Science, 353 (2016) 804-807.

[16] Z. Yang, H. Guo, C.Y. Tang, The upper bound of thin-film composite (TFC) polyamide membranes for desalination, J Membr Sci, 590 (2019) 117297.

[17] A.K. Ghosh, E.M.V. Hoek, Impacts of support membrane structure and chemistry on polyamide-polysulfone interfacial composite membranes, J Membr Sci, 336 (2009) 140-148.

[18] G.Z. Ramon, M.C.Y. Wong, E.M.V. Hoek, Transport through composite membrane, part 1: Is there an optimal support membrane?, J Membr Sci, 415 (2012) 298-305.

[19] L. Cheng, D.M. Wang, A.R. Shaikh, L.F. Fang, S. Jeon, D. Saeki, L. Zhang, C.J. Liu, H. Matsuyama, Dual Superlyophobic Aliphatic Polyketone Membranes for Highly Efficient Emulsified Oil-Water Separation: Performance and Mechanism, Acs Appl Mater Inter, 10 (2018) 30860-30870.

[20] Y.S. Jung, A. Canlier, T.S. Hwang, An efficient and facile method of grafting Allyl groups to chemically resistant polyketone membranes, Polymer, 141 (2018) 102-108.

[21] M. Yasukawa, S. Mishima, M. Shibuya, D. Saeki, T. Takahashi, T. Miyoshi, H. Matsuyama, Preparation of a forward osmosis membrane using a highly porous polyketone microfiltration membrane as a novel support, J Membr Sci, 487 (2015) 51-59.

[22] A.A. Tashvigh, T.S. Chung, Facile fabrication of solvent resistant thin film composite membranes by interfacial crosslinking reaction between polyethylenimine and dibromo-p-xylene on polybenzimidazole substrates, J Membr Sci, 560 (2018) 115-124.

[23] M. Ghadiri, M. Mohammadi, M. Asadollahzadeh, S. Shirazian, Molecular separation in liquid phase: Development of mechanistic model in membrane separation of organic compounds, J Mol Liq, 262 (2018) 336-344.

[24] J.H. Kim, S.J. Moon, S.H. Park, M. Cook, A.G. Livingston, Y.M. Lee, A robust thin film composite membrane incorporating thermally rearranged polymer support for organic solvent nanofiltration and pressure retarded osmosis, J Membr Sci, 550 (2018) 322-331.

[25] M. Mertens, C. Van Goethem, M. Thijs, G. Koeckelberghs, I.F.J. Vankelecom, Crosslinked PVDF-membranes for solvent resistant nanofiltration, J Membr Sci, 566 (2018) 223-230.

[26] S.C. Yu, M.H. Liu, X.S. Liu, C.J. Gao, Performance enhancement in interfacially synthesized thin-film composite polyamide-urethane reverse osmosis membrane for seawater desalination, J Membr Sci, 342 (2009) 313-320.

[27] Y. Li, E. Wong, Z. Mai, B. Van der Bruggen, Fabrication of composite polyamide/Kevlar aramid nanofiber nanofiltration membranes with high permselectivity in water desalination, J Membr Sci, 592 (2019) 117396.

[28] L.L. Xia, J. Ren, M. Weyd, J.R. McCutcheon, Ceramic-supported thin film composite membrane for organic solvent nanofiltration, J Membr Sci, 563 (2018) 857-863.

[29] S.P. Sun, S.Y. Chan, T.S. Chung, A slow-fast phase separation (SFPS) process to fabricate dual-layer hollow fiber substrates for thin-film composite (TFC) organic solvent nanofiltration (OSN) membranes, Chem Eng Sci, 129 (2015) 232-242.

[30] S.P. Sun, S.Y. Chan, W.H. Xing, Y. Wang, T.S. Chung, Facile Synthesis of Dual-Layer Organic Solvent Nanofiltration (OSN) Hollow Fiber Membranes, Acs Sustain Chem Eng, 3 (2015) 3019-3023.

[31] A. Buekenhoudt, F. Bisignano, G. De Luca, P. Vandezande, M. Wouters, K. Verhulst, Unravelling the solvent flux behaviour of ceramic nanofiltration and ultrafiltration membranes, J Membr Sci, 439 (2013) 36-47.

[32] S.M. Aharoni, The Solubility Parameters of Aromatic Polyamides, J Appl Polym Sci, 45 (1992) 813-817.

Chapter VI Improved organic solvent osmosis reverse (OSRO) membrane for organic liquid mixture separation by simple heat treatment

VI.1 Introduction

Organic liquid mixture separations, such as the separation of alcohols/alkanes, aromatics/aliphatic hydrocarbons, are crucial processes in petroleum, pharmacy and chemistry. Owing to the similarly small sizes and volatilities of these organic liquid molecules, the energy-intensive thermally driven separation approaches such as distillation are still dominating. These separations put a huge burden on energy resources, resulted from the heat for liquids vaporization and significant carbon dioxide emissions [1-3]. The success of reverse osmosis (RO) membrane process replacing distillation in seawater desalination and water reclamation verifies the bright prospects of membrane technology in separations, in terms of not only alleviated environmental burden, but also compact spacing and operational simplicity.

Considerable progress has been achieved in organic solvent nanofiltration (OSN), which exhibits high retentions toward molecules with molecular weight (M_w) larger than 200 Da [4-6], which can be catalysts [7], ionic liquids [8], dyes [9], antibiotics [10], however, OSN shows no selectivity toward organic liquid mixtures comprising molecules lower than 100 Da [11], such as methanol/toluene mixture. For this target, organic solvent reverse osmosis (OSRO) membranes hold promise due to the higher crosslinked selective layer than OSN membranes. State-of-the-art RO membranes are mainly thin-film composite (TFC) membranes, comprising a polyamide skin layer fabricated from interfacial polymerization (IP) and a polysulfone support. However, these RO membranes cannot be used as OSRO, because the supports would be dissolved or swell in organic solvents. Other developed support membranes, such as polyimide, polybenzimidazole, polyacrylonitrile, exhibit good

organic solvent resistance after an additional pretreatment [6]. Nevertheless, most TFC membranes made from these supports are only reported as OSN membranes. Our previous work showed the TFC membrane made from polyketone (PK) support can provide efficient OSRO searation of organic liquid mixtures, and a separation factor of 8.4 was achieved for methanol/toluene (90/10 wt%) mixture. The separation factor needs to be further improved for practical application. Polyamide layer plays a crucial role in separation performance, and thus, to acquire higher separation factor, higher crosslinked polyamide layer is needed.

Efforts to densificate the selective layer of polyamide based TFC membranes are mainly devoted by optimizing the reaction conditions in IP reaction including the monomer concentration, reaction time, acid acceptors, heat treatment, and so on [12]. Heat treatment is a facile approach to regulate the membrane performance. Two kinds of heat-treatment approaches have been reported in literatures. The most commonly used one is heating the membrane in a hot oven at desired temperature after the interfacial polymerization [13-15]. This step is usually applied to promote additional crosslinking through dehydration of amine and carboxylic acid residues [16], which has been proven to be useful in tightening the membrane structure and improving salt rejection. Another efficient approach is immersing the commerical membrane in high-temperature water before the usage [17]. It was found that after this hot water treatment, marginal changes occurred in the membrane surface characteristics, including zeta potential, hydrophobicity, roughness, chemistry, and also free-volume hole-radius of the skin layer, while a rejection enhancement of salt and netrual small sized compounds (e.g. boron) and lower water permeability were obtained. It was suggested that maybe the change in free-volume fraction and thickness affect the membrane performance [18, 19].

Even the effect of heat-treatment on membrane performance has been reported, the reported ones are for the membranes employing in aqueous media and in gas separation [12, 20]. The effect of heat-treatment on the OSRO membrane remains unclear. The main purpose of this work is to elucidate the effect of the above two kinds of heat treatments on OSRO performance in terms of flux and separation factor.

VI.2 Experimental

VI.2.1 Materials

The materials are the same as that in Chapter V.

VI.2.2 Membrane fabrication

The procedures of PK support membrane fabrication and IP reaction were the same as that in Chapter V, expect for the heat treatment procedure and no SDS addition in MPD solution. In this work, the membrane was heat-treated in a hot-air circulating oven as the Chapter V, but at a desired temperature (100 – 170 ℃) for 5 min. After that, the membrane was taken out from the oven, and put into Milli-Q water after cooling down to room temperature. After one night immersion for washing out the unreacted monomers, the membrane was heated in Milli-Q water at different temperature (25 – 97 ℃) for 3 h. Then, the membrane was taken out and stored in Milli-Q water under 4℃ in dark prior to use. The membrane was denoted as "AT1WT2". "A" represents the air heated process in oven, "T1" the temperature of oven; "W" represents water heated process, "T2" the temperature of water. For example, A100T60 represents the membrane treated in oven at 100 ℃ and subquently, in water at 60 ℃.

VI.2.3 Performance in organic media

RO performance of OSRO was characterized using a lab-scale cross-flow filtration setup at 25 ℃ with an effective area of 8.04 cm^2. This test unit was the same as that in Chapter V. All samples were prefiltrated using Milli-Q water as the feed solution for 1 h under 2 MPa to reach a steady state before testing. Next, the NaCl rejection was examined using 2000 ppm NaCl as the feed solution under 2 MPa. After NaCl rejection test, water was used as the feed solution to wash the unit for 1 h. Next, MeOH was used to balance the unit for 1 h, and the membrane was ready for the performance test in organic liquid.

For the permeabiliy test of pure organic liquid, the liquid was introduced as the feed solution untile a stable permeabiliy value was obtained. After this test, MeOH was used to wash the unit for 1 h, and the next liquid was tested. After all the permeability tests, finally, MeOH was used to balance the unit for 1 h.

For the performance test of binary oragnic liquid mixtures, the majority of mixture was denoted as solvent, and another one was solute. The mixture was noted as AxBy according to their compositions. A is the solvent (x wt%), and B is the solute (y wt%). MeOH and toluene were abbreviated as "M" and "T", respectively. The solvent was firstly filtrated for 1 h, and then the mixture was introduced, after getting the stable flux and separation factor, the solvent was fed again into the test unit to wash the uint. After that, MeOH was used to wash the unit again, before the test of next mixtures. For ternary oragnic liquid mixtures, 90 wt% of mixture was MeOH acting as solvent. The other two components was defined as solute 1 and solute 2.

VI.3 Results and discussion

VI.3.1 Membrane fabrication

VI.3.1.1 Effect of oven temperature

Fig. VI.1 (A) and (B) showed the oven temperature remarkably influenced separation performance. Both the solute retention in aqueous and organic liquids increased first and then decreased after reaching the maximum values at 130℃. The optimized NaCl rejection and toluene separation factor were 99.5 % and 18.4, repectively. From 100 to 130℃, the oven heat helps to evaporate water and solvent remaining in membrane and also promotes the reaction between unreacted amino and chloride groups. Therefore, the polyamide skin layer becomes more crosslinked, providing incresed retention ability. Considering the fact that the condensation polymerization between amino and chloride groups was exothermic reaction [21], further increased oven temperature may lead to an inhibition to the reaction, which led to a decreased retention ability. On the other hand, the variation tendency of retention in organic media keeps consistent with that in aqueous media, indicating that the performance in aqueous media can be a powerful indicator to predict the performance in organic media. This is the first attempt to connect the membrane performances in aqueous and organic media.

Meanwhile, it is worth to notice that higher oven temperature causes obvious PK support shrinkage. As shown in Fig. VI.1 (C), the membrane thinkness kept decreasing with oven temperature. Fig. VI.1 (D) shows the PK support became more compacted after higher oven

temperature treatment. The PK shinkage may have an effect on polyamide layer structure, because the shinkage and further MPD/TMC reaction occurred at the same time during the oven heating. Moderate PK support shrinkage is expected to promote the formation of more compacted polyamide layer. However, large degree of shrinkage may bring in membrane damage, because the membrane was fixed by frames during the oven heat-treatment.
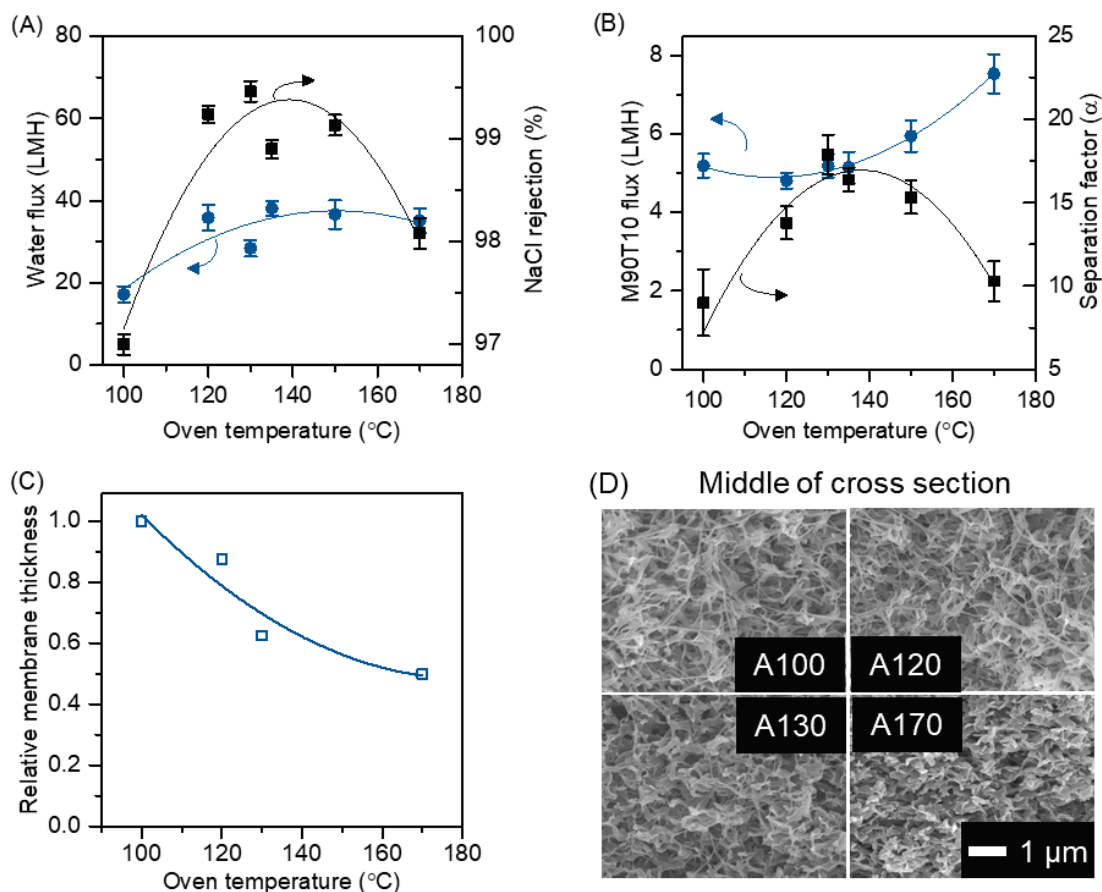

Fig. VI.1 The effect of oven temperature on the (A) water flux and NaCl rejection in aqueous media under 2 MPa, and (B) flux and separation factor in M90T10 mixture under 3 MPa. (C) The relative thickness of membranes fabricated with different oven temperatures. (D) The middle cross section SEM images of membranes.

As for the flux, in aqueous media, water flux increased a little from 100 to 130 °C, and this increased water flux may came from the enhanced roughness at 130 °C, due to the enhanced shrinkage of PK support at 130°C. Then the water flux kept constant among 130 to 170 °C, which was the balance of pore shinkage and decreased crosslinking reaction. However, the flux in organic media showed constant from 100 to 130 °C, which may come from the increased osmotic pressure created by toluene because of increased retention ability. Similarly, the increased flux from130 to 170 °C was due to the decreased osmotic pressure.

VI.3.1.2 Effect of water temperature

The effect of water temperature on membrane performance was investigated, choosing the optimized membrane in the oven treatment step (A130). The water treatment step is different from that in oven treatment. During oven treatment, both membrane shrinkage and crosslinking reaction occur, while in water treatment, it is reasonable to believe that mainly shrinkage occurrs. Because the reaction between -COOH and -NH$_2$ will produce water molecules, and aqueous media does not benefit this reaction.

As shown in Fig. VI.2 (A), the water flux obviouly decreased with water temperature, particularly at temeprature higher than 80 °C, which might come from the densifiation of polyamide layer in high-temperature water due to the pore shrinkage, even the observed salt rejection can not benefit from this. In organic media (Fig. VI.2(B)), the flux decreased, while the separation factor was improved continuously with the water temperature. The best performance was achieved by A130W95, with a separation factor of 50.0 and a flux of 2.9 LMH. This result showed the separation in organic liquid is more sensitive than salt seperation in water.
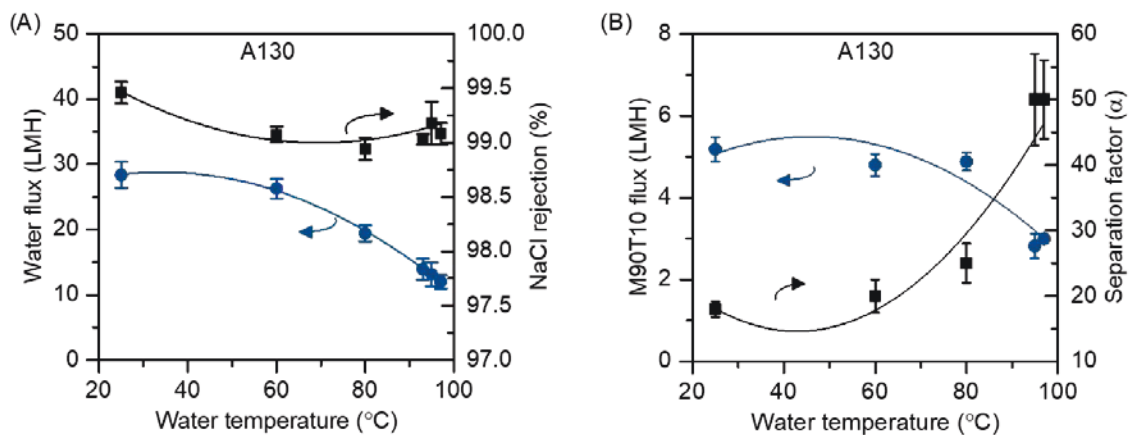
Fig. VI.2 The effect of water temperature on the performance of A130 (A) in aqueous media. (B) in organic media.

VI.3.2 Membrane characterization

To future investigate the difference of A100, A130 and A130W95, other characterizations were conducted. As shown in Fig. VI.3 (A), the pore size of A100 is higher than the other two membranes, due to the lowest crosslinking degree. A130W95 has a little bit smaller pore size than A130. Then, MWCO was determinated using 1wt% alcohols with different molecular weights as solutes, and using MeOH as solvent. Fig. VI.3 (B) showed the order of MWCO is A130W95 < A130 < A100, which was consistent with the above result in pore size. Fig. VI.3 (C) shows there are some differences in membrane morphology between these three membranes. It seems that A130W95 had the smoothest and the thickest polyamide layer, which was helpful to provide highest retention ability. The further characterizations will be conducted in the future.
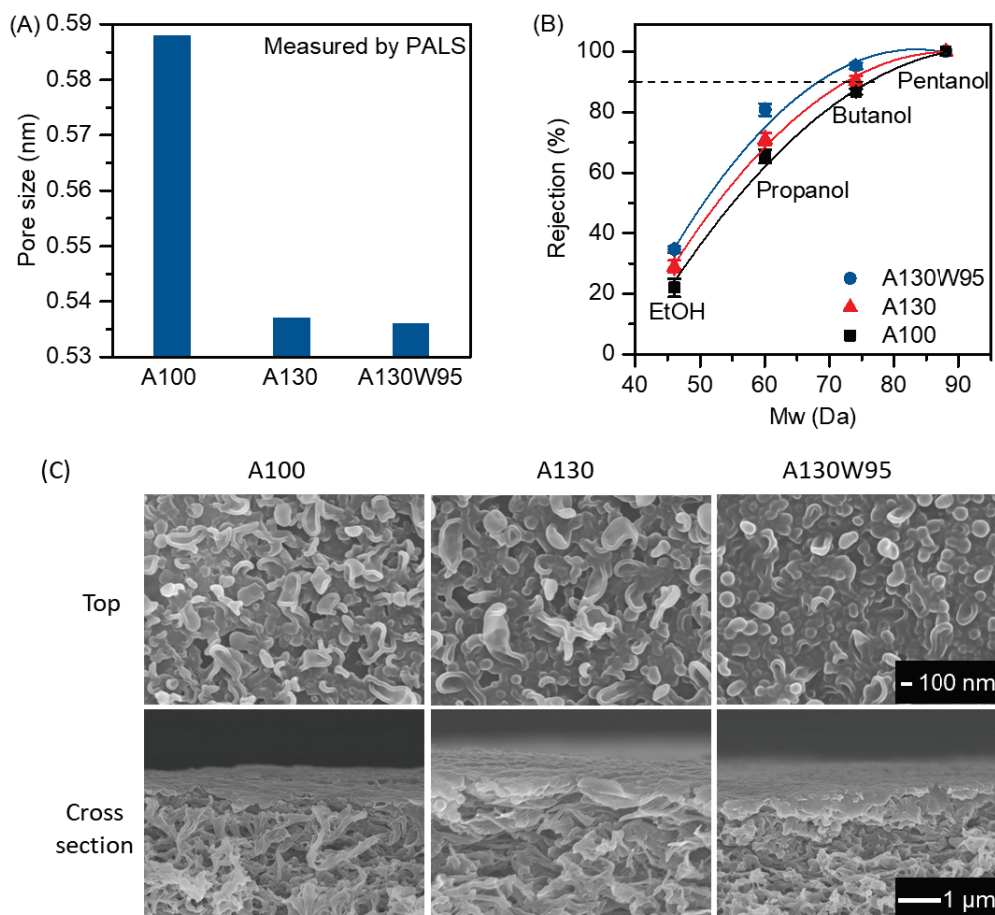
Fig. VI.3 Characterization of A100, A130, and A130W95 (A) Pore size measured by PALS. (B) MWCO determination. Feed solution is 1 wt% solute (ethanol, 1-propanol, 1- butanol, 1-pentanol) in MeOH. (C) SEM images of top surface and cross section.

VI.3.3 Membrane separation process

VI.3.3.1 Toluene separation from MeOH

In this section, toluene and MeOH separation was used as a binary mixture model. The toluene separation from MeOH solution can be affected by the operation conditions. Fig. VI.4 (A) showed higher applied pressure provided higher flux and separation factor, because largely enhanced MeOH transportion at higher pressure. Fig. VI.4 (B) indicated that decreasing the toluene fraction in feed led to higher flux and separation factor, resulting from the easier transporation of MeOH than toluene through the membrane. The temperature of

feed solution also had a big influence (Fig. VI.4 (C)). It was found that the the flux kept increasing with feed temperature. One reason is that the viscocity of liquids decreases with the increased temperature. Another possibility is that the mobility of polyamide chain was enhanced at higher temperature, leading to the enhanced liquid transportation. Although the flux increased with feed temperature, the separation factor decreased, which may be related to the weakened membrane stability as well as the temperature dependencies of the adsorption and diffusion of methanol and toluene. It was inferred that the enhancement of toluene adsorption and transporation at high feed temperature was higher that that of MeOH, so lower separation factor was obtained. Finally, the stability during 7 days was confirmed, providing the possibility to be used in practical applications. (Fig. VI.4 (B)).
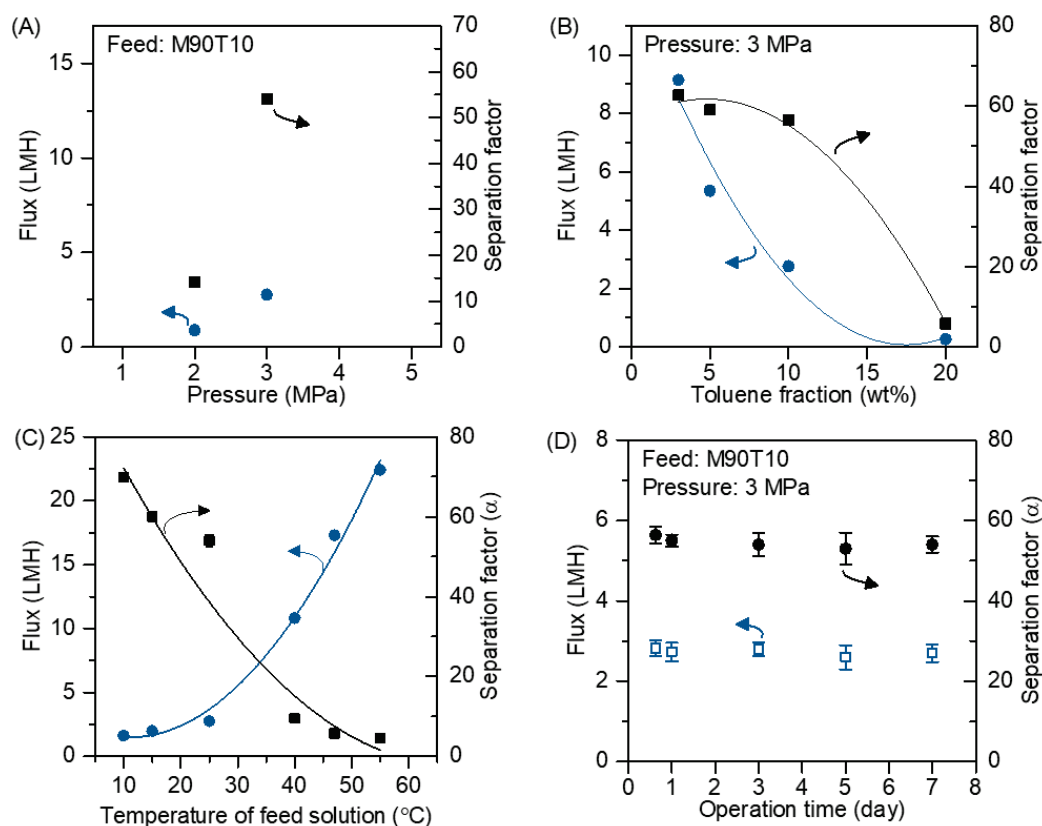

Fig. VI.4 The effect of (A) applied pressure, (B) feed solution ratio, and (C) feed solution temperature on the membrane performance of A130W95. (D) The stability in long time operation.

VI.3.3.2 Toluene separation from other polar liquids

The toluene separation from other polar liquids was investigated in this section. A130W95 showed decreased permeability of polar liquids than A100 (Fig. VI.5 (A)), because the decreased membrane pore size explained before. As expected, the highly crosslinked polyamide layer of A130W95 provided it higher separation factor of toluene in all the tested polar liquids than that of A100 (Fig. VI.5 (B)).
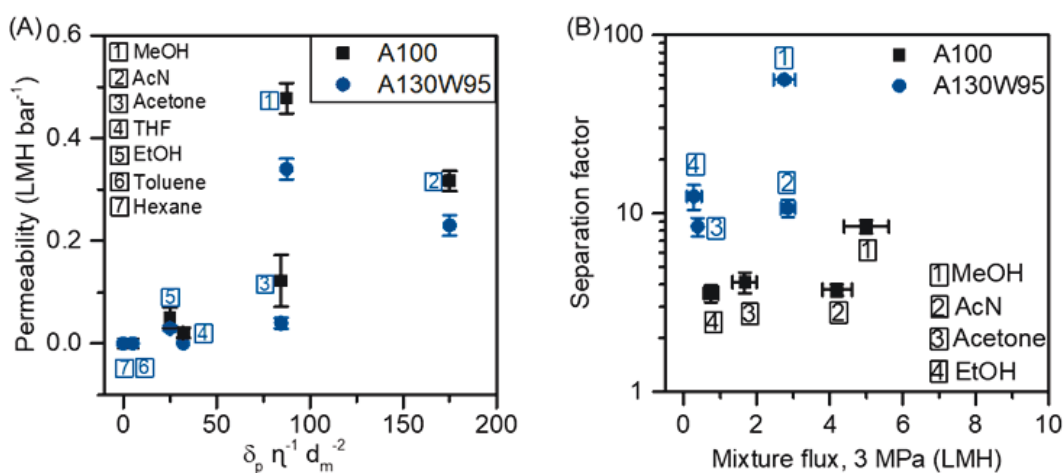

Fig. VI.5 The comparision of A100 and A130W95. (A) The permeability of several pure organic liquids. (B) The flux and separation flux of polar liquid/toluene binary systems.

VI.3.3.3 Toluene separation in tenary systems

There is of practical interest to study the separation performance of complex organic liquid mixtures, especially in petroleum and refining industries. In this section, ternary systems were selected. MeOH was chosen as a primary solvent and the ratio was fixed at 90 wt%. The ratio of the other two components was changed. Firstly, the toluene-hexane-MeOH system was investigated as shown in Fig. VI.6 (A). Similar fluxes of all mixtures were obtained, because the osmotic pressures of all mixtures are similar. A130W95 showed higher separation factor toward hexane than toluene, due to the higher non-polarity of hexane. Because hexane has an interaction with toluene, it will go through membrane easier with the existence of toluene. Higher toluene fraction in the feed brings in easier transportation of

hexane, and thus lower separation factor of hexane. On the other hand, the separation factor of toluene did not change in any ratios. It means that the existence of hexane has no influence for toluene retention. Continuously, pentanol was chosen as another co-solute with toluene, and the result was shown in Fig. VI.6 (B). It was found that similar result was obtained. That was the separation factor of pentanol (the solute with lower separation factor) was kept constant regardless of the ratio of toluene and pentanol, while the separation factor of toluene (the solute with higher separation factor) decreased with the increase of pentanol ratio. Because pentanol can help toluene to go through the membrane.

In summary, for tenary systems using MeOH as solvent, the solute with lower separation factor will kept similar separation factor whenever the solute ratio is. For the solute with higher separation factor, the separation factor decreased with the increase of the other component.
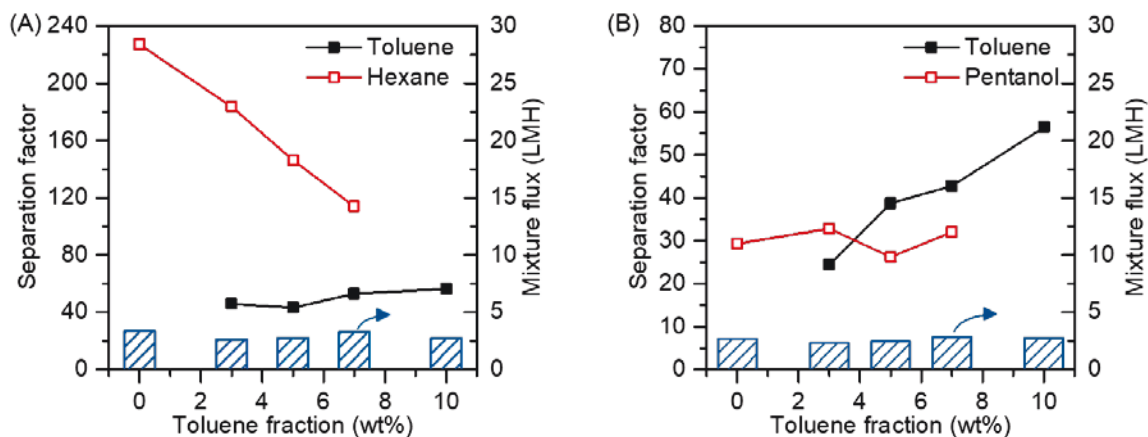

Fig. VI.6 The separation performance in tenary systems: (A) toluene-hexane-MeOH, (B) toluene-pentanol-MeOH.

VI.4 Conclusions

The implementation of membrane technology to replace energy-intensive distillation for separation of organic liquid mixtures proves an extremely important yet challenging task. Organic solvent reverse osmosis (OSRO) membranes fabricated via interfacial

polymerization on polyketone support are promising for this separation. Highly selective OSRO membrane was developed by facily adjusting heat treatment procedures. By virtue of synergistic effects of size sieving and hydropic replusion, an unprecedental combination of high flux (2.8 LMH) and high selectivity (50.0) was achieved with the optimized membrane (A130W95) for methanol (90 wt%) and toluene (10 wt%) mixture under 3 MPa at 25℃. The applied pressure, feed solution composition, and feed solution temperature have significant effect on the flux and separation performance. The tenary systems were also investaged in this work. This facial approach may open novel avenues to the design of high-performance membranes for organic liquid separations.

Reference

[1] K. Tang, P. Bai, J.W. Zhang, Y. Huo, Separation of Methanol-Toluene Azeotropic Mixture by Extractive Distillation, Asian J Chem, 25 (2013) 321-326.

[2] Y.K. Ong, G.M. Shi, N.L. Le, Y.P. Tang, J. Zuo, S.P. Nunes, T.S. Chung, Recent membrane development for pervaporation processes, Prog Polym Sci, 57 (2016) 1-31.

[3] W.J. Koros, R.P. Lively, Water and beyond: Expanding the spectrum of large-scale energy efficient separation processes, AIChE J, 58 (2012) 2624-2633.

[4] I. Soroko, A. Livingston, Impact of TiO2 nanoparticles on morphology and performance of crosslinked polyimide organic solvent nanofiltration (OSN) membranes, J Membr Sci, 343 (2009) 189-198.

[5] S. Karan, Z.W. Jiang, A.G. Livingston, Sub-10 nm polyamide nanofilms with ultrafast solvent transport for molecular separation, Science, 348 (2015) 1347-1351.

[6] P. Marchetti, M.F.J. Solomon, G. Szekely, A.G. Livingston, Molecular Separation with Organic Solvent Nanofiltration: A Critical Review, Chem Rev, 114 (2014) 10735-10806.

[7] L. Huang, J. Chen, T.T. Gao, M. Zhang, Y.R. Li, L.M. Dai, L.T. Qu, G.Q. Shi, Reduced Graphene Oxide Membranes for Ultrafast Organic Solvent Nanofi ltration, Adv Mater, 28 (2016) 8669-8674.

[8] H.T. Wong, C.J. Pink, F.C. Ferreira, A.G. Livingston, Recovery and reuse of ionic liquids and palladium catalyst for Suzuki reactions using organic solvent nanofiltration, Green Chemistry, 8 (2006) 373-379.

[9] B. Liang, H. Wang, X.H. Shi, B.Y. Shen, X. He, Z.A. Ghazi, N.A. Khan, H. Sin, A.M. Khattak, L.S. Li, Z.Y. Tang, Microporous membranes comprising conjugated polymers with rigid backbones enable ultrafast organic-solvent nanofiltration, Nat Chem, 10 (2018) 961-967.

[10] D.Q. Shi, Y. Kong, J.X. Yu, Y.F. Wang, J.R. Yang, Separation performance of polyimide nanofiltration membranes for concentrating spiramycin extract, Desalination, 191 (2006) 309-317.

[11] P. Silva, S.J. Han, A.G. Livingston, Solvent transport in organic solvent nanofiltration membranes, J Membr Sci, 262 (2005) 49-59.

[12] J. Zhao, Z. Wang, J.X. Wang, S.C. Wang, Influence of heat-treatment on CO2 separation performance of novel fixed carrier composite membranes prepared by interfacial polymerization, J Membr Sci, 283 (2006) 346-356.

[13] T. Shintani, H. Matsuyama, N. Kurata, Effect of heat treatment on performance of chlorine-resistant polyamide reverse osmosis membranes, Desalination, 247 (2009) 370-377.

[14] C.Y. Chong, W.J. Lau, N. Yusof, G.S. Lai, N.H. Othman, T. Matsuura, A.F. Ismail, Studies on the properties of RO membranes for salt and boron removal: Influence of thermal treatment methods and rinsing treatments, Desalination, 428 (2018) 218-226.

[15] S.C. Yu, M.H. Liu, X.S. Liu, C.J. Gao, Performance enhancement in interfacially synthesized thin-film composite polyamide-urethane reverse osmosis membrane for seawater desalination, J Membr Sci, 342 (2009) 313-320.

[16] A.K. Ghosh, B.H. Jeong, X.F. Huang, E.M.V. Hoek, Impacts of reaction and curing conditions on polyamide composite reverse osmosis membrane properties, J Membr Sci, 311 (2008) 34-45.

[17] T. Fujioka, K.P. Ishida, T. Shintani, H. Kodamatani, High rejection reverse osmosis membrane for removal of N-nitrosamines and their precursors, Water Res, 131 (2018) 45-51.

[18] T. Fujioka, L.D. Nghiem, Modification of a polyamide reverse osmosis membrane by heat treatment for enhanced fouling resistance, Water Sci Tech-W Sup, 13 (2013) 1553-1559.

[19] T. Fujioka, N. Oshima, R. Suzuki, M. Higgins, W.E. Price, R.K. Henderson, L.D. Nghiem, Effect of heat treatment on fouling resistance and the rejection of small and neutral solutes by reverse osmosis membranes, Water Sci Tech-W Sup, 15 (2015) 510-516.

[20] A.P. Rao, N.V. Desai, R. Rangarajan, Interfacially synthesized thin film composite RO membranes for seawater desalination, J Membr Sci, 124 (1997) 263-272.

[21] X.H. Ma, Z.K. Yao, Z. Yang, H. Guo, Z.L. Xu, C.Y.Y. Tang, M. Elimelech, Nanofoaming of Polyamide Desalination Membranes To Tune Permeability and Selectivity, Environ Sci Tech Let, 5 (2018) 123-130.

Chapter VII Conclusions

The application of membrane technology in various separations becomes more and more prosperous, due to its much lower energy cost compared with thermal based separation approaches. Therefore, the exploration of novel membrane and membrane materials is crucial for the development of membrane technology. For the separations in aqueous media, the membranes with easy functionalization and low fouling are desired. For the separations in organic media, the membranes with excellent organic solvent resistant are needed. This thesis focused on the development of polyketone (PK) polymer as membrane materials due to the following main properties:

- low fouling property resulted from the high hydrophilicity;

- easy functionalization due to ketone groups;

- excellent solvent resistance due to strong hydrogen bonds within the polymer chains.

First, targeting the environmental problems resulted from micropollutants in water resources, forward osmosis (FO) and microfiltration (MF) membranes with PK support are developed. The membranes were combined with enzyme catalysis for micropollutant degradation. Second, considering the large demand in separations of organic liquid mixtures, reverse osmosis (RO) membrane with PK support are designed. The conclusions of this study are summarized below.

1. Enzyme-aided forward osmosis (E-FO) process to enhance removal of micropollutants from water resources

The FO membrane with PK support (PK-IP) was fabricated using the methods reported in our previous study. The micropollutant removal efficiency of PK-IP was tested. It was found the performance of PK-IP outperformed the commercial FO membrane. Then, laccase enzyme catalysis was combined with FO separation process using PK-IP as a FO membrane. The degradation efficiency of laccase was enhanced in this hybrid system, due to the increased concentration of laccase in feed solution during FO separation. The amounts of

micropollutant on membrane and in permeate also sharply decreased compared to the single FO separation process, resulted from the degradation of micropollutant during separation. Low fouling was also confirmed. It showed that PK-IP was an excellent FO membrane, and enzyme-aided forward osmosis (E-FO) process could enhance removal of micropollutants from water resources.

2. A novel strategy to immobilize enzymes on microporous membranes via dicarboxylic acid halides

In the above study, free enzyme was used to combine with membrane process. Considering the limitations of free enzyme including non-recyclability and instability, immobilization of enzyme onto membrane was put forward. Trypsin and lipase were used as model enzyme, and covalently immobilized onto regenerated cellulose (RC) membranes by a newly developed method. The immobilized enzymes showed good activity retention, good reusability and improved stability in long time usage.

3. Polyketone-based membrane support improves the organic solvent resistance of laccase catalysis

In practical applications, organic solvents may exist in micropollutant-included aqueous media, which will sharply damage free enzyme. As proved above, enzyme could be immobilized onto membrane via the developed method, and the stability of enzyme was enhanced. It was suggested that immobilizing laccase onto membrane could increase the enzyme stability in the existence of organic solvent. A hydroxylated polyketon (PK-OH) MF membrane was used as a novel platform for enzyme immobilization and RC membrane was used as a contrast. Laccase was immobilized on to these membranes via the developed method. The result showed the PK-OH membrane could immobilize more amount of enzyme molecules than RC, because of the attraction between ketone groups and enzyme. The immobilized laccase showed higher catalytic efficiency than free laccase towards micropollutants in organic solvent-included aqueous media, because of the enzyme protection from the PK-OH MF membrane.

4. Organic liquid mixture separation using an aliphatic polyketone based organic solvent reverse osmosis (OSRO) membrane

As reported, PK polymer has excellent solvent resistance superior to nylon by 30%. In this part, the separation performance of PK based membrane in organic media was explored. One application is the separation of organic liquid mixtures. Reverse osmosis (RO) membrane with PK support was explored, named as PK-RO, fabricated via interfacial polymerization on PK MF support membrane. The highly crosslinked, polar, and stable polyamide skin layer was successfully formed. 15 kinds of mixtures were investigated, and the results suggested PK-RO had high selectivity towards big nonpolar liquids from small polar liquids. It showed the two key factors for separation performance were size and hydrophilicity of liquids. This work showed the high potential of OSRO process for organic liquid mixture separation.

5. Improved organic solvent osmosis reverse (OSRO) membrane for organic liquid mixture separation by simple heat treatment

Last part showed the efficient separation of organic liquid mixtures via PK-RO membrane. Higher crosslinking degree of skin layer is expected to provide higher separation factors. In this work, through adjusting the heat treatment procedure, the membrane was optimized. Higher separation factor was achieved.

Perspective

Further work can be done using PK polymer, and here are some potential applications:

- PK based FO membrane for the separation of organic liquid mixtures;
- PK based NF membrane for the separation of solutes larger than 200 Da from organic liquid.

List of Publications

Chapter II

Cuijing Liu, Ryosuke Takagi, Liang Cheng, Daisuke Saeki, Hideto Matsuyama*. Enzyme-aided forward osmosis (E-FO) process to enhance removal of micropollutants from water resources. *J. Membr. Sci.*, 2020, 593, 117399.

Chapter III

Cuijing Liu, Daisuke Saeki, Hideto Matsuyama*. A novel strategy to immobilize enzymes on microporous membranes via dicarboxylic acid halides. *RSC Adv.*, 2017, 7, 48199-48207.

Chapter IV

Cuijing Liu, Daisuke Saeki, Liang Cheng, Jianquan Luo, Hideto Matsuyama*. Polyketone-based membrane support improves the organic solvent resistance of laccase catalysis. *J. Colloid Interface Sci.*, 2019, 544, 230-240.

Chapter V

Cuijing Liu, Ryosuke Takagi, Takuji Shintani, Liang Cheng, Kuo Lun Tung, Hideto Matsuyama*. Organic liquid mixture separation using an aliphatic polyketone-based organic solvent reverse osmosis (OSRO) membrane. Submitted to *ACS Appl. Mater. Interfaces*.

Chapter VI

Cuijing Liu, Ryosuke Takagi, Liang Cheng, Takuji Shintani, Hideto Matsuyama*. Improved organic solvent osmosis reverse (OSRO) membrane for organic liquid mixture separation by simple heat treatment. *In preparation.*